An improved dust emission model. Part 1: Model description and comparison against measurements

Kok, J. F.[1,2], N. M. Mahowald[2], G. Fratini[3,*], J. A. Gillies[4], M. Ishizuka[5], J. F. Leys[6], M. Mikami[7], M.-S. Park[8,9], S.-U. Park[8], R. S. Van Pelt[10], and T. M. Zobeck[11]

[1] Department of Atmospheric and Oceanic Sciences, University of California, Los Angeles, CA 90095, USA
[2] Department of Earth and Atmospheric Sciences, Cornell University, Ithaca, NY 14850, USA
[3] Department for innovation in biological, agro-food and forest systems (DIBAF), University of Tuscia, Via San Camillo de Lellis snc, 01100 Viterbo, Italy
[4] Division of Atmospheric Sciences, Desert Research Institute, 2215 Raggio Parkway, Reno NV 89512, USA
[5] Faculty of Engineering, Kagawa University, Takamatsu, Kagawa, 761-0396, Japan
[6] Science Division, Office of Environment and Heritage, Department of Premier and Cabinet, Gunnedah, New South Wales, Australia
[7] Japan Meteorological Research Institute, Tsukuba, Japan
[8] Center for Atmospheric and Environmental Modeling, Seoul National University Research Park RM. 515 San 4-2, Bongcheon-dong, Gwanak-gu, Seoul, 151-919, Korea
9 Weather Information Service Engine Project, Center for Atmospheric Science & Earthquake Research, 12Fl. 434 Worldcupbukro Mapo-gu, Seoul, 121-835, Korea
10 USDA-Agricultural Research Service, Wind Erosion and Water Conservation Research Unit, Big Spring, TX 79720, USA
[11] USDA-Agricultural Research Service, Wind Erosion and Water Conservation Research Unit, Lubbock, TX, USA
[*] Now at LI-COR Biosciences GmbH, Siemensstr. 25A, 61352 Bad Homburg, Germany

Correspondence to J. F. Kok (jfkok@ucla.edu)

Abstract

Simulations of the dust cycle and its interactions with the changing Earth system are hindered by the empirical nature of dust emission parameterizations in weather and climate models. Here we take a step towards improving dust cycle simulations by using a combination of theory and numerical simulations to derive a physically-based dust emission parameterization. Our parameterization is straightforward to implement into large-scale models, as it depends only on the wind friction velocity and the soil's threshold friction velocity. Moreover, it accounts for two processes missing from most existing parameterizations: the increased scaling of the dust flux with wind speed as a soil becomes less erodible, and a soil's increased ability to produce dust under saltation bombardment as it becomes more erodible. Our treatment of both these processes is supported by a compilation of quality-controlled vertical dust flux measurements. Furthermore, our scheme reproduces this measurement compilation with substantially less error than the existing dust flux parameterizations we were able to compare against. A critical insight from both our theory and the measurement compilation is that dust fluxes are substantially more sensitive to the soil's threshold friction velocity than most current schemes account for.

1. Introduction

The emission of mineral dust aerosols produces important impacts on the Earth system, for instance through interactions with radiation, clouds, the biosphere, and atmospheric chemistry (e.g., Miller and Tegen (1998), Jickells et al. (2005), Cwiertny et al. (2008), Creamean et al. (2013)). The inclusion of an accurate dust cycle in climate and weather models is thus critical. Yet, the current generation of dust modules shows substantial disagreements with measurements (Cakmur et al., 2006; Huneeus et al., 2011; Evan et al., 2014), and commonly uses semi-empirical "dust source functions" to help parameterize dust emission processes (e.g., Ginoux et al. (2001), Tegen et al. (2002), Zender et al. (2003b)).

Here we aim to improve the dust cycle's representation in weather and climate models, in particular for climate regimes other than the current climate to which most models are tuned (Cakmur et al., 2006). We do so by presenting a physically-based theory for the vertical dust flux emitted by an eroding soil. The functional form of the resulting dust flux parameterization is supported by a compilation of quality-controlled dust flux measurements, and our new parameterization reproduces these measurements with substantially less error than the existing parameterizations we are able to test against. Moreover, our new parameterization is relatively straightforward to implement since it uses only variables that are readily available in weather and climate models. A critical insight from the theory is that the dust flux is substantially more sensitive to changes in the soil state than most climate and weather models account for.

We derive our new dust emission parameterization in Section 2, after which we compare our parameterization's predictions against a compilation of quality-controlled vertical dust flux measurements in Section 3. We discuss the implications of the new parameterization and conclude the article in Section 4.

2. Derivation of physically-based dust flux parameterization

Because of their small size, dust particles in soils (< 62.5 μm diameter (Shao, 2008)) experience cohesive forces that are large compared to aerodynamic and gravitational forces. Consequently, dust aerosols are usually not lifted directly by wind (Gillette et al., 1974; Shao et al., 1993; Sow et al., 2009) and instead are emitted through *saltation*, in which larger sand-sized particles (~70 – 500 μm) move in ballistic trajectories (Bagnold, 1941; Shao, 2008; Kok et al., 2012). Upon impact, these saltating particles can eject dust particles from the soil, a process known as *sandblasting*. Moreover, some saltating particles are actually aggregates containing dust particles. Upon impact, these aggregates can also emit dust aerosols (Shao et al., 1996).

We aim to obtain an analytical expression that captures the main dependencies of the emitted flux of dust aerosols on wind speed and soil properties. An important limitation is that, to allow implementation into climate models, this expression can only use parameters that are globally available. Our approach to achieve this objective combines a theoretical derivation with numerical simulations of dust emission. We start in the next section by providing a basic theoretical expression for the vertical dust flux, after which we derive the three main variables in this expression in the three subsequent sections. We then combine all these components together to give the full dust emission parameterization in Section 2.5.

2.1 Basic theoretical expression of the vertical dust flux

The starting point of our theory is the insight that a saltator impact will produce dust emission only if a threshold impact energy is exceeded (Rice et al., 1999), with the nature and value of this threshold depending on the soil type and state. For instance, for a soil with only a small fraction of suspendable particles, much of the dust is present as coatings on larger sand particles (Bullard et al., 2004), such that the relevant threshold is likely the energy required for rupturing these coatings (Crouvi et al., 2012). Conversely, for a soil containing a large fraction of suspendable dust particles, the threshold for fragmentation of brittle dust aggregates could be most important (Kok, 2011b). Since the theoretical size distribution predicted by brittle fragmentation theory is in good agreement with dust size distribution measurements (Albani et al., 2014; Mahowald et al., 2014; Rosenberg et al., 2014), and its implementation into large-scale models improves agreement with other measurements of the dust cycle (Johnson et al., 2012; Nabat et al., 2012; Li et al., 2013; Evan et al., 2014), the threshold for fragmentation of soil dust aggregates might be the most relevant threshold for dust emission under many conditions. For simplicity, we thus assume that the energy required for dust aggregate fragmentation is globally the most relevant dust emission threshold, but we note that the functional form of the dust flux parameterization derived below is likely relatively insensitive to the chosen threshold process (see further discussion in Section 3.6).

Following the discussion above, the vertical dust flux F_d (kg m^{-2} s^{-1}) generated by a soil during saltation can be written as

$$F_d = f_{bare} n_s f_{frag} m_{frag} \varepsilon , \quad (1)$$

where f_{bare} is the fraction of the surface that consists of bare soil, n_s is the number of saltator impacts on the soil surface per unit area and time, f_{frag} is the average fraction of saltator impacts resulting in fragmentation, m_{frag} is the mean mass of emitted dust produced per fragmenting impact, and ε is the mass fraction of emitted dust that does not reattach to the surface and is transported out of the near-surface layer where it can be measured (Gordon and McKenna Neuman, 2009). Since ε likely depends predominantly on the flow immediately above the surface, which remains relatively constant with wind speed (Ungar and Haff, 1987; Shao, 2008; Kok et al., 2012), we expect ε to be approximately constant for different wind conditions for a given soil. Finally, we obtain n_s from the balance of horizontal momentum in the saltation layer (Shao et al., 1996; Kok et al., 2012),

$$n_s = \frac{C_{ns}\left(\tau_s - \tau_{st}\right)}{m_s \overline{v_{imp}}}, \quad (2)$$

where τ_s denotes the wind stress exerted on the bare soil, and τ_{st} denotes the threshold value of τ_s above which saltation occurs. Furthermore, m_s and $\overline{v_{imp}}$ are the mean saltator mass and impact speed, and the constant $C_{ns} \approx 2$ (Kok et al., 2012). Substituting Eq. (2) into Eq. (1) yields

$$F_d = f_{bare} f_{clay} \gamma \varepsilon \frac{C_{ns}\left(\tau_s - \tau_{st}\right)}{\overline{v_{imp}}} f_{frag} , \quad (3)$$

where we assumed that $m_{frag}/m_s = \gamma f_{clay}$. That is, we assumed that m_{frag}/m_s scales with the volume fraction of the soil that contributes to the creation of dust aerosols (Sweeney and Mason, 2013). The size limit of dust relevant for climate is usually taken as ~10 μm (Mahowald et al., 2006; Mahowald et al., 2010), but since the mass fraction of soil particles ≤10 μm is not available on a global scale, we instead use the soil clay fraction (f_{clay}; ≤2 μm diameter), which is globally available (FAO, 2012). The dimensionless coefficient γ likely depends on the relative sizes of soil dust aggregates and saltators. Because many saltators are aggregates (Shao, 2008), we expect only modest variations in γ between soils and take it as a constant.

Since we thus expect variations of γ and ε with wind and soil conditions to be less important (see above), we seek to understand the dependence of τ_s, $\overline{v_{imp}}$, and f_{frag} on wind and soil conditions in order to complete our theoretical expression for F_d. In the next three sections, we derive these dependencies through a combination of insights from previous studies, new theoretical work, and simulations with the numerical saltation model COMSALT (Kok and Renno, 2009).

2.2 Friction velocity and the wind stress τ_s on the bare soil surface

The dust flux emitted by an eroding soil depends on both the soil's properties and on the wind shear stress τ exerted on the surface (Marticorena and Bergametti, 1995; Shao et al., 1996; Alfaro and Gomes, 2001; Shao, 2001; Klose and Shao, 2012; Kok et al., 2012). This shear stress is characterized by the friction velocity, which is defined as (e.g., Bagnold (1941); Shao (2008); Kok et al. (2012))

$$u'_* = \sqrt{\tau/\rho_a}\ , \qquad (4)$$

where ρ_a is the air density. Dust emission often occurs in the presence of non-erodible elements such as rocks and vegetation. Thus, τ can be partitioned between the stress τ_R exerted on non-erodible roughness elements and the stress τ_s exerted on the bare erodible soil; only τ_s produces dust emission (Raupach et al., 1993; Shao et al., 1996). In analogy with Eq. (4), we define the *soil friction velocity* corresponding to τ_s as

$$u_* = \sqrt{\frac{\tau_s}{f_{bare}\rho_a}}\ , \qquad (5)$$

where f_{bare} is the fraction of the surface that consists of bare, erodible soil (note that f_{bare} corresponds to the quantity *S'*/*S* in the terminology of Raupach (1992)).The soil friction velocity u_* can be derived from u_*' using knowledge of the soil's roughness elements - f_{bare}, the aerodynamic roughness length, and/or the spatial distribution and size of roughness elements - through the use of a drag partitioning model (e.g., Raupach et al. (1993), Marticorena and Bergametti (1995), Okin (2008)) that yields the stress τ_s exerted on the bare erodible soil.

Equation (5) thus accounts for the effect of wind momentum absorption by non-erodible roughness elements on aeolian transport through the wind stress on the bare soil, as captured by the soil friction velocity u_*. However, with the exception of Okin (2008), most previous studies have accounted for the effects of roughness elements by using the ratio of τ_s/τ to scale the value of the *threshold friction velocity* u_{*t}' at which transport is initiated (Raupach et al., 1993; Marticorena and Bergametti, 1995). Although phenomenologically correct, the result of this approach is that, in the presence of non-erodible roughness elements, the quantity $\rho_a u_*^{2\prime}$ overestimates the wind shear stress exerted on the bare soil. For instance, Marticorena and Bergametti (1995) equate the wind stress driving saltation to $\tau_{sand} = \rho_a \left(u_*^{\prime 2} - u_{*t}^{\prime 2}\right)$ (see Eq. 24 in MB95), rather than $\tau_{sand} = \left(\tau_s - \tau_{st}\right) = \rho_a \left(u_*^2 - u_{*t}^2\right)$ (Owen, 1964), where the *soil threshold friction velocity* u_{*t} is defined in more detail in the next paragraph. Therefore, using u_*' and u_{*t}' to parameterize saltation properties likely results in an overestimation of aeolian transport in the presence of non-erodible roughness elements (Webb et al., 2014), which our approach avoids.

In analogy to the threshold friction velocity u_{*t}', the soil threshold friction velocity u_{*t} is the minimum value of u_* for which the bare soil experiences erosion. u_{*t} depends on both the properties of the fluid and on the gravitational and interparticle cohesion forces that oppose the fluid lifting of sand particles that initiates saltation (Shao and Lu, 2000; Kok et al., 2012). In principle, u_{*t} can be estimated from dust or sand flux measurements, as long as a correction is made for the presence of non-erodible elements, as discussed above and in the Supplement.

However, the theoretical interpretation of this threshold is complicated by several factors. For instance, the threshold friction velocities at which saltation is initiated (the fluid or static threshold u_{*ft}) and terminated (the impact or dynamic threshold u_{*it}) are not equal. For most conditions, the impact threshold is thought to be smaller than the fluid threshold, of the order of ~85 % (Bagnold, 1941; Kok, 2010). Moreover, spatial and temporal variations in soil conditions (Wiggs et al., 2004; Barchyn and Hugenholtz, 2011), as well as large variations in instantaneous wind speed for a given friction velocity (Rasmussen and Sorensen, 1999), make it such that there is generally not a clear value of u_* above which saltation does and below which it does not occur (Wiggs et al., 2004). Despite these problems, we neglect here for simplicity the temporal and spatial variability of u_{*t} and also assume that $u_{*t} = u_{*ft} = u_{*it}$, as previous dust emission parameterizations have also done (e.g., Gillette and Passi (1988), Shao et al. (1996), Marticorena and Bergametti (1995)).

In addition to u_{*t}, we define the *standardized threshold friction velocity* (u_{*st}) as the value of u_{*t} at standard atmospheric density at sea level (ρ_{a0} = 1.225 kg/m^3). Consequently, u_{*st} is not only independent of the presence of roughness elements, but is also invariant to variations in ρ_a, and is thus equal for similar soils at different elevations. Therefore, u_{*st} is a measure of the soil's susceptibility to wind erosion that depends on the state of the bare soil only. Since $u_{*t} \propto \sqrt{\rho_a}$ (e.g., Bagnold (1941)),

$$u_{*st} \equiv u_{*t}\sqrt{\rho_a/\rho_{a0}}\,. \tag{6}$$

We hypothesize that u_{*st} is a proxy for many of the soil properties known to affect dust emission, including soil cohesion, size distribution, and mineralogy (Fecan et al., 1999; Alfaro and Gomes, 2001; Shao, 2001). That is, although we do not understand in detail the effect of each of these soil properties on the dust flux (Shao, 2008), changes in soil properties that decrease the dust flux tend to also increase u_{*st}. Consequently, it is possible that u_{*st} can be used to partially account for the poorly understood effect of these soil properties on the dust flux.

2.3 The mean saltator impact speed ($\overline{v_{imp}}$)

After saltation has been initiated by the aerodynamic lifting of surface particles, new particles are brought into saltation primarily through the ejection, or *splashing*, of surface particles by impacting saltators (Ungar and Haff, 1987; Duran et al., 2011; Kok et al., 2012). (Note that this is only correct for soils with a sufficient supply of loose sand particles. The present theory is not valid for soils that instead are *supply-limited*, which we discuss in further detail in Section 3.6) Saltation is thus in steady state when exactly one particle is ejected from the soil bed for each particle impacting it. Since the number of splashed particles increases with the impacting saltator's speed (Kok et al., 2012), this condition for steady state is met at a particular value of $\overline{v_{imp}}$. Consequently, theory and measurements indicate that $\overline{v_{imp}}$ is independent of u_* for steady-state saltation (Ungar and Haff, 1987; Duran et al., 2011; Kok, 2011a; Kok et al., 2012) (Supplement Fig. S1).

Although $\overline{v_{imp}}$ is independent of u_*, it does depend on soil properties. In particular, the soil's saltation threshold sets the wind speed in the near-surface layer (Bagnold, 1941), which in turn determines the particle speed (Duran et al., 2011; Kok et al., 2012). To first order then,

$$\overline{v_{imp}} = C_v u_{*st}\,, \tag{7}$$

where $C_v \approx 5$ since $\overline{v_{imp}} \approx 1$ m/s for loose sand with $u_{*st} \approx 0.20$ m/s (Supplement Fig. S1).

2.4 The fragmentation fraction (f_{frag})

An impacting saltator can fragment a dust aggregate in the soil if its impact energy exceeds a certain threshold (Kun and Herrmann, 1999; Kok, 2011b). The threshold impact energy per unit area ψ (J/m^2) required to fragment a soil dust aggregate scales with the sum of the energetic cohesive bonds E_{coh} between the constituent particles that make up the aggregate (Kun and Herrmann, 1999). That is,

$$\psi \propto \sum E_{\text{coh}} / D_{\text{s}}^2 , \tag{8}$$

where D_{s} is the saltator size, and the sum is over all interparticle bonds in the aggregate. Measurements and theory suggest that (Shao, 2001)

$$E_{\text{coh}} \propto \beta D_{\text{c}}^2 , \tag{9}$$

where D_{c} is the typical size of a constituent particle of the dust aggregate. The parameter β (J/m^2) scales the interparticle force, which is the sum of a complex collection of individual forces, including van der Waals, water adsorption, and electrostatic forces (Shao and Lu, 2000). Consequently, β depends on the state of the soil, including soil moisture content, mineralogy, and size distribution. Since the number of bonds in the aggregate scales with $D_{\text{ag}}^3 / D_{\text{c}}^3$, where D_{ag} is the aggregate size, Eq. (8) becomes

$$\psi \propto \beta D_{\text{ag}}^3 \big/ \left(D_{\text{s}}^2 D_{\text{c}}\right), \tag{10}$$

For highly erodible, dry soils, $\beta = \beta_0 \approx 1.5 \times 10^{-4}$ J/m^2 (Shao and Lu, 2000; Kok and Renno, 2006). Experiments suggest that most typical saltator impacts (i.e., D_{s} = 100 μm and v_{imp} = 1 m/s) eject dust for such highly erodible, dry soils (Rice et al., 1996), yielding $\psi_0 \approx 0.1$ J/m^2. Thus,

$$\tilde{\psi} = c_\psi \tilde{\beta} , \tag{11}$$

where $\tilde{\psi} = \psi / \psi_0$ and $\tilde{\beta} = \beta / \beta_0$. The dimensionless parameter c_ψ is of order unity and depends on the soil size distribution since it scales with $D_{\text{ag}}^3 \big/ \left(D_{\text{s}}^2 D_{\text{c}}\right)$. In particular, because saltators are often aggregates (Shao, 2008), with both D_{ag} and D_{s} having typical sizes of the order of 100 μm (Shao, 2001), the leading order scaling is likely $c_\psi \sim D_{\text{ag}}/D_{\text{c}}$. Here we take c_ψ as a constant, both because there are insufficient vertical dust flux data sets available that report a detailed soil size distribution, and because global soil data sets are not nearly detailed enough to represent spatial and temporal variability in the soil size distribution.

Since the soil's standardized threshold friction velocity ($u_{*\text{st}}$) depends on the strength of interparticle forces (Shao and Lu, 2000), ψ must increase monotonically with $u_{*\text{st}}$ (Shao et al., 1996). This is intuitive: soils that are more erosion resistant, for example with strongly-bound soil aggregates due to surface crusts or high moisture content, require a larger impact energy to fragment (Rice et al., 1996; Rice et al., 1999). For such soils, wind tunnel experiments show that only a small fraction of saltator impacts produce dust emission (Rice et al., 1996).

We calculate the fragmentation fraction f_{frag} from the overlap between the probability distributions of ψ and the saltator impact energy per unit area E_{imp}. Since ψ is the sum of a large number of individual cohesive bonds, its probability distribution $P_\psi(\psi)$ is normally distributed per the central limit theorem (Kallenberg, 1997), with a mean $\overline{\psi}$ and standard deviation σ_ψ. The total fraction of saltator impacts that produces dust emission through fragmentation then equals

$$f_{\text{frag}} = \int_0^\infty \int_0^{E_{\text{imp}}} P_{\text{Eimp}}\left(E_{\text{imp}}\right) P_\psi\left(\psi\right) d\psi \, dE_{\text{imp}} = \int_0^\infty P_{\text{Eimp}}\left(E_{\text{imp}}\right) \left\{ \frac{1}{2} + \frac{1}{2} \operatorname{erf}\left[\frac{E_{\text{imp}} - \overline{\psi}}{\sqrt{2}\sigma_\psi} \right] \right\} dE_{imp} , \tag{12}$$

where erf is the error function, which results from the integration of the normally-distributed ψ.

2.4.1 Determining P_{Eimp} with the numerical saltation model COMSALT. In order to calculate f_{frag} with Eq. (12), we require the probability distribution of saltator impact energies (P_{Eimp}) for given values of u_*, β, and D_s, which we obtain through simulations with the numerical saltation model COMSALT (Kok and Renno, 2009). This model explicitly simulates the trajectories of saltators due to gravitational and fluid forces, and accounts for the stochasticity of individual particle trajectories due to turbulence and collisions with the irregular soil surface. Moreover, COMSALT simulates the retardation of the wind profile by the drag of saltating particles, which is the process that ultimately limits the number of particles that can be saltating at any given time. Finally, in contrast to many previous models, COMSALT includes a physically-based parameterization of the ejection (‘splashing’) of surface particles, based on conservation of energy and momentum (Kok and Renno, 2009). Because of this explicit inclusion of splash, as well as other improvements over previous studies, COMSALT is the first numerical model capable of reproducing a wide range of measurements of naturally occurring saltation.

Since COMSALT was developed for saltation of soils made up of loose sand, it must be adapted in order to simulate saltation over dust-emitting soils. For soils made up of loose sand, the splashing of new saltating particles is constrained predominantly by the momentum transferred by impacting saltators (Kok and Renno, 2009). That is, the total momentum of splashed particles scales with the impacting saltator momentum (Beladjine et al., 2007; Oger et al., 2008). For dust emitting soils, this situation is likely different, because saltating particles are more strongly bound in the soil by cohesive forces (Shao and Lu, 2000; Kok and Renno, 2009). We therefore assume that, for dust emitting soils, the number of particles splashed by an impacting saltator scales with its impacting energy (Shao and Li, 1999). Furthermore, in order for a saltating particle to eject another saltator from the soil, the impact must be sufficiently energetic to overcome the cohesive the bonds with other soil particles. Therefore, the larger the soil cohesive forces, the stronger the cohesive binding energy $E_{\mathrm{coh,s}}$ with which sand-sized particles are bonded to other soil particles, resulting in a smaller number of splashed saltating particles N. That is,

$$N \propto \frac{m_s v_{\mathrm{imp}}^2 / 2}{E_{\mathrm{coh,s}}}, \qquad (13)$$

Since $E_{\mathrm{coh,s}}$ scales with βD_s^2 (see Eq. (9) and (Shao, 2001)), Eq. (13) becomes

$$N = a_E \frac{\rho_p D_s v_{\mathrm{imp}}^2}{\beta}, \qquad (14)$$

where $\rho_p \approx 2650$ kg/m^3 is the density of the saltating particle (Kok et al., 2012), and the dimensionless parameter a_E scales the number of splashed particles. We obtain $a_E = 6.1 \cdot 10^{-5}$ by forcing the minimum u_* for which saltation can occur in COMSALT with $\beta = \beta_0$ to equal the minimal value of $u_{*\mathrm{st}}$ for an optimally erodible soil. We define this minimal value as $u_{*\mathrm{st0}}$, and measurements show that $u_{*\mathrm{st0}} \approx 0.16$ m/s for a bed of 100 μm loose sand particles (Bagnold, 1941; Iversen and White, 1982; Kok et al., 2012).

Other parameters of the splash process, such as the speed of splashed particles, the coefficient of restitution, and the probability that an impacting saltator does not rebound, are treated as described in Kok and Renno (2009). We thus neglect any change in these parameters with changes in soil cohesion since there is very little experimental data available to account for any such dependences (O'Brien and McKenna Neuman, 2012). COMSALT also computes the soil's standardized threshold friction velocity u_{*st} as the minimum value of u_* at which saltation can be sustained for a given value of β, following the procedure outlined in Kok and Renno (2009).

COMSALT simulations of P_{Eimp} show that, although the mean saltator impact speed ($\overline{v_{imp}}$) remains approximately constant with u_* (see above), the distribution of E_{imp} does not (Fig. 1). Because the total drag exerted by saltators on the flow increases with u_*, the wind profile lower in the saltation layer is relatively insensitive to u_* (Owen, 1964; Ungar and Haff, 1987; Duran et al., 2011; Kok et al., 2012).Conversely, the wind speed higher up in the saltation layer does increase with u_* (Bagnold, 1941), which causes the speed and abundance of energetic particles moving higher in the saltation layer to also increase. This causes a non-linear increase in the high-energy tail of P_{Eimp} with u_* (Fig. 1; also see Duran et al. (2011) and Kok et al. (2012)).

2.4.2 Dependence of f_{frag} on u_* and u_{*st}. Since we can obtain P_{Eimp} for given values of u_*, D_s, and β (and thus u_{*st}) from COMSALT simulations, we can use Eq. (12) to determine f_{frag} for given values of c_ψ and σ_ψ. Given that the exact values of c_ψ and σ_ψ for any particular soil are unknown, our objective in using Eq. (12) is to understand the functional form of the dependence of f_{frag}, and thus F_d, on u_* and u_{*st}. To understand these dependencies, we consider the distributions of E_{imp} and ψ for two limiting cases: a highly erodible and an erosion-resistant soil (Fig. 1). For a highly erodible soil, a large fraction of saltator impacts can be expected to produce fragmentation (Rice et al., 1996 and Fig. 1a), such that $\overline{E_{imp}} \sim \overline{\psi}$. In this case, the value of f_{frag} is thus approximately constant with u_* (Fig. 1c). Conversely, when the soil is erosion-resistant, $\overline{E_{imp}} << \overline{\psi}$, and only the high-energy tail of the impact energy distribution results in dust emission through fragmentation (Fig. 1b). Since this high-energy tail increases sharply with u_*, f_{frag} also increases sharply with u_* (Fig. 1c). Consequently, F_d scales more strongly with u_* for erosion-resistant than for highly erodible soils.

Our results thus show that f_{frag} depends on both u_* and u_{*st} (Fig. 1c). Since f_{frag} is dimensionless, its dependency on u_* and u_{*st} should take the form of the non-dimensional ratios that capture the physical processes determining f_{frag} (Buckingham, 1914). That is, f_{frag} should depend only on (i) the dimensionless friction velocity u_*/u_{*t}, which sets the increase of the high-energy tail (Fig. 1), and (ii) the dimensionless standardized threshold velocity u_{*st}/u_{*st0}, which sets the soil's susceptibility to wind erosion. From Fig.1c, we infer

$$f_{frag} = C_{fr}\left(\frac{u_*}{u_{*t}}\right)^\alpha . \tag{15}$$

Since this power law accounts for the dependence of f_{frag} on u_*/u_{*t}, the dimensionless fragmentation constant C_{fr} and exponent α must depend only on the other dimensionless number, u_{*st}/u_{*st0} (Buckingham, 1914). Since highly erodible soils with $u_{*st} = u_{*st0}$ have $\alpha \approx 0$ (Fig. 1), we hypothesize that

$$\alpha = C_\alpha\left(\frac{u_{*st} - u_{*st0}}{u_{*st0}}\right), \tag{16}$$

where C_α is a dimensionless constant. Equation (16) is supported by numerical simulations of f_{frag} for a range of plausible values of the saltator diameter D_s and the threshold fragmentation energy's normal distribution parameters (Fig. 2a).

The proportionality constant C_{fr} in Eq. (15) must decrease sharply with u_{*st} (Fig. 1c), because increases in u_{*st} are primarily driven by increases in soil (aggregate) cohesion (Shao and Lu, 2000; Shao, 2008; Kok et al., 2012), for instance due to increases in soil moisture. Such increases in aggregate cohesion reduce the fragmentation fraction f_{frag}, and numerical simulations indicate that (Fig. 2b)

$$C_{fr} = C_{fr0} \exp\left(-C_e \frac{u_{*st} - u_{*st0}}{u_{*st0}} \right), \tag{17}$$

where $C_{fr0} \approx 0.5$ is the fragmentation fraction for highly erodible soils (Fig. 1c), and C_e is a dimensionless constant.

2.5 Full theoretical expression for the vertical dust flux

We complete our theoretical expression by substituting Eqs. (2), (5), and (15)-(17) into Eq. (3), yielding

$$F_d = C_d f_{bare} f_{clay} \frac{\rho_a \left(u_*^2 - u_{*t}^2\right)}{u_{*st}} \left(\frac{u_*}{u_{*t}} \right)^{C_\alpha \frac{u_{*st} - u_{*st0}}{u_{*st0}}}, \qquad \left(u_* > u_{*t}\right) \quad , \tag{18a}$$

where

$$C_d = C_{d0} \exp\left(-C_e \frac{u_{*st} - u_{*st0}}{u_{*st0}} \right), \tag{18b}$$

with $C_{d0} = \gamma \varepsilon C_{ns} C_{fr0} / C_v$. Eq. (18) thus predicts that the dust flux (F_d) scales with the soil friction velocity (u_*) to the power $a \equiv \alpha + 2$. We determine the dimensionless coefficients C_α, C_e, and C_{d0} through comparison against a quality-controlled compilation of vertical dust flux data sets in Section 3. The dimensionless dust emission coefficient C_d is independent of the soil friction velocity u_*, and is thus a measure of a soil's ability to produce dust under a given wind stress. This susceptibility to dust emission is termed the *soil erodibility* in the dust modeling literature (e.g., Zender et al. (2003b)), which is not to be confused with the identical term in the soil erosion literature referring more generally to the susceptibility of soil particles to detachment by erosive agents (e.g., Webb and Strong (2011)).

The increase in the dust emission coefficient C_d with decreasing u_{*st} accounts for a soil's increased ability to produce dust under saltation bombardment as the soil becomes more erodible (i.e., its threshold friction velocity decreases). This is an important result, as this process is not included in the previous dust flux parameterizations of Gillette and Passi (1988) and Marticorena and Bergametti (1995) that dominate dust modules in current climate models (e.g., Ginoux et al. (2001), Zender et al. (2003a), Huneeus et al. (2011)). In particular, this result implies that the dust flux is more sensitive to the soil's threshold friction velocity than climate models currently account for. We further discuss this result and its implications in Section 4 and in the companion paper (Kok et al., 2014).

Note that the dust flux parameterization of Eq. (18) is considerably simpler than previous physically-based dust emission models (Shao et al., 1996; Shao, 2001). This was achieved in large part by using u_{*st} as a measure of soil erodibility, which allowed us to substantially simplify the energetics of dust emission. Furthermore, since our parameterization's main variables (u_*, u_{*t}, and f_{clay}) are available in weather and climate models, its implementation is relatively straightforward, in contrast to these more complex models (Darmenova et al., 2009).

3. Assessment of parameterization performance using a quality-controlled compilation of dust flux measurements

We test our proposed dust emission parameterization using a compilation of quality-controlled literature data sets. We do so by first separately testing the two main improvements of Eq. (18) over previous theories: the linear increase of the dust emission coefficient a with u_{*st}, and the exponential decrease of the dust emission coefficient C_d with u_{*st}. This procedure also yields estimates of the dimensionless parameters C_α, C_{d0}, and C_e, subsequently allowing us to directly compare the measured dust flux against the predictions of Eq. (18).

The following section discusses the quality-control criteria that data sets need to meet in order to allow an accurate comparison against our theoretical expression. Section 3.2 then describes the various corrections applied to bring all data sets on an equal footing, after which Section 3.3 describes the procedure for determining the dust emission coefficient (C_d) and fragmentation exponent (α) from literature data sets of dust flux measurements. We then test the functional form of the parameterization against the estimates of C_d and α extracted from the literature data sets in Section 3.4, and test the parameterization's predictions of the vertical dust flux against our dust flux compilation in Section 3.5. Finally, we discuss the limitations of our parameterization in Section 3.6.

3.1 Data set quality-control criteria

We strive to obtain a compilation of high-quality vertical dust flux measurements that we can use to test our new parameterization. We thus apply several quality-control criteria that data sets need to meet in order to be included in our compilation; these criteria are designed to ensure that the measured dust flux is governed by a soil in an approximately constant state. This is critical, because any changes in the soil state affects u_{*t}, which is one of the main parameters in our parameterization. Since changes in the threshold friction velocity can occur on timescales as short as an hour (Wiggs et al., 2004; Barchyn and Hugenholtz, 2011), we only use data sets for which all data was taken within a limited time period of up to ~12 hours. This requirement excludes many of the data sets on which previous dust flux schemes were based, in particular data sets by Gillette (1979), Nickling and colleagues (Nickling, 1978, 1983; Nickling and Gillies, 1993; Nickling et al., 1999), and Gomes et al. (2003). In addition, we require that a data set contains sufficient measurements to reliably determine the threshold friction velocity for the measurements. Furthermore, we only use data sets of natural dust emission taken in the field, because the characteristics of saltation and dust emission simulated in (portable) wind tunnels have been shown to, in some cases, be substantially different from the characteristics of natural saltation (Sherman and Farrell, 2008; Kok, 2011a). Finally, the measurements should be made for relatively homogeneous terrain, such that the soil state is spatially approximately constant. This last constraint is only required for predicting the dust emission coefficient C_d. Therefore, data sets that meet all criteria except that of homogeneous terrain (i.e., the data sets of Fratini et al. (2007) and Park et al. (2011)) are not used for comparison against the theoretical equations for C_d and F_d, but are still used for assessing the fragmentation exponent α.

Our literature search for vertical dust flux measurements that met the above quality-control criteria resulted in the identification of six studies: Gillies and Berkofsky (2004) (hereinafter referred to as GB04), Zobeck and Van Pelt (2006) (ZP06), Fratini et al. (2007) (FC07), Sow et al. (2009) (SA09), Shao et al. (2011) (SI11), and Park et al. (2011) (PP11). Images of the experimental sites of these six studies are shown in Fig. 3, and the main properties of each data set are summarized in Table 1. We used the original data for each of these six studies, and extracted 11 individual data sets from them. We describe the general procedures for correcting for differences between data sets and for extracting estimates of u_{*t}, α, and C_d in the next two sections. A detailed description of the analysis of each individual data set is provided in the Supplement.

3.2 Correcting for differences in averaging period and measured size range

A critical property of dust flux data sets is the time period over which measurements are averaged. In particular, since the vertical dust flux is non-linear in the friction velocity, the averaging period needs to be consistent among data sets (Sow et al., 2009; Martin et al., 2013). In setting the averaging period, an important consideration is that the friction velocity, being a turbulence parameter, is only meaningful when obtained over averaging periods long enough to sample a sufficient range of the turbulent eddies contributing to the downward flux of horizontal fluid momentum (Kaimal and Finnigan, 1994; Namikas et al., 2003; van Boxel et al., 2004). Moreover, the averaging period needs to be short enough such that the meteorological forcing of the boundary layer, which partially sets the downward momentum transfer, remains approximately constant. A compromise between these constraints is an averaging period of 30 minutes (Goulden et al., 1996; Aubinet et al., 2001; van Boxel et al., 2004; Fratini et al., 2007), which conveniently is also of the order of the typical time step in global models. We thus reanalyzed each data set using a 30 minute averaging period. In order to get maximum use out of each data set, the data were averaged over 30 minutes with a running average (e.g., a 60-minute continuous data set with 1-minute resolution yielded 31 data points).

In addition to using the same averaging period for each data set, we also need to correct for differences in the measured dust size range between the data sets. We therefore corrected each data set to represent the mass flux of dust aerosols with a geometric diameter D_d between 0 - 10 μm, which is a size range commonly represented in atmospheric circulation models (Mahowald et al., 2006). Several of the dust flux data sets (e.g., GB04, ZP06) reported size ranges not in terms of the geometric diameter D_d, which is defined as the diameter of a sphere having the same volume as the irregularly-shaped dust aerosol, but in terms of the aerodynamic diameter, D_{ae}, which is defined as the diameter of a spherical particle with density ρ_0 = 1000 kg/m^3 with the same aerodynamic resistance as the dust aerosol (Hinds, 1999). Therefore, depending on the data set, two separate corrections need to be made: one to correct from aerodynamic diameter to geometric diameter, and one to correct the measured geometric size range to 0 – 10 μm.

The geometric and aerodynamic diameters are related by (Hinds, 1999; Reid et al., 2003)

$$D_d = \sqrt{\frac{\chi \rho_0}{\rho_p}} D_{ae}, \qquad (19)$$

where $\rho_p \approx 2.5 \pm 0.2 \times 10^3$ kg/m^3 is the typical density of a dust aerosol particle (Kaaden et al., 2009), and χ is the dynamic shape factor, which is defined as the ratio of the drag force experienced by the irregular particle to the drag force experienced by a spherical particle with diameter D_d (Hinds, 1999). Measurements of the dynamic shape factor for mineral dust particles with a geometric diameter of ~10 μm find $\chi \approx 1.4 \pm 0.1$ (Cartwright, 1962; Davies, 1979; Kaaden et al., 2009). Inserting this into equation (19) then yields that $D_d \approx (0.75 \pm 0.04)\, D_{ae}$, where the standard error was obtained using error propagation (Bevington and Robinson, 2003).

After converting each data set's measured aerodynamic particle size range to a geometric size range as necessary, we corrected the measured dust flux by assuming that the size distribution at emission is well-described by the theoretical dust size distribution expression of

Kok (2011b), which is in excellent agreement with measurements. For instance, equation (6) in Kok (2011b) predicts that 71 ± 5 % of emitted dust in the geometric 0 – 10 μm size range lies in the aerodynamic 0 – 10 μm size range (which is equivalent to the geometric 0 – 7.5 ± 0.4 μm size range). We thus apply a correction factor of $(0.71 \pm 0.05)^{-1} = 1.42 \pm 0.10$ in order to correct a measured aerodynamic PM10 flux (e.g., GB04, ZP06) to a geometric ≤ 10 μm flux. Note that the uncertainty in the correction factor is propagated into the uncertainty on the value of C_d extracted from each data set (see the Supplement).

In addition to correcting for differences between data sets in the averaging time and the measured size range, we also corrected for differences in the fetch length when possible (see Supplement text).

3.3 Procedure for obtaining $u_{*\mathrm{t}}$, α, and C_d

After putting all data on an equal footing using the above procedures, we extracted the parameters $u_{*\mathrm{t}}$, α, and C_d from the dust flux data sets. Because $u_{*\mathrm{t}}$ is required to determine the other parameters, we first determined the soil's threshold friction velocity for each data set.

Since many field experiments did not report the threshold friction velocity, and because of differences in the definition of threshold between data sets that did report a threshold friction velocity, we estimated $u_{*\mathrm{t}}$ in a similar manner for each data set as described in detail in Appendix B in the Supplement. In brief, we estimated $u_{*\mathrm{t}}$ using least-squares fitting of a second order Taylor series of Eq. (22) below to saltation flux measurements within a limited range around the threshold (Barchyn and Hugenholtz, 2011). If the data set did not contain sand flux measurements, we instead used a least-squares fit of a second order Taylor series of equation (18) to measurements of the dust flux.

After determining $u_{*\mathrm{t}}$ in this manner, we used the following procedure to extract C_d and α from each data set's dust flux measurements. Following Eq. (5), we start by calculating the dimensionless dust flux for each measurement of F_d at given values of u_* and $u_{*\mathrm{t}}$ (obtained as described below) as

$$\tilde{F}_d = \frac{F_d}{f_\mathrm{bare} f_\mathrm{clay} \rho_\mathrm{a} \left(u_*^{\,2} - u_{*\mathrm{t}}^2\right) / u_{*\mathrm{st}}} . \tag{20}$$

Through substitution of Eq. (18) we now obtain an analytical expression for $\tilde{F}_d$ as a function of C_d and α,

$$\tilde{F}_d = C_\mathrm{d} \left(\frac{u_*}{u_{*_t}} \right)^{\alpha} . \tag{21}$$

We then use least-squares fitting of Eq. (21) to the values of $\tilde{F}_d$ calculated from dust flux measurements to determine the dust emission coefficient C_d and the fragmentation exponent α, as well as their uncertainties, for each data set. The least-squares fitting procedure and the calculation of uncertainties is described in more detail in the Supplement.

In addition, we obtain an independent estimate of the fragmentation exponent α, and thus the dust emission exponent $a = \alpha + 2$, by using measurements of the *sandblasting efficiency*, which is defined as the ratio of the vertical dust flux to the horizontal saltation flux (Gillette, 1979). The sandblasting efficiency is thus defined for the data sets that reported measurements of both the dust flux and the (impact) flux of saltators at a certain height (i.e., ZP06, SA09, and SI11). This latter variable was usually measured with the Sensit piezoelectric instrument (Stockton and

Gillette, 1990), which has been shown to provide a good measure of the horizontal saltation flux (Gillette et al., 1997; van Donk et al., 2003).

We extract α from measurements of the sandblasting efficiency as follows. We start with the saltation mass flux, which is given by (Bagnold, 1941; Kok et al., 2012)

$$Q = \rho_a \left(u_*^2 - u_{*t}^2\right)\frac{L}{\Delta v}, \tag{22}$$

where L is the typical saltation hop length, and Δv is the average difference between saltators' impact and lift-off speeds. The ratio $L/\Delta v$ is thought to scale with the friction velocity,

$$\frac{L}{\Delta v} \propto u_*^r, \tag{23}$$

where the exponent r ranges from 0 (Ungar and Haff, 1987; Duran et al., 2011; Ho et al., 2011; Kok et al., 2012) to 1 (Owen, 1964; Shao et al., 1993), such that we take $r = 0.5 \pm 0.5$. We now obtain an analytical expression for the sandblasting efficiency by combining equations (18, 22, 23)

$$\frac{F_d}{Q} = C_s u_*^{\alpha - r}, \tag{24}$$

where the dimensional constant C_s contains all parameters that do not depend on u_*. We then obtain α and its uncertainty by fitting measurements of the sandblasting efficiency to the power law in u_* of Eq. (24); this procedure is described in more detail in the Supplement. Note that an important advantage of the calculation of α from the sandblasting efficiency is that, unlike the calculation of α from the dimensionless dust flux described above, the result does not depend on the determination of the threshold friction velocity u_{*t}. Therefore, errors that arise due to the procedure for assessing u_{*t} do not affect the estimate of α derived from the sandblasting efficiency.

3.4 Test of parameterization's functional form with dust flux measurements

All 11 data sets from the six studies that met the quality-control criteria discussed in Section 3.1 were used to determine the fragmentation exponent α through non-linear least-squares fitting of Eq. (21) to the vertical dust flux (see Supplement Fig. S5). Furthermore, five data sets featured simultaneous dust flux and saltation flux measurements, which we used to determine α by fitting Eq. (24) to the ratio of the vertical dust and horizontal saltation (impact) fluxes (see Supplement Fig. S6), and seven data sets were taken over spatially homogeneous terrain and thus were used to determine the dust emission coefficient C_d (see Supplement Fig. S5).

The resulting analysis of the compilation of quality-controlled dust flux data sets shows an approximately linear increase in the dust emission exponent α with u_{*st} (Fig. 4a), as predicted by Eq. (16). We obtain the dimensionless constant C_α using least-squares fitting of Eq. (16), yielding $C_\alpha = 2.7 \pm 1.0$. Moreover, the literature-extracted data sets show an approximately exponential decrease of the dust emission coefficient C_d with u_{*st}, as also predicted from our theory (Eq. 18) and numerical simulations (Fig. 4b). We obtain $C_e = 2.0 \pm 0.3$ and $C_{d0} = (4.4 \pm 0.5) \times 10^{-5}$ from least squares fitting of Eq. (18b).

3.5 Test of parameterization's predictions with dust flux measurements

After testing the parameterization's functional form and determining the values of its dimensionless coefficients, we can compare the predictions of Eq. (18) against our quality-controlled compilation of dust flux measurements. To avoid testing the model with the same data used to obtain its dimensionless coefficients (see previous section), we use the cross-correlation method (e.g., Wilks (2011), p. 252-3). That is, we use the following method for each data set: first, we obtain the dimensionless coefficients using the procedure in the previous section, but without using that particular data set or any other data sets from the same study. We then use the obtained dimensionless coefficients, which are thus specific for each of the six studies in our compilation, to predict the dust flux for each of the 11 data sets in our compilation. The resulting comparison between model and measurements is reported in Fig. 5c and Table 2.

For reference, we also compare against the predictions of the previous dust flux parameterizations GP88 (Gillette and Passi, 1988) and MB95 (Marticorena and Bergametti, 1995). Note that we unfortunately cannot compare our measurements compilation against the physically-explicit dust flux parameterizations of Shao and colleagues (Shao et al., 1993; Shao et al., 1996; Shao, 2001), because these parameterizations use detailed soil properties that are unavailable for most data sets.

The MB95 dust flux parameterization is given by

$$F_\mathrm{d} = C_\mathrm{MB}\eta f_\mathrm{bare}\frac{\rho_\mathrm{a}}{g}u_*'^3\left(1+\frac{u_{*\mathrm{t}}'}{u_*'}\right)\left(1-\frac{u_{*\mathrm{t}}'^2}{u_*'^2}\right), \qquad (u_*' > u_{*\mathrm{t}}'), \tag{25}$$

where the *threshold friction velocity* $u_{*\mathrm{t}}$' is the minimum value of the friction velocity u_*' above which the bare soil experiences erosion. The dimensionless parameter C_MB is a proportionality constant, and the sandblasting efficiency η (units of m^{-1}) depends on the clay fraction following $\eta = 10^{13.4 f_\mathrm{clay} - 6}$. Note that Eq. (25) simplifies Eq. (34) in Marticorena and Bergametti (1995) by using a single value of $u_{*\mathrm{t}}$' for the soil rather than different thresholds for different soil particle size bins. This is a common simplification necessary for the implementation of MB95 into most large-scale models (e.g., Zender et al. (2003a)). Furthermore, measurements, numerical models, and theory indicate that this simplification is actually more realistic (Bagnold, 1938; Rice et al., 1995; Namikas, 2006; Kok et al., 2012). Furthermore, note that $u_{*\mathrm{t}}$' in MB95 is calculated through a drag partition parameterization (Eq. 20 in MB95), which we use for consistency for the comparison of MB95 against the measurement compilation (see Supplement).

The GP88 parameterization is given by

$$F_\mathrm{d} = C_\mathrm{GP} f_\mathrm{bare} u_*^4 \left(1 - u_{*\mathrm{t}}/u_*\right), \qquad \left(u_* > u_{*\mathrm{t}}\right), \tag{26}$$

where C_GP (kg m^{-6} s^3) is a proportionality constant. Note that GP88 is thus formulated in terms of the soil friction velocity u_* since it converts wind speed measurements taken over an airport with approximate roughness length of 1 cm to the u_* over a bare eroding field with roughness length of 20 μm (p. 14,234 in GP88).

Our new parameterization reproduces the compilation of dust flux measurements with substantially less error than the parameterizations of GP88 and MB95 (Figs. 5a-c, Table 2, and Fig. S3). Equation (18) also produces better agreement when each parameterization's proportionality constant is tuned to each individual data set (Table 2 and Fig. S2).

3.6 Limitations of the dust emission theory and parameterization

We derived the dust emission parameterization of Eq. (18) for dust emission occurring primarily through the fragmentation of soil aggregates of dust particles by impacting saltators. Nonetheless, the main assumption used in deriving Eq. (18) is the existence of a normally-distributed threshold controlling dust emission. Consequently, Eq. (18) theoretically applies to any dust emission processes controlled by an approximately normally-distributed threshold. This point is underscored by the insensitivity of the functional form of Eqs. (16) and (17) to the threshold's normal distribution parameters and the saltator size (Fig. 2). Examples of dust emission processes other than fragmentation that are controlled by a normally-distributed threshold could include dust emission from crusted soils (Rice et al., 1996) and from sand particles with clay coatings (Bullard et al., 2004). Since we do not know what the relative contribution of different dust emission processes is to each of the dust flux data sets used to calibrate the dimensionless coefficients in Eq. (18), it is likely that the obtained values of these coefficients represents some weighted average of the relative contribution of each dust emission process. As discussed in Section 2.2, we consider it most likely that the fragmentation process contributes the largest fraction of the dust flux for each data set. Thus, although our parameterization theoretically applies to dust emission from soils dominated by processes other than fragmentation, the dimensionless coefficients in Eq. (18) could be quite different for such soils. We are not aware of any experimental data sets that meet our quality-control criteria that could be used to estimate the dimensionless coefficients for soils for which dust emission is dominated by any specific process other than fragmentation.

Furthermore, as mentioned in Section 2.2.1, our theory applies only to soils for which the saltation flux is limited by the availability of wind momentum, and are thus *transport limited* (e.g., Nickling and McKenna Neuman (2009)). The present theory is thus not valid for soils for which the horizontal saltation flux at a given point in time is limited by the availability of sand-sized sediment. Such *supply-limited* soils are inherently inefficient sources of dust aerosols (Rice et al., 1996), and are thus probably less important in the global dust budget. Note that dust emission from some prominent sources can be limited by the sediments supplied to these sources, for instance through the deposition of fluvially-eroded sediment (Bullard et al., 2011; Ginoux et al., 2012). However, when substantial emission occurs from such regions, the soil is generally not supply limited at that point in time (Bullard et al., 2011), such that Eq. (18) could be used to parameterize the dust flux.

Our parameterization attempts to include only the most important processes affecting the dust flux. Eq. (18) thus does not explicitly account for many other processes that might affect dust emission, including changes in the parameters γ and ε with u_* and u_{*t}, and the dependence of c_ψ and σ_ψ on the soil size distribution, mineralogy, and other soil properties. Future studies should consider these effects, especially if more extensive global (or regional) soil data sets become available, or if more dust flux data sets that sufficiently characterize these soil properties become available. However, as mentioned above, many of these processes partially affect the dust emission flux F_d by increasing or decreasing u_{*st}, such that some of their effect might be captured in the calibration of the dimensionless coefficients of Eq. (18) to our compilation of vertical dust flux data sets.

Another limitation of our theory is that it does not account for dust emission due to saltator impacts that do not produce fragmentation but that nonetheless produce dust by 'damaging' the dust aggregate (Kun and Herrmann, 1999). It also does not account for the lowering of an aggregate's fragmentation threshold through the rupturing of cohesive bonds by impacting saltators. These effects might dominate for very erosion-resistant soils, such as crusted soils. A further limitation of our theory is that it simplifies the energetics of dust emission by considering u_{*st} the prime determinant of soil erodibility (Shao and Lu, 2000). Although the threshold for saltation (u_{*st}) and the threshold energy required to fragment dust aggregates (ψ) are likely strongly coupled for many soils (Shao et al., 1993; Rice et al., 1996; Rice et al., 1999), increases in ψ might not produce corresponding increases in u_{*st} for some soils. An example of such a soil is a sandy soil for which dust emissions occurs primarily from the removal of dust coatings on sand grains (Bullard et al., 2004), and emission from such soils might thus be poorly captured by the present theory.

4. Discussion and conclusions

We have used a combination of theory and numerical simulations to derive a physically-based parameterization of the vertical dust flux emitted by an eroding soil. Our new dust flux parameterization includes two main improvements over previous schemes used in large-scale models. First, it accounts for the predicted (Figs. 1, 2a) and observed (Fig. 4a) increasing scaling of F_{d} with u_* that occurs with increasing threshold friction velocity$_{\mathrm{t}}$; this advance helps explain the numerous observed scalings of F_{d} with u_* (Shao, 2008; Kok et al., 2012). Second, our parameterization accounts for a soil's increased ability to produce dust under saltation bombardment as the soil becomes more erodible (Figs. 1, 2b, and 4b). This second improvement is especially important, as it implies that previous parameterizations have underestimated the sensitivity of the dust flux to the soil's dust emission threshold (u_{*st}) (also see Fig. 1 in Kok et al. (2014)). This underestimation is not sensitive to the details of our parameterization because it follows directly from the energetics of dust emission: increases in soil cohesion both raise the dust emission threshold and cause dust emission to require more energy, thereby reducing the dust flux for a given saltator kinetic impact energy. Previous work by Shao and colleagues (Shao et al., 1993; Shao et al., 1996; Shao, 2001) has noted that soils with stronger interparticle forces should produce less dust per saltator impact, but this insight had not been included in dust emission parameterizations commonly implemented in large-scale models (e.g., Ginoux et al. (2001), Zender et al. (2003a), Cakmur et al. (2006), Menut et al. (2013), Zhao et al. (2013)).

Partially as a result of the inclusion of these two additional physical processes, our parameterization is in better agreement with a quality-controlled compilation of dust flux measurements than the previous dust flux parameterizations of Gillette and Passi (1988) and Marticorena and Bergametti (1995) (see Fig. 5). Although our parameterization thus appears to account for more of the processes driving the dust flux than these previous parameterizations, it is straightforward to implement as it uses only variables that are readily available in weather and climate models (note that the code to implement the parameterization in the Community Earth System Model is freely available from the main author). This is made possible because of several advances and simplifications over previous theories. Arguably the main advance is that we use the soil's standardized threshold friction velocity (u_{*st}) as a measure of soil erodibility (i.e., the soil's ability to emit dust), allowing us to substantially simplify the energetics of dust emission relative to previous physically-explicit schemes (Shao et al., 1996; Shao, 2001). Furthermore, many previous parameterizations used a different threshold friction velocity for each soil particle size bin. However, experiments, numerical modeling, and theory all indicate that, once the saltation threshold is exceeded, particles of a wide range of sizes are set into motion (e.g., Bagnold (1938), Rice et al. (1995), Namikas (2006), Kok and Renno (2009), Kok et al. (2012)). We therefore characterized the threshold friction velocity with a single value, which can for instance be calculated using the models of Iversen and White (1982), Fecan et al. (1999), or Shao and Lu (2000).

Our result that the dust flux is more sensitive to the soil's threshold friction velocity than most current parameterizations account for emphasizes the importance for models to accurately represent spatial and temporal variations in soil erodibility. Our parameterization provides a convenient way of doing so through variations in the standardized dust emission threshold u_{*st}. However, the parameterization of u_{*st} in most models is relatively primitive (e.g., (Zender et al., 2003a)). For instance, one of the main determinants of u_{*st} is the moisture content of the top layer of soil particles. Yet, the most commonly-used parameterization of the effect of soil moisture on u_{*st} (Fecan et al., 1999) is found to produce unrealistic results in some models, requiring the use of a tuning constant (Zender et al., 2003a; Mokhtari et al., 2012). Furthermore, effects of soil aggregation and crust formation on u_{*t} are not included in the most widely-used global dust modules (Ginoux et al., 2001; Zender et al., 2003a; Huneeus et al., 2011). Considering the paramount importance of u_{*st} in determining dust fluxes (see Eq. 18), an effective way to improve the fidelity of dust cycle simulations would be to develop improved parameterizations of u_{*st} as a function of soil properties, precipitation events, atmospheric relative humidity, and other relevant parameters. Alternatively, for simulations of the current dust cycle, u_{*st} could be remotely sensed (Chomette et al., 1999; Chappell et al., 2005; Draxler et al., 2010). Doing so requires the simultaneous determination of the threshold wind speed and the surface roughness (Marticorena et al., 2004), such that the remotely-sensed threshold wind stress can be partitioned between the portion causing dust emission (τ_S) and that absorbed by non-erodible elements (τ_R) (Raupach et al., 1993; Marticorena and Bergametti, 1995).

Current large-scale models commonly use semi-empirical dust source functions (e.g., Ginoux et al. (2001), Tegen et al. (2002), Zender et al. (2003b)) to help parameterize dust emissions. The use of these source functions usually shift emissions towards the most erodible regions. Because our parameterization accounts for a soil's increased ability to produce dust under saltation bombardment as the soil becomes more erodible, its implementation in models would also result in a shift of emissions to the most erodible regions. We therefore hypothesize that our parameterization reduces the need for empirical source functions in dust modules. We test this hypothesis in our companion paper (Kok et al., 2014).

Notation

a – dust emission exponent
a_E – dimensionless constant scaling the number of splashed particles
α – fragmentation exponent
β – scales energy of energetic bond between constituent particles in dust aggregate (E_{coh}), J/m^2
β_0 – approximate value of β for an optimally erodible soil, J/m^2
c_ψ – dimensionless constant linking ψ to β
C_d – dimensionless dust emission coefficient, scaling the vertical dust flux
C_{d0} – dimensionless constant scaling the dust emission coefficient
C_e – dimensionless constant scaling the exponential decrease of C_d with u_{*st}
C_{fr} - dimensionless constant scaling the fragmentation fraction (f_{frag})
C_{fr0} – value of C_{fr} for a highly erodible soil
C_{GP} – dimensionless constant scaling the dust flux in GP88
C_{MB} – dimensionless constant scaling the dust flux in MB95
C_{ns} – dimensionless constant scaling the number of saltator impacts (n_s)
C_s – dimensional constant scaling the ratio of vertical dust flux to horizontal saltation flux
C_v – dimensionless constant scaling the mean saltator impact speed ($\overline{v_{imp}}$)
C_α - dimensionless constant scaling the fragmentation exponent (α)
γ – dimensionless constant scaling the emitted dust per saltator fragmenting impact (m_{frag})

D_{ae} – dust aerosol aerodynamic diameter, m
D_{ag} – size of soil dust aggregate, m
D_{c} – typical size of constituent particles of a soil dust aggregate, m
D_{d} – dust aerosol geometric diameter, m
D_{s} – Size of saltating particle, m
Δv – average difference between saltators' impact and lift-off speeds
E_{coh} – Energy of the energetic bond between constituent particles of soil dust aggregate, J
$E_{\mathrm{coh,s}}$ – Energy of the energetic bond between sand particles and other soil particles, J
ε – mass fraction of emitted dust that does not reattach to the surface
f_{bare} – fraction of the surface consisting of bare soil
f_{clay} – soil clay fraction
f_{frag} – average fraction of saltator impacts resulting in fragmentation
F_{d} – vertical dust flux, kg m^{-2} s^{-1}
$\tilde{F}_d$ – dimensionless vertical dust flux
L – typical saltation hop length
m_{frag} – average mass of suspended dust produced per fragmenting saltator impact, kg
m_{s} – mean saltator mass, kg
n_{s} – number of saltator impacts on soil surface per unit area and time, m^{-2} s^{-1}
N – number of particles splashed by impacting saltator
P_{Eimp} – probability distribution of saltator impact energy E_{imp}, J^{-1}
P_{ψ} – probability distribution of threshold fragmentation energy ψ, J^{-1} m^{2}
P_0 – standard density of aerosol particle, kg m^{-3}
Q – saltation mass flux, kg m^{-1} s^{-1}
r – exponent of u_* scaling the ratio of saltating particle hop length and impact speed differential
ρ_{a} – air density, kg m^{-3}
ρ_{a0} – air density at standard atmosphere, kg m^{-3}
ρ_{d} – density of a dust aerosol particle, kg m^{-3}
ρ_{p} – density of a saltating particle, kg m^{-3}
σ_{ψ} – standard deviation of normal distribution of the threshold impact energy ψ, J m^{-2}
τ – total wind stress exerted on surface, N m^{-2}
τ_{R} – wind stress exerted on non-erodible roughness elements only, N m^{-2}
τ_{s} – wind stress exerted on bare soil only, N m^{-2}
τ_{st} – threshold wind stress exerted on bare soil above which saltation occurs, N m^{-2}
u_* - soil friction velocity, derived from shear stress on bare soil τ_{s}, m s^{-1}
u_*' - friction velocity, derived from total shear stress on surface τ, m s^{-1}
$u_{*\mathrm{st}}$ – the threshold friction velocity standardized to standard atmospheric density, m s^{-1}
$u_{*\mathrm{st0}}$ – the standardized threshold friction velocity of an optimally erodible soil, m s^{-1}
$u_{*\mathrm{t}}$ – threshold soil friction velocity above which saltation occurs, m s^{-1}
$u_{*\mathrm{t}}'$ – threshold friction velocity above which saltation occurs, m s^{-1}
$\overline{v_{\mathrm{imp}}}$ - mean saltator impact speed, m s^{-1}
χ – dynamic shape factor for irregularly-shaped aerosol particle
ψ – threshold impact energy per unit area required to fragment a soil dust aggregate, J m^{-2}
$\overline{\psi}$ - mean value of normal distribution of the threshold impact energy ψ, J m^{-2}

Acknowledgments. We thank Stéphane Alfaro, Jean Louis Rajot, and Béatrice Marticorena for providing the measurements of Sow et al. (2009), and for providing comments that helped improve the manuscript. Comments by two anonymous referees, the editor Yves Balkanski, Shanna Shaked, and Greg Okin improved this paper. This work was supported by the National Science Foundation (NSF) under grant numbers 0932946 and 1137716.

References

Albani, S., Mahowald, N. M., Perry, A. T., Scanza, R. A., Zender, C. S., Heavens, N. G., Maggi, V., Kok, J. F., and Otto-Bliesner, B. L.: Improved dust representation in the Community Atmosphere Model, J. Adv. Model. Earth Syst., doi: 10.1002/2013MS000279, 2014. 2014.

Alfaro, S. C. and Gomes, L.: Modeling mineral aerosol production by wind erosion: Emission intensities and aerosol size distributions in source areas, J. Geophys. Res., 106, 18075-18084, 2001.

Aubinet, M., Chermanne, B., Vandenhaute, M., Longdoz, B., Yernaux, M., and Laitat, E.: Long term carbon dioxide exchange above a mixed forest in the Belgian Ardennes, Agric. For. Meteorol., 108, 293-315, 2001.

Bagnold, R. A.: The measurement of sand storms, Proceedings of the Royal Society of London Series a-Mathematical and Physical Sciences, 167, 0282-0291, 1938.

Bagnold, R. A.: The Physics of Blown Sand and Desert Dunes, Methuen, New York, 1941.

Barchyn, T. E. and Hugenholtz, C. H.: Comparison of four methods to calculate aeolian sediment transport threshold from field data: Implications for transport prediction and discussion of method evolution, Geomorphology, 129, 190-203, 2011.

Beladjine, D., Ammi, M., Oger, L., and Valance, A.: Collision process between an incident bead and a three-dimensional granular packing, Phys. Rev. E, 75, 061305, 2007.

Bevington, P. R. and Robinson, D. K.: Data reduction and error analysis, McGraw-Hill, New York, 2003.

Buckingham, E.: On physically similar systems, illustrations of the use of dimensional equations, Physical Review, 4, 345-376, 1914.

Bullard, J. E., Harrison, S. P., Baddock, M. C., Drake, N., Gill, T. E., McTainsh, G., and Sun, Y. B.: Preferential dust sources: A geomorphological classification designed for use in global dust-cycle models, Journal of Geophysical Research-Earth Surface, 116, 2011.

Bullard, J. E., McTainsh, G. H., and Pudmenzky, C.: Aeolian abrasion and modes of fine particle production from natural red dune sands: an experimental study, Sedimentology, 51, 1103-1125, 2004.

Cakmur, R. V., Miller, R. L., Perlwitz, J., Geogdzhayev, I. V., Ginoux, P., Koch, D., Kohfeld, K. E., Tegen, I., and Zender, C. S.: Constraining the magnitude of the global dust cycle by minimizing the difference between a model and observations, Journal of Geophysical Research-Atmospheres, 111, D06207, 2006.

Cartwright, J.: Particle shape factors, Ann. Occup. Hyg., 5, 163-171, 1962.

Chappell, A., Zobeck, T. M., and Brunner, G.: Using on-nadir spectral reflectance to detect soil surface changes induced by simulated rainfall and wind tunnel abrasion, Earth Surface Processes and Landforms, 30, 489-511, 2005.

Chomette, O., Legrand, M., and Marticorena, B.: Determination of the wind speed threshold for the emission of desert dust using satellite remote sensing in the thermal infrared, Journal of Geophysical Research-Atmospheres, 104, 31207-31215, 1999.

Creamean, J. M., Suski, K. J., Rosenfeld, D., Cazorla, A., DeMott, P. J., Sullivan, R. C., White, A. B., Ralph, F. M., Minnis, P., Comstock, J. M., Tomlinson, J. M., and Prather, K. A.: Dust and Biological Aerosols from the Sahara and Asia Influence Precipitation in the Western U.S, Science, 339, 1572-1578, 2013.

Crouvi, O., Schepanski, K., Amit, R., Gillespie, A. R., and Enzel, Y.: Multiple dust sources in the Sahara Desert: The importance of sand dunes, Geophysical Research Letters, 39, 2012.

Cwiertny, D. M., Young, M. A., and Grassian, V. H.: Chemistry and photochemistry of mineral dust aerosol, Annu. Rev. Phys. Chem., 59, 27-51, 2008.
Darmenova, K., Sokolik, I. N., Shao, Y. P., Marticorena, B., and Bergametti, G.: Development of a physically based dust emission module within the Weather Research and Forecasting (WRF) model: Assessment of dust emission parameterizations and input parameters for source regions in Central and East Asia, Journal of Geophysical Research-Atmospheres, 114, 2009.
Davies, C. N.: Particle-fluid interaction, Journal of Aerosol Science, 10, 477-&, 1979.
Draxler, R. R., Ginoux, P., and Stein, A. F.: An empirically derived emission algorithm for wind-blown dust, Journal of Geophysical Research-Atmospheres, 115, 2010.
Duran, O., Claudin, P., and Andreotti, B.: On aeolian transport: Grain-scale interactions, dynamical mechanisms and scaling laws, Aeolian Research, 3, 243-270, 2011.
Evan, A. T., Flamant, C., Fiedler, S., and Doherty, O.: An analysis of aeolian dust in climate models, Geophysical Research Letters, doi: 10.1002/2014GL060545, 2014. 2014.
FAO: Harmonized World Soil Database (version 1.2), FAO, Rome, Italy and IIASA, Laxenburg, Austria, 2012.
Fecan, F., Marticorena, B., and Bergametti, G.: Parametrization of the increase of the aeolian erosion threshold wind friction velocity due to soil moisture for arid and semi-arid areas, Ann Geophys-Atm Hydr, 17, 149-157, 1999.
Fratini, G., Ciccioli, P., Febo, A., Forgione, A., and Valentini, R.: Size-segregated fluxes of mineral dust from a desert area of northern China by eddy covariance, Atmospheric Chemistry and Physics, 7, 2839-2854, 2007.
Gillette, D. A.: Environmental factors affecting dust emission by wind erosion. In: Saharan dust, Morales, C. (Ed.), Wiley, New York, 1979.
Gillette, D. A., Blifford, I. H., and Fryrear, D. W.: Influence of wind velocity on size distributions of aerosols generated by wind erosion of soils, Journal of Geophysical Research, 79, 4068-4075, 1974.
Gillette, D. A., Hardebeck, E., and Parker, J.: Large-scale variability of wind erosion mass flux rates at Owens Lake .2. Role of roughness change, particle limitation, change of threshold friction velocity, and the Owen effect, Journal of Geophysical Research-Atmospheres, 102, 25989-25998, 1997.
Gillette, D. A. and Passi, R.: Modeling dust emission caused by wind erosion, Journal of Geophysical Research-Atmospheres, 93, 14233-14242, 1988.
Gillies, J. A. and Berkofsky, L.: Eolian suspension above the saltation layer, the concentration profile, Journal of Sedimentary Research, 74, 176-183, 2004.
Ginoux, P., Chin, M., Tegen, I., Prospero, J. M., Holben, B., Dubovik, O., and Lin, S. J.: Sources and distributions of dust aerosols simulated with the GOCART model, J. Geophys. Res., 106, 20255-20273, 2001.
Ginoux, P., Prospero, J. M., Gill, T. E., Hsu, N. C., and Zhao, M.: Global-scale attribution of anthropogenic and natural dust sources and their emission rates based on MODIS Deep Blue aerosol products, Reviews of Geophysics, 50, Rg3005, 2012.
Gomes, L., Rajot, J. L., Alfaro, S. C., and Gaudichet, A.: Validation of a dust production model from measurements performed in semi-arid agricultural areas of Spain and Niger, Catena, 52, 257-271, 2003.
Gordon, M. and McKenna Neuman, C.: A comparison of collisions of saltating grains with loose and consolidated silt surfaces, Journal of Geophysical Research-Earth Surface, 114, 2009.

Goulden, M. L., Munger, J. W., Fan, S. M., Daube, B. C., and Wofsy, S. C.: Measurements of carbon sequestration by long-term eddy covariance: Methods and a critical evaluation of accuracy, Global Change Biology, 2, 169-182, 1996.
Hinds, W. C.: Aerosol technology: Properties, Behavior, and measurement of airborne particles, John Wiley & Sons, New York, 1999.
Ho, T. D., Valance, A., Dupont, P., and El Moctar, A. O.: Scaling Laws in Aeolian Sand Transport, Phys. Rev. Lett., 106, 2011.
Huneeus, N., Schulz, M., Balkanski, Y., Griesfeller, J., Prospero, J., Kinne, S., Bauer, S., Boucher, O., Chin, M., Dentener, F., Diehl, T., Easter, R., Fillmore, D., Ghan, S., Ginoux, P., Grini, A., Horowitz, L., Koch, D., Krol, M. C., Landing, W., Liu, X., Mahowald, N., Miller, R., Morcrette, J. J., Myhre, G., Penner, J., Perlwitz, J., Stier, P., Takemura, T., and Zender, C. S.: Global dust model intercomparison in AeroCom phase I, Atmospheric Chemistry and Physics, 11, 7781-7816, 2011.
Iversen, J. D. and White, B. R.: Saltation threshold on earth, mars and venus, Sedimentology, 29, 111-119, 1982.
Jickells, T. D., An, Z. S., Andersen, K. K., Baker, A. R., Bergametti, G., Brooks, N., Cao, J. J., Boyd, P. W., Duce, R. A., Hunter, K. A., Kawahata, H., Kubilay, N., laRoche, J., Liss, P. S., Mahowald, N., Prospero, J. M., Ridgwell, A. J., Tegen, I., and Torres, R.: Global iron connections between desert dust, ocean biogeochemistry, and climate, Science, 308, 67-71, 2005.
Johnson, M. S., Meskhidze, N., and Kiliyanpilakkil, V. P.: A global comparison of GEOS-Chem-predicted and remotely-sensed mineral dust aerosol optical depth and extinction profiles, J. Adv. Model. Earth Syst., 4, 2012.
Kaaden, N., Massling, A., Schladitz, A., Muller, T., Kandler, K., Schutz, L., Weinzierl, B., Petzold, A., Tesche, M., Leinert, S., Deutscher, C., Ebert, M., Weinbruch, S., and Wiedensohler, A.: State of mixing, shape factor, number size distribution, and hygroscopic growth of the Saharan anthropogenic and mineral dust aerosol at Tinfou, Morocco, Tellus Ser. B-Chem. Phys. Meteorol., 61, 51-63, 2009.
Kaimal, J. C. and Finnigan, J. J.: Atmospheric boundary layer flows: Their structure and measurement Oxford Univ. Press, New York, 1994.
Kallenberg, O.: Foundations of Modern Probability, Springer-Verlag, New York, 1997.
Klose, M. and Shao, Y.: Stochastic parameterization of dust emission and application to convective atmospheric conditions, Atmospheric Chemistry and Physics, 12, 7309-7320, 2012.
Kok, J. F.: Does the size distribution of mineral dust aerosols depend on the wind speed at emission?, Atmospheric Chemistry and Physics, 11, 10149-10156, 2011a.
Kok, J. F.: An improved parameterization of wind-blown sand flux on Mars that includes the effect of hysteresis, Geophysical Research Letters, 37, 2010.
Kok, J. F.: A scaling theory for the size distribution of emitted dust aerosols suggests climate models underestimate the size of the global dust cycle, Proc. Natl. Acad. Sci. U. S. A., 108, 1016-1021, 2011b.
Kok, J. F., Albani, S., Mahowald, N. M., and Ward, D. S.: An improved dust emission model. Part 2: Evaluation in the Community Earth System Model, with implications for the use of dust source functions, Atmospheric Chemistry and Physics, this issue, 2014.
Kok, J. F., Parteli, E. J. R., Michaels, T. I., and Karam, D. B.: The physics of wind-blown sand and dust, Reports on Progress in Physics, 75, 106901, 2012.
Kok, J. F. and Renno, N. O.: A comprehensive numerical model of steady state saltation (COMSALT), Journal of Geophysical Research-Atmospheres, 114, D17204, 2009.

Kok, J. F. and Renno, N. O.: Enhancement of the emission of mineral dust aerosols by electric forces, Geophysical Research Letters, 33, 2006.
Kun, F. and Herrmann, H. J.: Transition from damage to fragmentation in collision of solids, Phys. Rev. E, 59, 2623-2632, 1999.
Li, Z., Kok, J. F., Henze, D. K., Li, Q., and Zhao, C.: Improving simulations of fine dust surface concentrations over the western United States by optimizing the particle size distribution, Geophysical Research Letters, 40, 3270-3275, 2013.
Mahowald, N. M., Albani, S., Kok, J. F., Engelstaedter, S., Scanza, R., Ward, D. S., and Flanner, M. G.: The size distribution of desert dust aerosols and its impact on the Earth system, Aeolian Research, doi: 10.1016/j.aeolia.2013.09.002, 2014. 2014.
Mahowald, N. M., Kloster, S., Engelstaedter, S., Moore, J. K., Mukhopadhyay, S., McConnell, J. R., Albani, S., Doney, S. C., Bhattacharya, A., Curran, M. A. J., Flanner, M. G., Hoffman, F. M., Lawrence, D. M., Lindsay, K., Mayewski, P. A., Neff, J., Rothenberg, D., Thomas, E., Thornton, P. E., and Zender, C. S.: Observed 20th century desert dust variability: impact on climate and biogeochemistry, Atmospheric Chemistry and Physics, 10, 10875-10893, 2010.
Mahowald, N. M., Muhs, D. R., Levis, S., Rasch, P. J., Yoshioka, M., Zender, C. S., and Luo, C.: Change in atmospheric mineral aerosols in response to climate: Last glacial period, preindustrial, modern, and doubled carbon dioxide climates, J. Geophys. Res., 111, D10202, 2006.
Marticorena, B. and Bergametti, G.: Modeling the atmospheric dust cycle .1. Design of a soil-derived emission scheme, Journal of Geophysical Research-Atmospheres, 100, 16415-16430, 1995.
Marticorena, B., Chazette, P., Bergametti, G., Dulac, F., and Legrand, M.: Mapping the aerodynamic roughness length of desert surfaces from the POLDER/ADEOS bi-directional reflectance product, International Journal of Remote Sensing, 25, 603-626, 2004.
Martin, R. L., Barchyn, T. E., Hugenholtz, C. H., and Jerolmack, D. J.: Timescale dependence of aeolian sand flux observations under atmospheric turbulence, Journal of Geophysical Research-Atmospheres, 118, 9078-9092, 2013.
Menut, L., Perez, C., Haustein, K., Bessagnet, B., Prigent, C., and Alfaro, S.: Impact of surface roughness and soil texture on mineral dust emission fluxes modeling, Journal of Geophysical Research-Atmospheres, 118, 6505-6520, 2013.
Miller, R. L. and Tegen, I.: Climate response to soil dust aerosols, Journal of Climate, 11, 3247-3267, 1998.
Mokhtari, M., Gomes, L., Tulet, P., and Rezoug, T.: Importance of the surface size distribution of erodible material: an improvement on the Dust Entrainment And Deposition (DEAD) Model, Geoscientific Model Development, 5, 581-598, 2012.
Nabat, P., Solmon, F., Mallet, M., Kok, J. F., and Somot, S.: Dust emission size distribution impact on aerosol budget and radiative forcing over the Mediterranean region: a regional climate model approach, Atmospheric Chemistry and Physics, 12, 10545-10567, 2012.
Namikas, S. L.: A conceptual model of energy partitioning in the collision of saltating grains with an unconsolidated sediment bed, J. Coast. Res., 22, 1250-1259, 2006.
Namikas, S. L., Bauer, B. O., and Sherman, D. J.: Influence of averaging interval on shear velocity estimates for aeolian transport modeling, Geomorphology, 53, 235-246, 2003.
Nickling, W. G.: Eolian sediment transport during dust storms - Slims river valley, Yukon territory, Canadian Journal of Earth Sciences, 15, 1069-1084, 1978.
Nickling, W. G.: Grain-size characteristics of sediment transported during dust storms, Journal of Sedimentary Petrology, 53, 1011-1024, 1983.

Nickling, W. G. and Gillies, J. A.: Dust emission and transport in Mali, West-Africa, Sedimentology, 40, 859-868, 1993.
Nickling, W. G. and McKenna Neuman, C.: Aeolian sediment transport. In: Geomorphology of Desert Environments, Parsons, A. J. and Abrahams, A. D. (Eds.), Springer Science+Business Media, New York, 2009.
Nickling, W. G., McTainsh, G. H., and Leys, J. F.: Dust emissions from the Channel Country of western Queensland, Australia, Zeitschrift fur Geomorphologie NF Supplementband, 116, 1-17, 1999.
O'Brien, P. and McKenna Neuman, C.: A wind tunnel study of particle kinematics during crust rupture and erosion, Geomorphology, 173, 149-160, 2012.
Oger, L., Ammi, M., Valance, A., and Beladjine, D.: Study of the collision of one rapid sphere on 3D packings: Experimental and numerical results, Computers & Mathematics with Applications, 55, 132-148, 2008.
Okin, G. S.: A new model of wind erosion in the presence of vegetation, Journal of Geophysical Research-Earth Surface, 113, F02s10, 2008.
Owen, P. R.: Saltation of uniform grains in air, Journal of Fluid Mechanics, 20, 225-242, 1964.
Park, M. S., Park, S. U., and Chun, Y.: Improved parameterization of dust emission (PM10) fluxes by the gradient method using the Naiman tower data at the Horqin desert in China, Science of the Total Environment, 412, 265-277, 2011.
Rasmussen, K. R. and Sorensen, M.: Aeolian mass transport near the saltation threshold, Earth Surface Processes and Landforms, 24, 413-422, 1999.
Raupach, M. R.: Drag and drag partition on rough surfaces, Boundary-Layer Meteorology, 60, 375-395, 1992.
Raupach, M. R., Gillette, D. A., and Leys, J. F.: The effect of roughness elements on wind erosion threshold, Journal of Geophysical Research-Atmospheres, 98, 3023-3029, 1993.
Reid, J. S., Jonsson, H. H., Maring, H. B., Smirnov, A., Savoie, D. L., Cliff, S. S., Reid, E. A., Livingston, J. M., Meier, M. M., Dubovik, O., and Tsay, S. C.: Comparison of size and morphological measurements of coarse mode dust particles from Africa, Journal of Geophysical Research-Atmospheres, 108, 2003.
Rice, M. A., McEwan, I. K., and Mullins, C. E.: A conceptual model of wind erosion of soil surfaces by saltating particles, Earth Surface Processes and Landforms, 24, 383-392, 1999.
Rice, M. A., Willetts, B. B., and McEwan, I. K.: An experimental-study of multiple grain-size ejecta produced by collisions of saltating grains with a flat bed, Sedimentology, 42, 695-706, 1995.
Rice, M. A., Willetts, B. B., and McEwan, I. K.: Observations of collisions of saltating grains with a granular bed from high-speed cine-film, Sedimentology, 43, 21-31, 1996.
Rosenberg, P. D., Parker, D. J., Ryder, C. L., Marsham, J. H., Garcia-Carreras, L., Dorsey, J. R., Brooks, I. M., Dean, A. R., Crosier, J., McQuaid, J. B., and Washington, R.: Quantifying particle size and turbulent scale dependence of dust flux in the Sahara using aircraft measurements, Journal of Geophysical Research-Atmospheres, 119, 7577-7598, 2014.
Shao, Y.: A model for mineral dust emission, Journal of Geophysical Research-Atmospheres, 106, 20239-20254, 2001.
Shao, Y., Ishizuka, M., Mikami, M., and Leys, J. F.: Parameterization of size-resolved dust emission and validation with measurements, Journal of Geophysical Research-Atmospheres, 116, D08203, 2011.
Shao, Y. P.: Physics and Modelling of Wind Erosion, Springer, Heidelberg, 2008.

Shao, Y. P. and Li, A.: Numerical modelling of saltation in the atmospheric surface layer, Boundary-Layer Meteorology, 91, 199-225, 1999.
Shao, Y. P. and Lu, H.: A simple expression for wind erosion threshold friction velocity, Journal of Geophysical Research-Atmospheres, 105, 22437-22443, 2000.
Shao, Y. P., Raupach, M. R., and Findlater, P. A.: Effect of saltation bombardment on the entrainment of dust by wind, Journal of Geophysical Research-Atmospheres, 98, 12719-12726, 1993.
Shao, Y. P., Raupach, M. R., and Leys, J. F.: A model for predicting aeolian sand drift and dust entrainment on scales from paddock to region, Australian Journal of Soil Research, 34, 309-342, 1996.
Sherman, D. J. and Farrell, E. J.: Aerodynamic roughness lengths over movable beds: Comparison of wind tunnel and field data, Journal of Geophysical Research-Earth Surface, 113, F02s08, 2008.
Sow, M., Alfaro, S. C., Rajot, J. L., and Marticorena, B.: Size resolved dust emission fluxes measured in Niger during 3 dust storms of the AMMA experiment, Atmospheric Chemistry and Physics, 9, 3881-3891, 2009.
Stockton, P. H. and Gillette, D. A.: Field measurement of the sheltering effect of vegetation on erodible land surfaces, Land Degradation & Rehabilitation, 2, 77-85, 1990.
Sweeney, M. R. and Mason, J. A.: Mechanisms of dust emission from Pleistocene loess deposits, Nebraska, USA, Journal of Geophysical Research, 118, 1460-1471, 2013.
Tegen, I., Harrison, S. P., Kohfeld, K., Prentice, I. C., Coe, M., and Heimann, M.: Impact of vegetation and preferential source areas on global dust aerosol: Results from a model study, Journal of Geophysical Research-Atmospheres, 107, 2002.
Ungar, J. E. and Haff, P. K.: Steady-state saltation in air, Sedimentology, 34, 289-299, 1987.
van Boxel, J. H., Sterk, G., and Arens, S. M.: Sonic anemometers in aeolian sediment transport research, Geomorphology, 59, 131-147, 2004.
van Donk, S. J., Huang, X. W., Skidmore, E. L., Anderson, A. B., Gebhart, D. L., Prehoda, V. E., and Kellogg, E. M.: Wind erosion from military training lands in the Mojave Desert, California, USA, Journal of Arid Environments, 54, 687-703, 2003.
Webb, N. P., Okin, G. S., and Brown, S.: The effect of roughness elements on wind erosion: The importance of surface shear stress distribution, Journal of Geophysical Research-Atmospheres, 119, 6066-6084, 2014.
Webb, N. P. and Strong, C. L.: Soil erodibility dynamics and its representation for wind erosion and dust emission models, Aeolian Research, 3, 165-179, 2011.
Wiggs, G. F. S., Atherton, R. J., and Baird, A. J.: Thresholds of aeolian sand transport: establishing suitable values, Sedimentology, 51, 95-108, 2004.
Wilks, D. S.: Statistical Methods in the Amtospheric Sciences, Academic Press, Oxford, UK, 2011.
Zender, C. S., Bian, H. S., and Newman, D.: Mineral Dust Entrainment and Deposition (DEAD) model: Description and 1990s dust climatology, Journal of Geophysical Research-Atmospheres, 108, 4416, 2003a.
Zender, C. S., Newman, D., and Torres, O.: Spatial heterogeneity in aeolian erodibility: Uniform, topographic, geomorphic, and hydrologic hypotheses, Journal of Geophysical Research-Atmospheres, 108, 4543, 2003b.

Zhao, C., Chen, S., Leung, L. R., Qian, Y., Kok, J. F., Zaveri, R. A., and Huang, J.: Uncertainty in modeling dust mass balance and radiative forcing from size parameterization, Atmospheric Chemistry and Physics, 13, 10733-10753, 2013.
Zobeck, T. M. and Van Pelt, R. S.: Wind-induced dust generation and transport mechanics on a bare agricultural field, Journal of Hazardous Materials, 132, 26-38, 2006.

Tables

Table 1. Summary of main characteristics of the quality-controlled data sets used in this study. Data set names are defined in Section 3.1.

Study	Event	Measurement method	Range of u_* (m/s)	Estimated u_{*t} (m/s)	Fetch length	Event duration	Number of data points	Soil type (clay fraction in %)
GB04	Feb 16	Gradient method	0.26 – 0.43	0.24 ± 0.02	> 5 km	3h 51m	203	Loamy sand (9.1 % clay)
GB04	March 20	Gradient method	0.33 – 0.62	0.31 ± 0.02	> 5 km	2h 50m	142	Loamy sand (9.1 %clay)
ZP06	March 4	Gradient method	0.39 - 0.54	0.41 ± 0.03	200 m	4h 02m	148	Fine sandy loam (13% clay)
ZP06	March 18	Gradient method	0.38 – 0.48	0.36 ± 0.03	200 m	2h 26m	113	Fine sandy loam (13% clay)
FC07	Event 1	Eddy covariance	0.232 – 0.693	0.203 ± 0.016	> 5 km	9h 40m	57	Sand (< 1% clay)
FC07	Event 2	Eddy covariance	0.171 - 0.606	0.170 ± 0.014	> 5 km	11h 50m	54	Sand (< 1% clay)
SA09	ME1	Gradient method	0.238 – 0.321	0.237 ± 0.019	575 m	1h 57m	76	Sand (2.8% clay)
SA09	CE4	Gradient method	0.314 – 0.358	0.232 ± 0.019	420 m	1h 53m	61	Sand (2.8% clay)
SI11	N/A	Gradient method	0.164 – 0.246	0.161 ± 0.013	> 1 km	7h 21m	399	Loamy sand (11 % clay)
PP11	Event 1	Gradient method	0.192 – 1.444	0.171 ± 0.014	> 2 km	9h 40m	50	Sand (4 % clay)
PP11	Event 2	Gradient method	0.218 – 1.627	0.197 ± 0.016	> 2 km	12h 50m	52	Sand (4 % clay)

Table 2. Root mean square error (RMSE) of the vertical dust flux predicted by the parameterizations of Gillette and Passi (1988) (denoted as GP88), Marticorena and Bergametti (1995) (MB95), and Eq. (18). RMSE values were calculated for three separate cases. For the first case, the proportionality constant was tuned to a single value that minimized the mean RMSE for all data sets. The resulting RMSE for this case is thus a measure of the parameterization's ability to reproduce variations in the dust flux due to variations in both u_* and soil conditions (u_{*t} and f_{clay}). For the second case, the proportionality constant in each parameterization was tuned separately for each data set. The resulting RMSE is thus a measure of a parameterization's ability to reproduce the dust flux's dependence on u_* for each individual data set. Data set names are defined in Section 3.1.

Study	**Event**	**GP88, Case 1**[*]	**MB95, Case 1**[*]	**Eq. 18, Case 1**	**GP88, Case 2**[†]	**MB95, Case 2**[†]	**Eq. 18, Case 2**[†]
GB04	Feb 16	0.400	**0.182**	0.739	0.203	**0.181**	0.182
GB04	March 20	0.247	**0.214**	0.215	0.112	0.108	**0.106**
ZP06	March 4	1.043	1.147	**0.345**	0.306	0.325	**0.297**
ZP06	March 18	0.390	0.566	**0.137**	0.088	0.111	**0.085**
FC07	Event 1	-	-	-	0.377	0.155	**0.147**
FC07	Event 2	-	-	-	0.389	0.192	**0.132**
SA09	ME1	**0.299**	0.541	0.410	**0.054**	0.072	0.058
SA09	CE4	**0.387**	0.571	0.555	**0.104**	0.114	0.111
SI11	N/A	1.286	0.382	**0.101**	0.161	0.107	**0.099**
PP11	Event 1	-	-	-	0.609	0.347	**0.295**
PP11	Event 2	-	-	-	0.656	0.356	**0.333**
Average		**0.579**	**0.515**	**0.357**	**0.278**	**0.188**	**0.168**

Figures

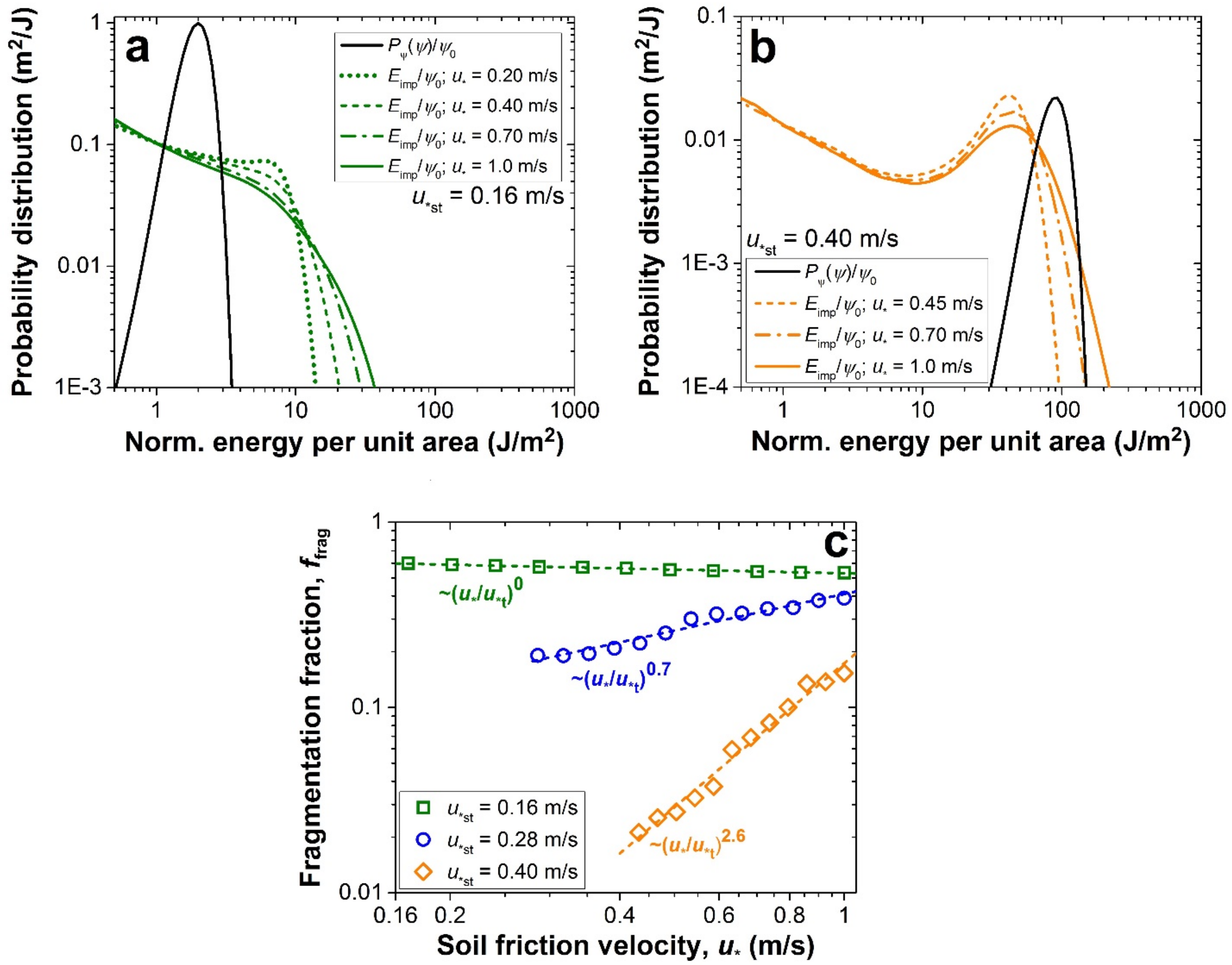

Figure 1. Probability distributions of the threshold impact energy per unit area (ψ) required for aggregate fragmentation (solid black line), and of the saltator impact energy per unit area (E_{imp}) for different values of u_* (colored lines). Shown are results for (**a**) a highly erodible soil (u_{*st} = 0.16 m/s) and (**b**) an erosion-resistant soil (u_{*st} = 0.40 m/s). The value of f_{frag} increases with u_* for erosion-resistant soils, but not for highly erodible soils, as shown explicitly in (**c**). All plotted energy values are normalized by ψ_0, the energy per unit area of a 100 μm saltator impacting at 1 m/s, and $P_\psi(\psi)$ was calculated using $c_\psi = 2$ and $\sigma_\psi = 0.2\overline{\psi}$.

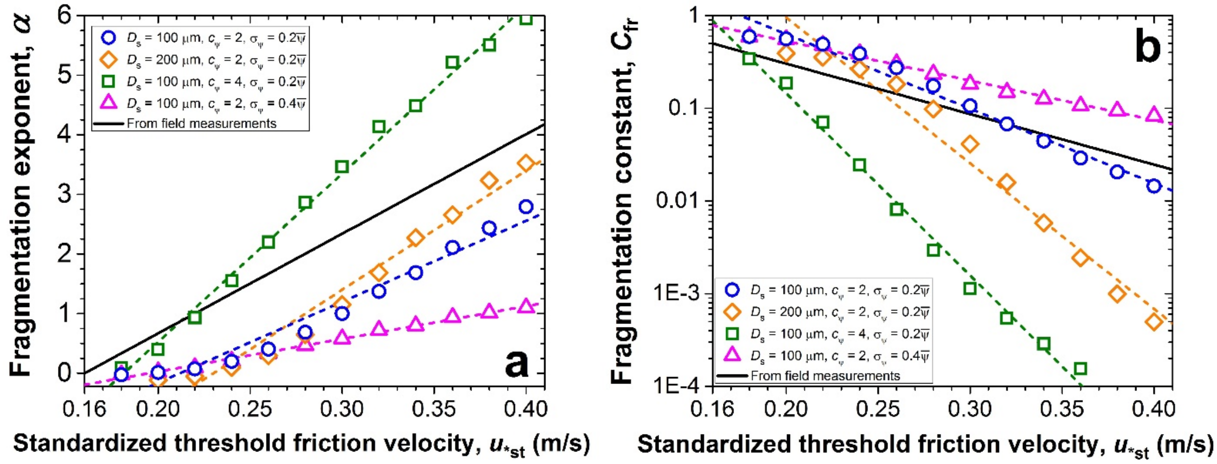

Figure 2. Simulations of the fragmentation exponent α (**a**) and constant C_{fr} (**b**) with the numerical saltation model COMSALT (Kok and Renno, 2009) for different values of the saltating particle size (D_s) and the threshold fragmentation energy's normal distribution parameters (c_ψ and σ_ψ). The colored dashed lines represent the best fits of the functional forms of Eqs. (16) and (17) to the corresponding simulation results, and the solid black lines represents the best fit to the experimental data in Fig. 4.

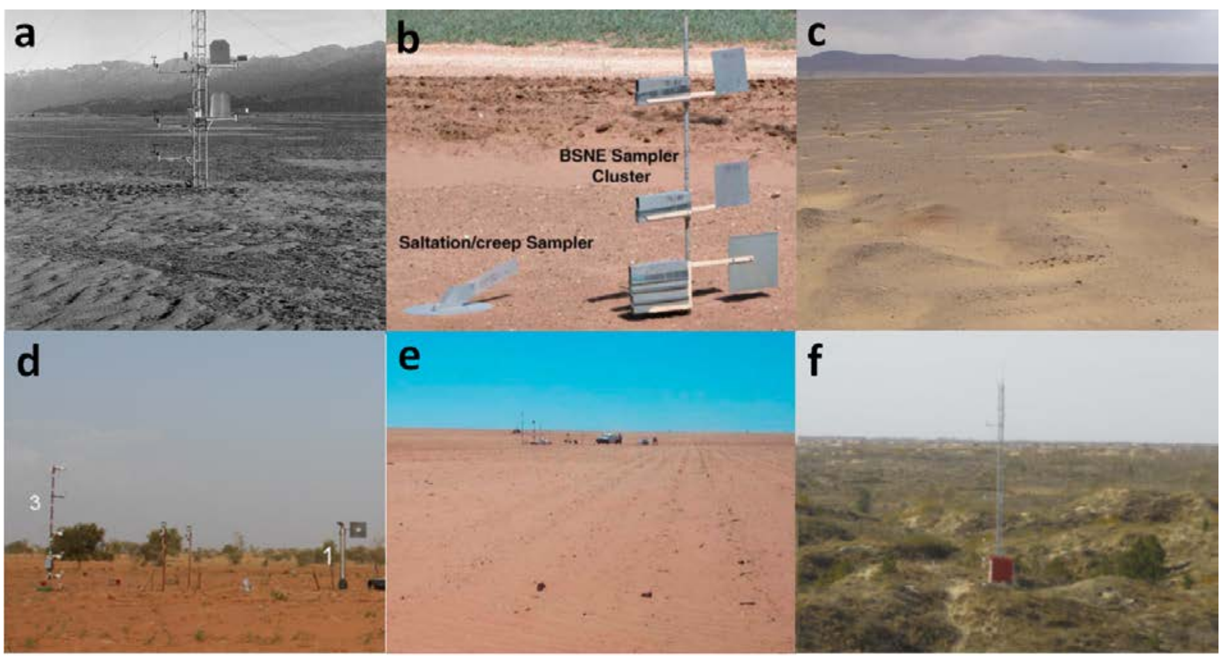

Figure 3. The experimental field sites of the six studies in our vertical dust flux compilation: (**a**) Gillies and Berkofsky (2004) (36.48º N, 117.90º W), (**b**) Zobeck and Van Pelt (2006) (32.27° N, 101.49° W), (**c**) Fratini et al. (2007) (100.54° E, 41.88° N), (**d**), Sow et al. (2009) (13.5° N, 2.6° E), (**e**) Shao et al. (2011) (33.85° S, 142.74° E), and (**f**) Park et al. (2011) (42.93° N, 120.70° E).

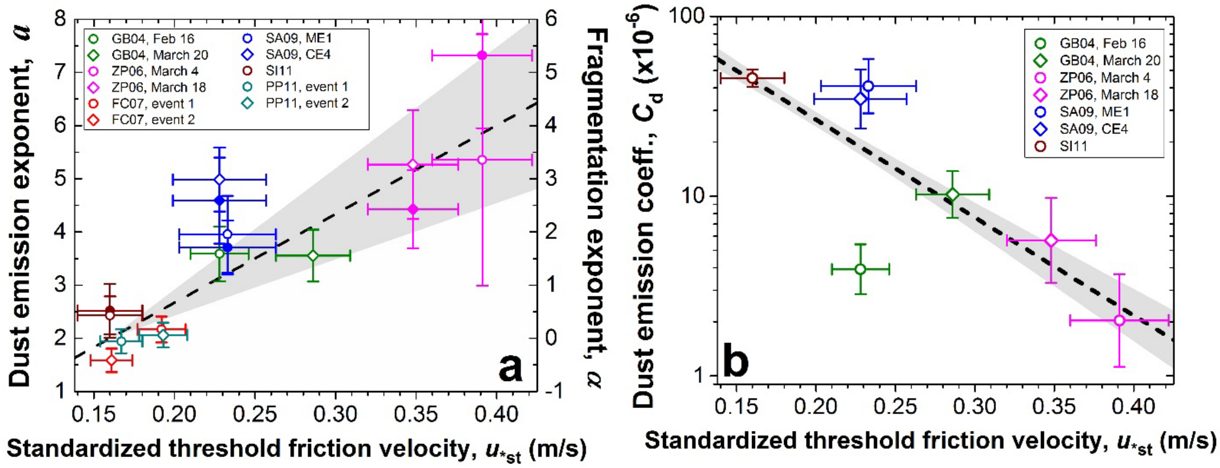

Figure 4. Values of (**a**) the dust emission exponent a (= α + 2) and (**b**) the dust emission coefficient C_d as a function of the standardized threshold friction velocity u_{*st}, determined from the analysis of available quality-controlled data sets. Open symbols refer to estimates of C_d and a from the least-squares fit of the measured dust flux to Eq. (18), whereas filled symbols refer to estimates of a from a least-squares fit to ratios of the measured vertical dust flux and the horizontal saltation flux (see text for details). The dashed line indicates the best-fit forms of Eqs. (16) and (18b), and the grey shaded area denotes one standard error from the fitted relation. Data set names are defined in Section 3.1.

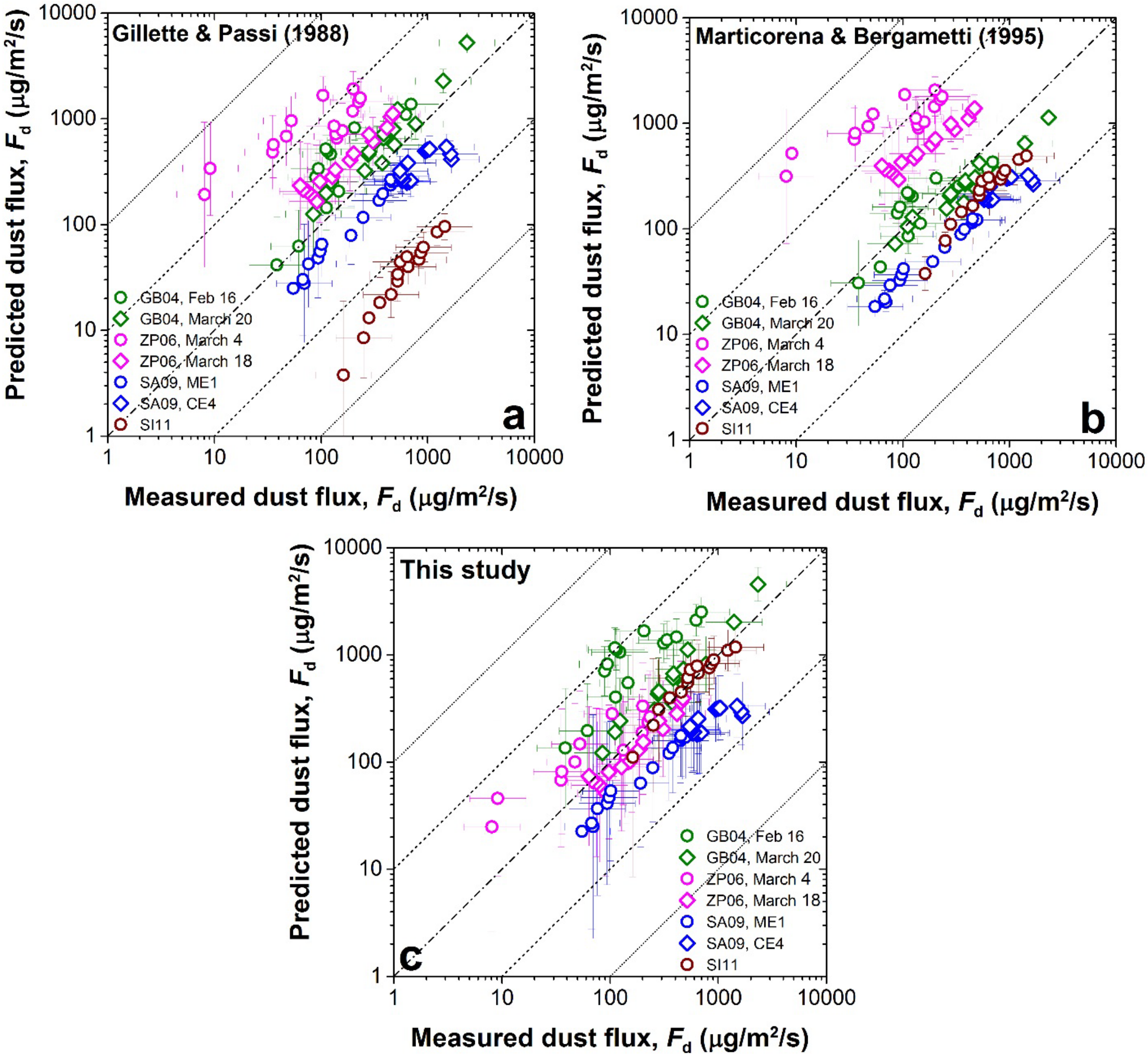

Figure 5. Comparison of measured dust fluxes with the predictions of the parameterizations of (**a**) Gillette and Passi (1988), (**b**) Marticorena and Bergametti (1995), and (**c**) this study. The proportionality constant in each parameterization was adjusted to maximize agreement with the compilation of measurements. To prevent cluttering of the graph, only 15 representative measurements are shown for each data set. Error bars denote uncertainty arising from the measurement of u_{*t}, u_*, and F_d (see the Supplement). Data set names are defined in Section 3.1.

An improved dust emission model. Part 2: Evaluation in the Community Earth System Model, with implications for the use of dust source functions

Kok, J. F.[1], S. Albani[2], N. M. Mahowald[2], and D. S. Ward[2]

[1] Department of Atmospheric and Oceanic Sciences, University of California, Los Angeles, CA 90095, USA
[2] Department of Earth and Atmospheric Sciences, Cornell University, Ithaca, NY 14850, USA

Correspondence to J. F. Kok (jfkok@ucla.edu)

Abstract

The complex nature of mineral dust aerosol emission makes it a difficult process to represent accurately in weather and climate models. Indeed, both measurements and the new physically-based dust emission parameterization presented in the companion paper indicate that many large-scale models underestimate the dust flux's sensitivity to the soil's threshold friction velocity. We hypothesize that this finding explains why many dust cycle simulations are improved by using an empirical dust source function that shifts emissions towards the world's most erodible regions. Here, we both test this hypothesis and evaluate the performance of the new dust emission parameterization. We do so by implementing the new emission scheme into the Community Earth System Model (CESM) and comparing the resulting dust cycle simulations against an array of measurements. We find that the new scheme shifts emissions towards the world's most erodible regions in a manner that is strikingly similar to the effect of implementing a widely-used source function based on satellite observations by the Total Ozone Mapping Spectrometer. Furthermore, model comparisons against aerosol optical depth measurements show that the new physically-based scheme produces a statistically significant improvement in CESM's representation of dust emission, which exceeds the improvement produced by implementing a source function. These results indicate that the need to use an empirical source function is (partially) eliminated, at least in CESM, by the additional physics in the new scheme, and in particular by its increased sensitivity to the soil's threshold friction velocity. Since the threshold friction velocity is affected by climate changes, our results further suggest that many large-scale models underestimate the global dust cycle's climate sensitivity.

1. Introduction

Mineral dust aerosols affect the Earth system through a wide variety of interactions, including scattering and absorbing radiation, altering cloud lifetime and reflectance, and serving as a nutrient source (Martin et al., 1991; Miller and Tegen, 1998; Forster et al., 2007). Conversely, the global dust cycle is highly sensitive to changes in climate (Tegen et al., 2004; Mahowald et al., 2006b; Washington et al., 2009), as evidenced both by global dust deposition being several times larger during glacial maxima than during interglacials (Rea, 1994; Harrison et al., 2001) and by the apparent increase in global dust deposition over the past century (Prospero and Lamb, 2003; Mahowald et al., 2010). The radiative forcing resulting from such changes in the dust cycle might have played a critical role in amplifying past climate changes (Jansen et al., 2007), and may play an important role in present and future climate changes (Harrison et al., 2001; Mahowald et al., 2010).

Unfortunately, an accurate quantification of dust interactions with the Earth system in past and future climates is hindered by the empirical nature of dust emission parameterizations in climate models. Since these parameterizations are generally tuned to reproduce the current dust cycle (Ginoux et al., 2001; Zender et al., 2003a; Cakmur et al., 2006), applying them to a past or future climate, with substantial differences in global circulation and land surface, could produce large systematic errors. In particular, many dust modules in climate models use a *dust source function S* (Ginoux et al., 2001; Tegen et al., 2002; Zender et al., 2003b; Grini et al., 2005; Koven and Fung, 2008) to help account for global variations in *soil erodibility* (defined in the dust modeling community as the efficiency of a soil in producing dust aerosols under a given wind stress (Zender et al., 2003b)).

The flux of dust emitted through wind erosion in a model grid cell is thus commonly represented by (Ginoux et al., 2001; Zender et al., 2003a; Grini et al., 2005; Colarco et al., 2014)

$$\phi_{\mathrm{d}} = C_{\mathrm{tune}} S F_{\mathrm{d}}, \tag{1}$$

where C_{tune} is a global tuning constant, usually set to maximize agreement against observations (Cakmur et al., 2006), and F_{d} is the vertical dust flux produced by an eroding soil per unit time and area, as predicted by a dust emission parameterization such as Gillette and Passi (1988), Marticorena and Bergametti (1995), or Kok et al. (2014). The dust source function *S* is a function of latitude and longitude, and usually shifts emissions towards the world's most erodible regions, such as North Africa (Ginoux et al., 2001; Tegen et al., 2002; Zender et al., 2003b).

The need to use a source function to improve agreement against observations was first noted by the pivotal study of Ginoux et al. (2001). They used the observation of Prospero et al. (2002) that dust "hot spots" tend to be co-located with topographic depressions to design a source function based on the relative height of a model grid cell compared to its surrounding cells. However, some subsequent studies challenged this association of dust hot spots with topographic depressions by Prospero et al. (2002) because (i) the used remote sensing product from the Total Ozone Mapping Spectrometer (TOMS) is sensitive to boundary layer height, which tends to be higher over depressions in central desert regions (Mahowald and Dufresne, 2004), and because (ii) advection causes the remotely sensed dust loading to be shifted downwind from source regions (Schepanski et al., 2009). Nonetheless, the use of source functions, and the consequent shift of emissions towards regions with observed high dust loadings (Ginoux et al., 2001; Prospero et al., 2002), can substantially improve the agreement of dust cycle simulations with measurements (Zender et al., 2003b; Cakmur et al., 2006).

This improvement of dust cycle simulations by semi-empirical source functions suggests that a key piece of physics is missing from existing dust emission parameterizations in models. And indeed, dust flux parameterizations in most large-scale models account for variations in soil erodibility in mostly empirical manners. The dust emission parameterization of Gillette and Passi (1988), which is used in the Goddard Chemistry Aerosol Radiation and Transport (GOCART) model (Ginoux et al., 2001) and many other models (Huneeus et al., 2011), does not account for the effect of either sediment availability or other soil properties on the dust flux. Similarly, the dust flux parameterization of Marticorena and Bergametti (1995), which is used in simplified form in the Dust Entrainment And Deposition model (Zender et al., 2003a) that is used in many climate models (Huneeus et al., 2011), accounts for the effect of fine sediment availability on the dust flux using an empirical fit to data from a single study (Gillette, 1979). Since such empirical parameterizations and source functions cannot accurately capture changes in soil erodibility produced by climate changes, which for instance affect soil moisture content and soil aggregation (Zobeck, 1991; Fecan et al., 1999; Shao, 2008; Kok et al., 2012), their use could cause substantial errors in model estimates of climate-induced changes in the global dust cycle.

This paper and its companion paper (Kok et al., 2014) strive to take a step towards an improved representation of the global dust cycle in climate models, in particular for climate regimes other than the current climate to which most models are tuned (Cakmur et al., 2006). The first component of this objective was achieved in our companion paper (Kok et al., 2014), by presenting a physically-based theory for the vertical dust flux emitted by an eroding soil. The resulting parameterization (henceforth referred to as K14) was able to reproduce a quality-controlled compilation of dust flux measurements with substantially less error than the existing dust flux parameterizations we were able to test against, and is relatively straightforward to implement since it uses only globally-available parameters. A critical insight from our companion paper is that the dust flux is likely substantially more sensitive to changes in the soil state than most climate models account for. The resulting underestimation of the dust flux sensitivity to the soil state might explain why an empirical source function that shifts emissions towards more erodible regions improves agreement against measurements (Cakmur et al., 2006). Since the new K14 scheme accounts for the increased sensitivity of the dust flux to the soil state, our companion paper hypothesized that K14 can reduce the need to use a source function in dust cycle simulations.

Here we use simulations with the Community Earth System Model (CESM) to both test the above hypothesis, and to evaluate the performance of the K14 parameterization in a climate model. Through a detailed comparison against measurements, we find that the K14 scheme produces a statistically significant improvement in the representation of dust emission in CESM, and that this improvement exceeds that produced by a source function. These results indicate that the additional physics accounted for by K14, which result in an increased sensitivity of the dust flux to the soil's threshold friction velocity, reduces the need for a source function in dust cycle simulations, at least in CESM. Since the threshold friction velocity is affected by climate changes, our finding that many models underestimate the dust flux's sensitivity to this threshold further suggests that these models have underestimated the global dust cycle's climate sensitivity.

The next section describes CESM's dust module and the implementation of the K14 dust emission parameterization, as well as the measurements used to evaluate the fidelity of CESM's dust cycle simulations. We then present results of the comparison between simulations and measurements in Section 3, discuss the implications of the results in Section 4, and summarize and conclude the paper in Section 5.

2. Methods

We use simulations with CESM version 1.1 (Hurrell et al., 2013) to evaluate the performance of the K14 dust emission scheme. Specifically, we simulate the present-day dust cycle with four different combinations of source functions and dust flux parameterizations (see Table 1). In order to assess whether K14 improves the representation of dust emission in CESM, we compare the simulation results against measurements of aerosol optical depth (AOD) by the AERosol RObotic NETwork (AERONET; Holben et al. (1998)), as well as to satellite-derived estimates of dust optical depth and dust mass path close to source regions (Evan et al., 2014). Note that the code to implement the K14 parameterization in CESM is freely available from the main author.

We also evaluate how each of the four dust cycle simulations performs against measurements further from source regions, namely dust surface concentration and dust deposition. Since these measurements were thus generally taken far from source regions, the simulation performance against these measurements depends on the model's ability to simulate a variety of other processes in addition to dust emission, especially transport and deposition.

The next section briefly describes CESM and its treatment of the dust cycle for each of the four simulations (Table 1). We then describe the properties of the data sets used to evaluate the model performance in Sections 2.2 and 2.3. In Section 2.4, we describe the method to assess whether improvements in the ability of the different simulations to reproduce these measurements are statistically significant.

Table 1. Summary of the four CESM simulations used in this study, and the statistics of their comparison against the data set most characteristic of dust emission, namely AERONET AOD measurements at dusty stations (see text). Model results are compared to measurements of AERONET AOD climatology (fourth and fifth columns), the mean correlation to the measured seasonal cycle at each station (sixth column), and the mean correlation to the measured daily variability at each station (seventh column). Statistically significant improvements (see Section 2.4) of Simulations II-IV relative to the 'control' Simulation I are indicated with bold font. Additionally, simulation results that are statistically significantly improved over the results of each of the other three simulations are both bold and underlined.

Simulation	Dust flux parameterization	Dust source function	AERONET climatology, *r*	AERONET climatology, RMSE	AERONET seasonal cycle, *r*	AERONET daily variability, *r*
I	Zender et al. (2003a)	None	0.55	0.149	0.79	0.43
II	Zender et al. (2003a)	Zender et al. (2003b)	0.57	0.146	0.75	0.43
III	Zender et al. (2003a)	Ginoux et al. (2001)	0.62	0.138	0.79	0.42
IV	Kok et al. (2014)	None	**0.72**	**0.117**	**0.82**	**0.46**

2.1. Dust cycle simulations with the Community Earth System Model

Emission of dust aerosols in CESM was calculated using its land model, the Community Land Model version 4.0 (CLM4, Lawrence et al. (2011)). These emissions were then used by CESM's atmosphere model, the Community Atmosphere Model version 4 (CAM4), to calculate the three-dimensional transport and deposition of dust, as well as the dust aerosol optical depth (Mahowald et al., 2006b; Albani et al., 2014). In addition to accounting for the global dust cycle and the consequent optical depth produced by dust aerosols (see next section), CESM also includes the effects of other kinds of aerosols, including sea salt, biomass burning, and sulfate aerosols. Black and organic carbon, dimethyl-sulphide, and sulphur oxides emissions are prescribed based on AeroCom specifications (Neale et al., 2010), whereas sea salt aerosol emission is prognostic, based on 10 m wind speed and humidity (Mahowald et al., 2006a).

2.1.1. General treatment of the dust cycle in CESM

The emission of dust aerosols in CLM4 follows the treatment of Zender et al. (2003a), with modifications described in Mahowald et al. (2006b, 2010), and further adjustments described below. Specifically, the vertical dust flux ϕ_d in a model grid cell is parameterized using Eq. (1), with the source function S and the vertical dust flux F_d given in Table 1 for the four simulations (also see 2.1.2). We adjust the global tuning factor C_{tune} to maximize agreement against AERONET AOD measurements (see Section 2.1.2).

The threshold friction velocity u_{*t}' at which dust emission is initiated is critical to determining dust emissions. The value of u_{*t}' depends on air density, soil properties, and the presence of non-erodible roughness elements (Marticorena and Bergametti, 1995; Shao and Lu, 2000; Kok et al., 2014). However, CLM4 does not account for the effect of non-erodible roughness elements on dust emissions, and the effect of air density on u_{*t}' is limited. Consequently, u_{*t}' in CLM4 is mostly determined by soil moisture content; the treatment of the effect of soil moisture on u_{*t}' follows Eqs. (12) and (14) in Fécan et al. (1999):

$$\frac{u_{*t}'}{u_{*dt}'} = 1, \qquad (w < w') \tag{2}$$

$$\frac{u_{*t}'}{u_{*dt}'} = \sqrt{1 + 1.21(w - w')^{0.68}} \qquad (w \geq w'), \tag{3}$$

where u_{*t}' and u_{*dt}' are respectively the threshold friction velocities in the presence and absence of soil moisture, and u_{*dt}' is calculated following the semi-empirical relation of Iversen and White (1982), as described on p. 3 of Zender et al. (2003a). Furthermore, w is the gravimetric water content in percent for CLM4's top soil layer, which has a thickness of 1.75 cm (Oleson et al., 2010). The threshold gravimetric water content w' of the top soil layer above which w increases u_{*t}' is given by (Fecan et al., 1999; Zender et al., 2003a)

$$w' = b\left(17 f_{clay} + 14 f_{clay}^2\right), \tag{4}$$

where w' is given in percent, b is a tuning parameter introduced by Zender et al. (2003a), and f_{clay} is the soil's clay fraction, which is taken from the FAO (2012) soil database (see Fig. S1).

The larger the value of the tuning parameter b, the smaller the effect of soil moisture on the dust emission threshold u_{*t}'. The range of plausible values of b extends from less than 1, to 1 (i.e., no tuning constant; Fecan et al. (1999)) to 3 (Mokhtari et al., 2012) to $1/f_{clay}$ (Zender et al., 2003a). Since dust emissions are non-linear in u_{*t}' (e.g., Kok et al. (2014)), and since u_{*t}' is a critical variable in the K14 dust emission scheme tested in this paper, the choice of b can be expected to substantially affect the simulated dust cycle. Unfortunately, the 'correct' value of b is highly uncertain, in part because the parameterization of Fecan et al. (1999) is based on wind tunnel studies. Implementing this small-scale parameterization into a climate model scales it up by many orders of magnitude, potentially producing physically unrealistic results. Furthermore, the inhibition of dust emission by soil moisture depends on the moisture content of the top layer of soil particles (McKenna Neuman and Nickling, 1989), which is in direct contact with the surface air. In contrast, the top soil layer of hydrology models in climate models usually has a thickness of multiple centimeters and thus responds differently to precipitation and changes in atmospheric humidity, which are important in determining the dust emission threshold (Ravi et al., 2004; Ravi et al., 2006). The 'correct' value of *b* in a climate model is therefore likely to depend substantially on the model methodology, and in particular on the specifics of the model's hydrology module. Since the choice of *b* is thus ambiguous, we investigated the sensitivity of our results to the particular value of *b* by running simulations with a wide range of values (Table S1). We emphasize that other models using the K14 scheme should do a similar sensitivity study to avoid an unrealistic influence of the model's hydrology on the dust emission fluxes. Because we found that the simplest case of not using a tuning constant (i.e., $b = 1$) produces the best overall results for all four model configurations, we used $b = 1$ for the results reported in Section 3. But note that the wide range of values of *b* that we tested all produced results qualitatively similar to those presented here (see Table S1).

In addition to the effects of soil moisture, CLM4 also accounts for the inhibition of dust emissions by vegetation. Specifically, CLM4 assumes that the fraction of the grid cell consisting of bare soil capable of emitting dust aerosols (f_{bare}) decreases linearly with the leaf area index (LAI), which is the ratio of the total surface area of leaves with the land surface area. That is,

$$f_{\mathrm{bare}} = 1 - \lambda / \lambda_{\mathrm{thr}}, \qquad (\lambda \leq \lambda_{\mathrm{thr}}) \tag{5}$$

where λ denotes LAI, and $\lambda_{\mathrm{thr}} = 0.3$ is the threshold LAI above which no dust emission is assumed to occur (Mahowald et al., 2010). (Note that the Ginoux et al. (2001) source function already includes the effects of vegetation, such that f_{bare} is set to 1 for all grid cells in Simulation III (see Table 1) to prevent accounting for the effects of vegetation twice.)

After CLM4 has calculated the dust flux, CAM4 distributes the emitted dust aerosols into 4 size bins (Mahowald et al., 2006b), from 0.1 – 1.0 μm, 1.0 – 2.5 μm, 2.5 – 5.0 μm, and 5.0 – 10 μm. The fraction distributed into each bin follows the 'brittle fragmentation' dust size distribution derived in Kok (2011b), which is in good agreement with a wide range of measurements (Mahowald et al., 2014). The emitted dust size distribution does not depend on the wind speed at emission, as shown by measurements (Kok, 2011a). The optical properties for each bin are specified in Albani et al. (2014) and are derived from a representation of dust as an internal mixture of the primary mineral classes of dust (quartz, aluminosilicates, clays, carbonates, iron-bearing minerals), combined into an effective medium using the Maxwell Garnett approximation (e.g., Videen and Chylek (1998)). The proportions of the mineral classes are consistent with the ranges reported in atmospheric dust and its parent soils (Claquin et al., 1999), and they are in agreement with bulk optical properties observed in dusty regions (Albani et al., 2014). The resulting radiative effects of dust aerosols do not feed back onto the simulated atmospheric dynamics.

CAM4 simulates both dry and wet deposition of dust. Dry deposition includes turbulent and gravitational settling, and follows the treatment in Zender et al. (2003a). Wet deposition accounts for in- and below-cloud scavenging and follows Neale et al. (2010) with the modifications described in Albani et al. (2014), which improve the model's ability to simulate the observed spatial gradients of dust. Specifically, the dust solubility (i.e., the fraction of dust available for in-cloud removal) was changed from 0.15 to 0.30, in line with a more recent version of the model (Liu et al., 2012). In addition, instead of using a constant below-cloud scavenging coefficient (collection efficiency) of 0.1 (Balkanski et al., 1993; Neale et al., 2010), the scavenging coefficient was made size-dependent (Andronache, 2003; Zender et al., 2003a), and was set to 0.1 for dust diameters below 2.5 μm and 0.3 for larger dust particles.

2.1.2. Dust emission schemes of the four CESM simulations

We used CESM to conduct four simulations, each with a different dust emission scheme (Table 1). The ‘control’ Simulation I uses CESM’s default dust emission parameterization of Zender et al. (2003a) (henceforth referred to as Z03) and does not use a source function; Simulations II and III then respectively add the source functions of Zender et al. (2003b) and Ginoux et al. (2001); and Simulation IV replaces the Zender et al. (2003a) parameterization with the K14 parameterization and also does not use a source function.

For Simulations I – III, F_d thus follows Z03, which is essentially a simplified version of the Marticorena and Bergametti (1995) parameterization. It is given by

$$F_{\mathrm{d}} = C_{\mathrm{MB}} \eta f_{\mathrm{bare}} \frac{\rho_{\mathrm{a}}}{g} u_*'^3 \left(1 - \frac{u_{*\mathrm{t}}'^2}{u_*'^2}\right)\left(1 + \frac{u_{*\mathrm{t}}'}{u_*'}\right), \qquad \left(u_*' > u_{*\mathrm{t}}'\right), \tag{6}$$

where C_{MB} is a dimensionless proportionality constant, ρ_{a} is the air density, g is the gravitational acceleration, and the sandblasting efficiency η (units of m^{-1}) depends on the soil clay fraction f_{clay} (see Fig. S1) following $\eta = 10^{13.4 f_{\mathrm{clay}} - 6}$. Note that, whereas the soil friction velocity u_* is defined from the wind stress on the bare erodible soil, the friction velocity u_*' is defined by the wind stress on the entire surface, so including the stress on non-erodible roughness elements (see Kok et al. (2014) for exact definitions). But since Z03 (and thus CLM4) does not account for the presence of non-erodible roughness elements, we have that $u_* = u_*'$, and $u_{*\mathrm{t}} = u_{*\mathrm{t}}'$, where $u_{*\mathrm{t}}$ and $u_{*\mathrm{t}}'$ are respectively the threshold friction velocity and the threshold soil friction velocity above which dust emissions occur.

Simulation IV uses the K14 dust emission parameterization (Kok et al., 2014), which is given by

$$F_{\mathrm{d}} = C_{\mathrm{d}} f_{\mathrm{bare}} f_{\mathrm{clay}} \frac{\rho_{\mathrm{a}}\left(u_*^2 - u_{*\mathrm{t}}^2\right)}{u_{*\mathrm{st}}} \left(\frac{u_*}{u_{*\mathrm{t}}}\right)^{C_\alpha \frac{u_{*\mathrm{st}} - u_{*\mathrm{st0}}}{u_{*\mathrm{st0}}}}, \qquad \left(u_* > u_{*\mathrm{t}}\right). \tag{7a}$$

The standardized threshold friction velocity $u_{*\mathrm{st}}$ is the value of $u_{*\mathrm{t}}$ at standard atmospheric density (ρ_{a0} = 1.225 kg/m^3), that is, $u_{*\mathrm{st}} \equiv u_{*\mathrm{t}} \sqrt{\rho_{\mathrm{a}} / \rho_{\mathrm{a0}}}$. $u_{*\mathrm{st0}}$ is then the minimal value of $u_{*\mathrm{st}}$ for an optimally-erodible soil, and measurements show that $u_{*\mathrm{st0}} \approx 0.16$ m/s (Kok et al., 2012). Furthermore, the dust emission coefficient C_{d} is a measure of soil erodibility (i.e., a soil’s ability to produce dust) that depends only on the standardized threshold friction velocity, and is defined as

$$C_{\mathrm{d}} = C_{\mathrm{d0}} \exp\left(-C_{\mathrm{e}} \frac{u_{*\mathrm{st}} - u_{*\mathrm{st0}}}{u_{*\mathrm{st0}}}\right). \tag{7b}$$

The dimensionless coefficients in Eq. (7) were determined in Kok et al. (2014) from comparison against a quality-controlled compilation of dust flux measurements, and are as follows: $C_\alpha = 2.7 \pm 1.0$, $C_{\mathrm{e}} = 2.0 \pm 0.3$ and $C_{\mathrm{d0}} = (4.4 \pm 0.5) \times 10^{-5}$.

As discussed in Kok et al. (2014), Eq. (7) accounts for the experimental observation that a more erodible soil produces a larger flux of dust per saltator impact. That is, per Eq. (7b), the dust flux F_{d} increases exponentially with a decrease in the standardized threshold $u_{*\mathrm{st}}$. Consequently, the dust flux is substantially more sensitive to the soil’s threshold friction velocity in K14 than in Z03 (Fig. 1), which is in agreement with measurements (Kok et al., 2014). We discuss the implications of the increased sensitivity of the dust flux to the threshold friction velocity in Sections 4.2 and 4.3.

The simulations used the capability of CESM to be forced with reanalysis winds instead of predicting winds, and used the ERA-Interim reanalysis meteorology from the European Centre for Medium-range Weather Forecasts (ECMWF) (Dee et al., 2011; Ma et al., 2013). CESM uses Monin-Obukhov Similarity Theory to obtain the friction velocity u_*' from the wind field (see section 5.1 in Oleson et al. (2010)). All simulations were run at a resolution of 1.9º latitude by 2.5º longitude, and cover the period 1994 to 2011 to produce substantial overlap with the data set of AERONET AOD measurements. The first year of each simulation was used as model spin-up and thus not used for analysis.

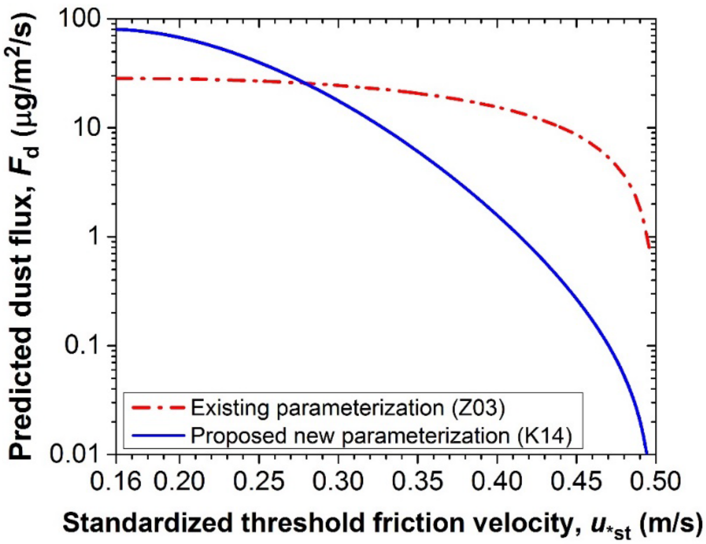

Figure 1. The vertical dust flux (F_d) as a function of the soil's standardized threshold friction velocity (u_{*st}) in CESM for the default Z03 dust flux parameterization (Eq. 6; dash-dotted red line), and for the K14 parameterization (Eq. 7; solid blue line). Results are shown for u_* = 0.50 m/s and for f_{clay} = 15%, which is a typical value for dust emitting regions (see Fig. S1). The predicted dust fluxes include the global tuning factors that eliminates the bias against AERONET AOD measurements for Simulations I and IV, respectively (see Eq. 1 and Section 2.2.1).

2.2. Measurements used to evaluate the representation of dust emission in CESM

We evaluate the representation of dust emission in the four dust cycle simulations by comparing their predictions against dust cycle measurements close to source regions. Arguably the best available data to test a model's dust emission scheme are the extensive and accurate (Eck et al., 1999) AOD measurements by the AERONET network (Holben et al., 1998). In addition to these measurements, we also compare the simulation results against a satellite-derived estimate of dust optical depth and dust mass path (DMP) off the West African coast (Evan et al., 2014).

2.2.1. AERONET AOD measurements

AERONET sites use sun photometers to measure radiances at a range of wavelengths, which are then inverted to retrieve aerosol properties (Dubovik et al., 2002; Dubovik et al., 2006). For this study, we used the daily-averaged level 2.0 quality-assured AOD (pre and post-field calibrated and manually inspected), obtained from the Version 2 Direct Sun Algorithm.

We select ‘dusty’ AERONET stations by only using stations for which our simulations indicate that over 50% of the annually-averaged AOD is due to dust aerosols (i.e., stations for which at least three of the four simulations find that over 50% of AOD is due to dust for the grid box in which the station is located; see Fig. S2). Furthermore, for each station, we select only days for which the Angstrom exponent α (in the 440-870 nm wavelength range) is smaller than 1 (Eck et al., 1999; Dubovik et al., 2002). Since α is a measure of particle size, with smaller values indicating coarser aerosols, values of $\alpha < 1$ indicate that a substantial fraction of AOD is due to dust (Eck et al., 1999; Dubovik et al., 2002), which is a relatively coarse aerosol. Choosing a different plausible cut-off for AE does not qualitatively affect our results. Finally, we select only stations for which at least 6 months of data (i.e., at least 183 days) is available over the simulation period.

The above procedure resulted in the selection of 42 ‘dusty’ AERONET stations: 18 in North Africa, 4 in the North Atlantic, 11 in the Middle East, 6 in the rest of Asia, and 3 in Australia (Figs. 3 – 5, S5). Comparisons between simulated and measured AOD at these stations is sensitive to the value of the parameter C_{tune} (see Eq. 1), which scales the size of the global dust cycle. Because of the many uncertainties in parameterizing dust emission on both small scales (Barchyn et al., 2014; Kok et al., 2014) and the much larger global model grid box scale (Cakmur et al., 2004), the value of C_{tune} is poorly constrained (Cakmur et al., 2006; Huneeus et al., 2011). We therefore choose the value of C_{tune} for each of the four simulations such that the bias vanishes. That is, we determine C_{tune} by forcing the average modeled optical depth at AERONET stations to equal the average observed optical depth:

$$\sum_{i}^{N} \tau_{\text{model},i} = \sum_{i}^{N} \tau_{\text{meas},i} , \qquad (8)$$

where i sums over the $N = 42$ ‘dusty’ AERONET stations, and τ_{model} is the AOD in the visible wavelength (550 nm) simulated at the AERONET station location, the component of which that is due to dust aerosols scales with C_{tune}. The measured AERONET AOD (τ_{meas}) is obtained at 550 nm, the central wavelength in the visible spectrum, by correcting the AOD measured at 675 nm to 550 nm using the measured value of the Angstrom exponent α. That is,

$$\tau_{\text{meas},i} = \tau_{675,i} \left(\frac{\lambda_{675}}{\lambda_{550}} \right)^{\alpha} \qquad (9)$$

where τ_{675} is the measured AOD at 675 nm, and λ_{550} and λ_{675} equal 550 and 675 nm, respectively.

We use the above procedure to generate three quantitative comparisons between the simulated and the measured AERONET AOD. First, we obtain the measured ‘climatological’ AOD for each station over the period of the model simulations (1995-2011) by averaging over all days for which AERONET data is available (subject to the quality-control criteria discussed above). For each station, we compare this average measured AOD to the simulated AOD averaged over the same days. Second, we obtain a comparison for the seasonal cycle of AOD by (i) calculating the measured monthly-averaged AOD for months with at least 10 days of data, (ii) calculating the corresponding simulated monthly AOD averaged over the same days, and (iii) averaging all simulated and modeled monthly-averaged AOD values for each of the 12 months in the year, and comparing them. And, third, we obtain a comparison between daily-averaged variations in AOD at each station. In order to prevent mismatches between model time and local time, we restrict the analysis of daily-averaged AOD variations to the 31 stations with longitude between 60W – 60E.

2.2.2. Satellite-derived estimates of dust mass path (DMP)

In addition to assessing the fidelity of the four different dust emission parameterizations through comparisons against AERONET AOD, we use recent satellite-derived estimates of dust optical depth and dust mass path (DMP; g/m^2) off the West African coast around Cape Verde by Evan et al. (2014). This study followed Kaufman et al. (2005) and Evan and Mukhopadhyay (2010) in separating the dust contribution to AOD from the (smaller) contributions of anthropogenic and marine aerosols for the long-term records of the Advanced Very High Resolution Radiometer (AVHRR) and the Moderate Resolution Imaging Spectroradiometer (MODIS) satellites. Evan et al. (2014) subsequently obtained the DMP by using the result of Kaufman et al. (2005) that a unit dust AOD corresponds to 2.7 ± 0.4 g/m^2 of suspended dust. Since DMP simulated at Cape Verde by climate models participating in the Climate Model Intercomparison Phase 5 (CIMP5) is strongly correlated to the simulated total North African emissions (Evan et al., 2014), and since the fraction of AOD contributed by dust in the study area exceeds the 50% threshold for which we consider the area 'dusty'(see Section 2.2.1 and Fig. S2), we use the dust AOD and the DMP off the West African coast as additional tests of the dust emission component of CESM.

2.3. Other measurements of the dust cycle

The measurement comparisons described in the previous section are designed to evaluate possible improvements in CESM's representation of dust emission. This section describes measurement comparisons to test whether such improvements propagate into an improved simulation of dust cycle properties further from source regions. Specifically, we compare the model results against measurements of dust surface concentration (Prospero and Nees, 1986) and deposition (Albani et al., 2014), which are generally taken far from source regions.

2.3.1. Surface concentration measurements

We compare the simulation results against a data set of dust concentration measurements at the surface. These data are a compilation of measurements taken in the North Atlantic during the Atmosphere-Ocean Chemistry Experiment (AEROCE; Arimoto et al. (1995)) and in the Pacific Ocean during the sea/air exchange program (SEAREX; Prospero et al. (1989)). Since the majority of these stations measure long-range transported dust, the ability of the model to reproduce these measurements depends on the accuracy of model parameterizations of several processes in addition to dust emission, including transport, and wet and dry deposition. We only use stations where CESM predicts at least some dust (> 0.05 $\mu g/m^3$ on an annual basis), such that the comparisons between the four simulations are meaningful. This results in a total of 15 stations (see Fig. S6).

The data sets from AEROCE and SEAREX were obtained by drawing large volumes of air through a filter when the wind was onshore and not very light (i.e., > 1 m/s); this was done to help reduce the effects of anthropogenic aerosols on the measurements (Prospero et al., 1989). The mineral dust fraction of the collected airborne particulates was determined either from their Al content (assumed to be 8%, corresponding to the Al abundance in the Earth's crust), or by burning the sample and assuming the ash residue to represent the mineral dust fraction (Prospero, 1999).

For each station, we first calculate the average dust concentration for each of the 12 months in the year using the data provided by Joseph Prospero to the AeroCom project (Joseph Prospero and Nicolas Huneeus, personal communication, 2014). We then calculate a 'climatological' average for each site by averaging over the seasonal cycle. We compare these measures to the seasonal cycle and 'climatological' dust concentration predicted by CESM over the period 1995 – 2011 (Table 2). We emphasize that, since the data of the AEROCE and SEAREX campaigns were taken for different dates at each site in the period 1981-2000, the 'climatology' derived from these measurements is for a different period than that of the model simulation, introducing systematic errors of unknown size. Similar comparisons in previous studies have suffered from the same problem (e.g., Huneeus et al. (2011); Albani et al. (2014); (Colarco et al., 2014)).

2.3.2. Deposition measurements

We further compare the simulation results against the data set of dust deposition measurements compiled by Albani et al. (2014), which consists of 110 stations. This compilation was produced by merging pre-existing datasets (Ginoux et al., 2001; Tegen et al., 2002; Lawrence and Neff, 2009; Mahowald et al., 2009), and retaining only measurements representative of modern climate (i.e., excluding sites representing a sediment flux integrated over hundreds or thousands of years). Furthermore, the size range of the measured deposition flux was adjusted to be consistent with the dust size range simulated in CESM of 0.1 – 10 μm (Albani et al., 2014).

Since the deposition fluxes represent an integration over long time scales (generally years to decades), we can only compare the global distribution of the deposition fluxes to those simulated by CESM, and cannot compare seasonal or daily variations. Specifically, we compare the measured annual deposition flux at each station against the mean annual deposition flux simulated by CESM with the various dust emission configurations over the period 1995 – 2011 (Table 1). As with the concentration comparison, the dates over which the measurements were obtained were by and large not coincident in time with the simulations, introducing systematic errors of unknown size. Furthermore, note that model representation of the dust deposition flux depends on the realistic simulation of a variety of processes. In addition to dust emission and transport, this notably includes wet and dry deposition, which is generally poorly captured by models (Huneeus et al., 2011).

2.4. Bootstrapping method to assess statistical significance of model improvements

We quantify the model performance for the range of comparisons outlined above by calculating the Pearson correlation coefficient r and the root mean square error (RMSE) (Bevington and Robinson, 2003; Wilks, 2011). An increase in r or a decrease in RMSE thus denotes an improvement in the model's ability to reproduce a given data set. To assess whether such an improvement is statistically significant, we use the *bootstrap method* (Efron, 1982). That is, we randomly select a number of samples from the 'distribution' of the observed data points, equal to the total number of data points. This is done with replacement, such that each data point can be chosen several times, or not at all. For each of the four simulations, we then calculate the value of r and RMSE for the model comparison with this randomly-chosen sample. By repeating this procedure a large number of times, the uncertainty of any arbitrary statistical measure can be estimated (Efron, 1982). In our case, we assess the significance of a model improvement by checking whether the statistical measure (r or RMSE) is improved for $\geq 95\%$ of the bootstrap samples, which is equivalent to the p-value of ≤ 0.05 generally used to represent statistical significance (e.g., Wilks (2011)). Table S2 lists the p-values of all comparisons between model results reported in Tables 1 and 2.

3. Results

This section presents the results of the four simulations. Below, we first present and qualitatively discuss the spatial patterns of the source functions, and the resulting dust emissions and dust AOD. Section 3.2 then reports the quantitative comparison of simulation results against aerosol optical depth measurements in dusty regions, after which Section 3.3 presents comparisons against dust cycle measurements further from source regions (i.e., dust concentration and deposition measurements).

3.1. The spatial patterns of source functions, dust emissions, and dust AOD

One of the objectives of the present study is to evaluate the hypothesis that use of the K14 scheme reduces the need for a source function in dust cycle simulations. We investigate this hypothesis by comparing the simulated spatial pattern of the dust emission coefficient C_d in K14, which scales the dust flux in Simulation IV, to the Zender et al. (2003b) and Ginoux et al. (2001) source functions (Figs. 2 and S3). As such, we interpret C_d as a physically-based and temporally-variable source function because C_d scales the dust emission flux in K14 in a manner that is similar (but not identical) to that of a source function (compare Eqs. 1 and 7a). We find that the large-scale spatial pattern of C_d, which is highly anti-correlated to the soil moisture content of the top soil layer (Fig. S4), is strikingly similar to that of the Ginoux et al. (2001) source function. That is, although Figs. 2b and 2c can show different patterns within source regions, both show a clear shift of emissions towards the "dust belt" of North Africa and the Middle East. In the case of Fig. 2b (Simulation III), this shift is empirically parameterized based on TOMS satellite observations (Ginoux et al., 2001). In contrast, in Fig. 2c (Simulation IV) this shift arises from the additional physics accounted for in K14 over Z03. Specifically, the shift of emissions to the most erodible regions arises from the greater sensitivity of the dust flux to the soil's threshold friction velocity (Fig. 1), which occurs because K14 accounts for a soil's increased ability to produce dust as it becomes more erodible.

The spatial patterns of the source functions and the dust emission coefficient C_d partially determine the dust flux (Figs. 3 and S2a-d), which in turn determines the dust optical depth (Figs. 4 and S2e-h). The simulation results show that application of a source function tends to shift dust emissions (Fig. 3) and dust AOD (Fig. 4) from less erodible regions, such as North America, to more erodible regions, such as North Africa. As hypothesized in our companion paper (Kok et al., 2014), and consistent with the similarity between C_d and the Ginoux et al. (2001) source function (Fig. 2), replacing Z03 with K14 has an effect that is similar to the application of an empirical source function. That is, it shifts emissions and dust AOD to the most erodible regions, producing increases in emissions and AOD over most of North Africa, and decreases over less erodible regions such as North America and Southern Africa (Figs. 3d, 4d). Moreover, K14 shifts dust AOD within North Africa westward, as well as southward towards the 15º – 25º N latitude belt. This appears to bring the simulations in better agreement with qualitative satellite observations of North African dust emitting regions (Prospero et al., 2002; Schepanski et al., 2009; Crouvi et al., 2012; Ginoux et al., 2012; Ashpole and Washington, 2013). Furthermore, applying K14 substantially increases dust emissions in Patagonia (Figs. 2c, 3d, and 4d), which in the default version of CESM needs to be increased by about two orders of magnitude to match available observations (Albani et al., 2014).

The simulation results further show that dust emissions depend quite differently on soil properties for the different dust emission schemes. In particular, the soil clay fraction f_{clay} has two competing effects, and the relative strength of these differ between the schemes. On the one hand, f_{clay} scales the threshold moisture content above which additional soil moisture increases the soil's threshold friction velocity (see Eq. 4), and on the other hand f_{clay} scales the dust emission flux (see Eq. 7a). Since the scaling of the dust flux with f_{clay} is exponential in Z03, it overwhelms the effect of f_{clay} on the threshold friction velocity, such that dust fluxes in Simulation I correlate strongly with f_{clay} (compare Figs. 3a and S1). In contrast, in the K14 scheme the dust flux scales merely linearly with f_{clay}, such that both effects of the clay fraction on the dust flux are important. Consequently, the effect of f_{clay} on dust emissions in K14 is not straightforward, and the map of Simulation IV's dust emission fluxes (Fig. S2d) does not show an obvious correlation with the map of the clay fraction (Fig. S1). However, because the strong exponential dependence of the dust flux on f_{clay} in Z03 is replaced by a linear dependence in K14, areas with low clay content, such as sand dunes, produce consistently more dust in Simulation IV than in Simulation I (compare Figs. 3d and S1). This brings the results of Simulation IV in better qualitative agreement with the observation by Crouvi et al. (2012) that a large fraction of North African dust plumes originate from sand dunes. Furthermore, since CESM does not use a map of the spatially variable aerodynamic roughness length to more accurately calculate the aerodynamic drag on the bare (erodible) soil, it is likely that improving the model by using such a map (Laurent et al., 2008; Menut et al., 2013) would produce even higher fluxes in regions covered in sand dunes, since these regions tend to have low roughness length.

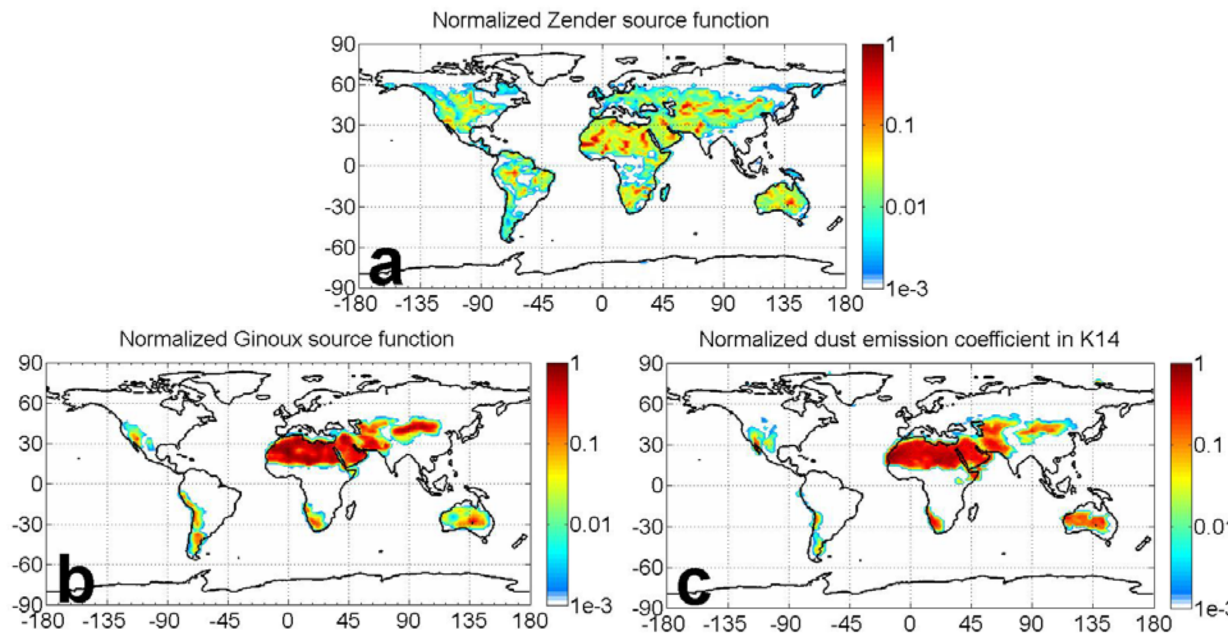

Figure 2. Global maps of (**a**) the Zender et al. (2003b) geomorphic source function used in Simulation II, (**b**) the Ginoux et al. (2001) source function used in Simulation III, and (**c**) the K14 dust emission coefficient C_d (see Eq. 7b) averaged over the model run (1995 – 2011). The seasonal cycle of C_d is reported in Fig. S3. Since the Ginoux et al. (2001) source function inherently includes the fraction of the grid cell that consists of bare soil, both the Zender et al. (2003b) source function and the dust emission coefficient C_d were multiplied by the grid cell's bare soil fraction (see Eq. 5). To further facilitate comparison, the source functions and C_d are each normalized by their highest occurrence in any of the grid boxes.

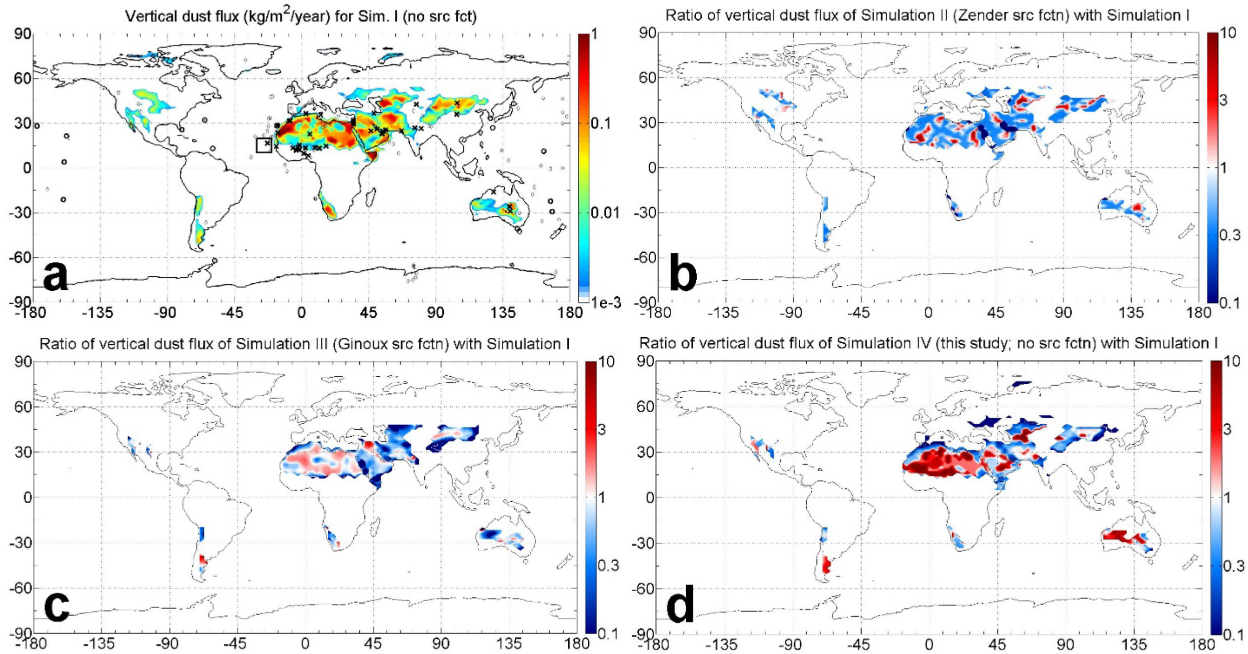

Figure 3. Global maps of (**a**) the simulated vertical dust flux for Simulation I and (**b - d**) the ratios of the dust flux in Simulations II – IV to the flux in Simulation I. Red (blue) coloring in panels (**b**) – (**d**) denotes increases (decreases) in dust emission fluxes relative to the 'control' (Simulation I). In panel (**a**), crosses, circles, and diamonds respectively mark the locations of measurements of AERONET AOD, dust surface concentration, and dust deposition flux. The square denotes the area off the West African coast for which the satellite-derived dust AOD and DMP were used.

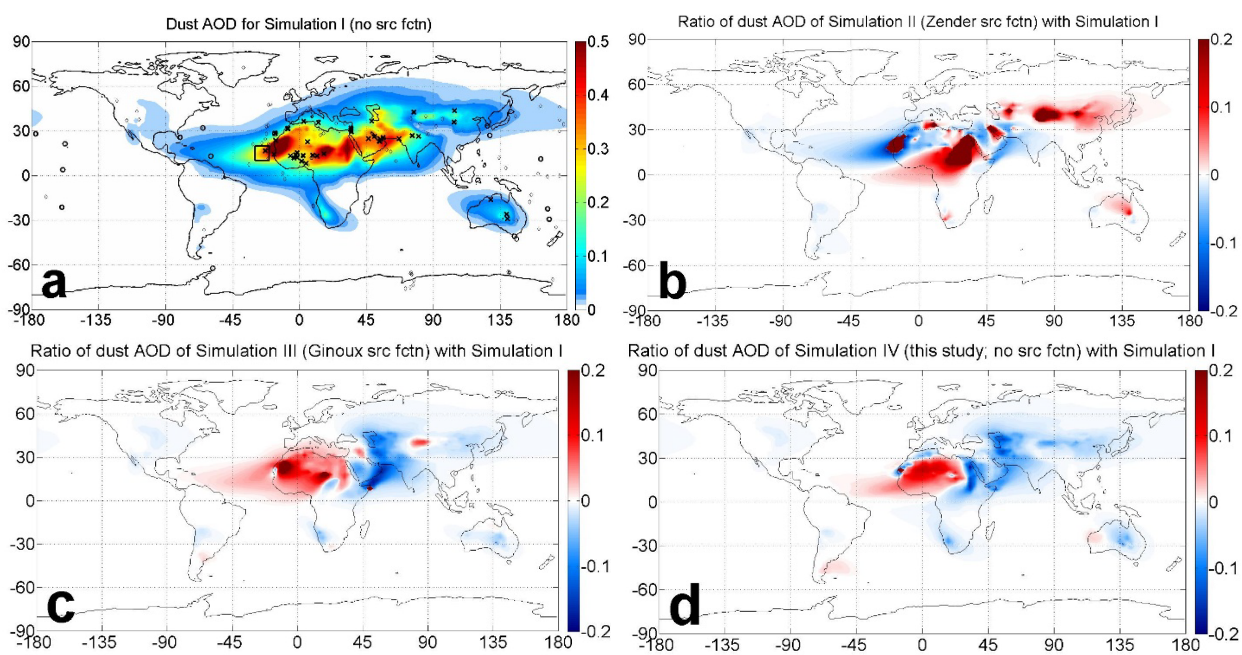

Figure 4. Global maps of (**a**) the dust aerosol optical depth (AOD) of Simulation I, and (**b - d**) the difference of dust AOD of Simulations II – IV with that of Simulation I. Red shading denotes

increases in dust AOD relative to the 'control' (Simulation I). Black symbols in panel (**a**) are as defined in Fig. 3.

3.2. Measurement comparisons evaluating CESM's representation of dust emission

3.2.1. AOD climatology

As discussed previously, the data sets of AOD at the 42 'dusty' AERONET stations (see Section 2.2.1) are arguably the most reliable currently available data to quantitatively evaluate the dust emission components of large-scale models. We therefore perform an extensive comparison against the AERONET AOD data sets (Table 1 and Figs. 5, S5). As expected, the application of the source functions of both Zender et al. (2003b) and Ginoux et al. (2001) improve model agreement against the average ('climatological') AERONET AOD data (Figs. 5a-c). However, a substantially larger and statistically significant improvement is obtained with Simulation IV, which uses the K14 scheme and does not use a source function (Fig. 5d and Table 1). In particular, Simulation IV produces improved agreement over North Africa, the Middle East, and Australia, and somewhat lesser agreement over Asia.

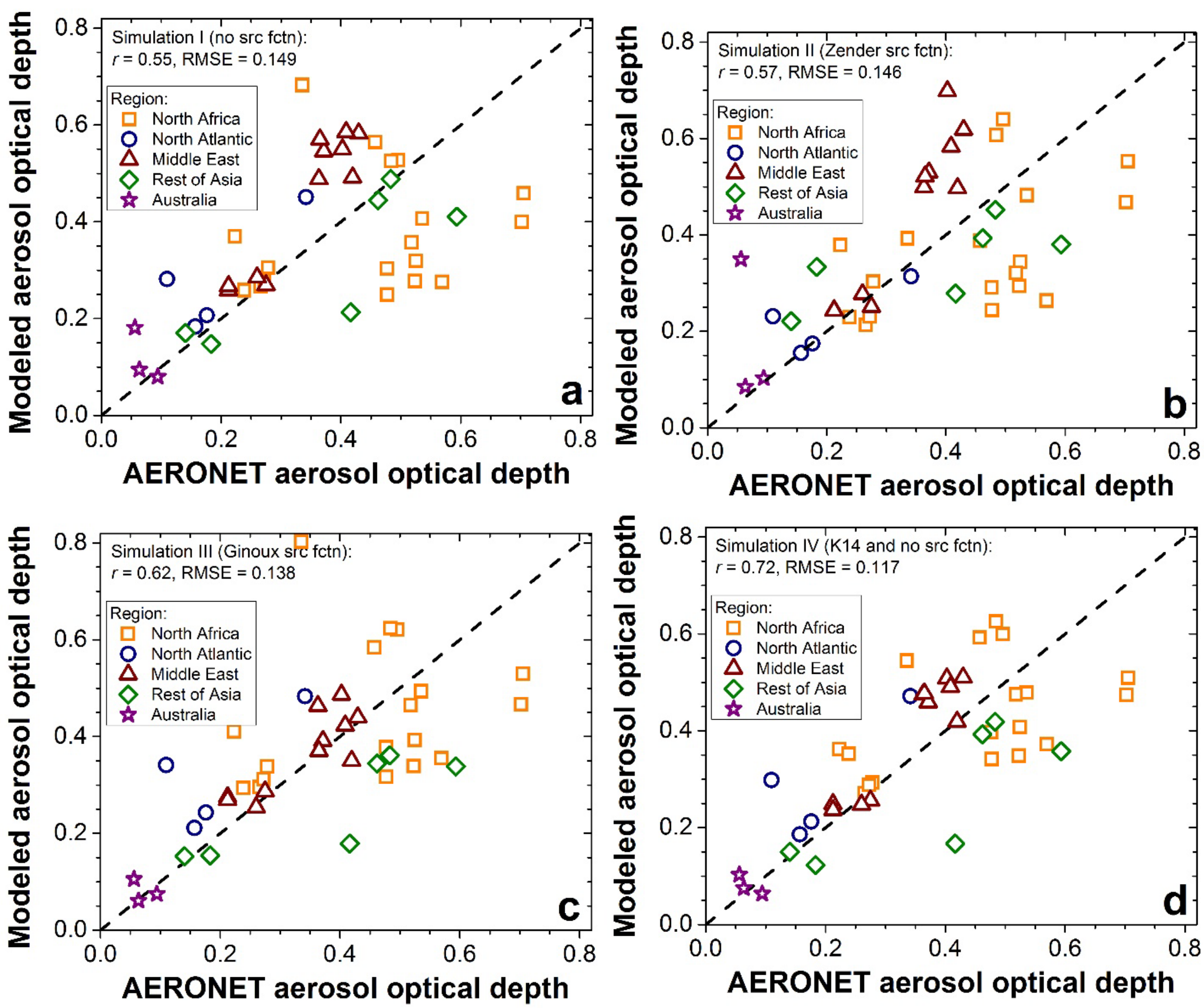

Figure 5. Comparison of measured and modeled aerosol optical depth (AOD) at 42 dust-dominated AERONET stations. Results are shown for (**a**) Simulation I (no source function), (**b**) Simulation II (Zender et al. (2003b) geomorphic source function), (**c**) Simulation III (Ginoux et al. (2001) source function), and (**d**) Simulation IV (no source function, and dust flux is parameterized following K14 instead of Z03). For each simulation, the root mean square error (RMSE) and correlation coefficient (*r*) are noted.

3.2.2. AERONET AOD seasonal cycle and daily variability

In addition to improving the representation of AOD climatology, applying K14 also produces a statistically significant improvement of CESM's simulation of the seasonal AOD cycle at the AERONET stations (Fig. S5 and Table 1). Indeed, Simulation IV produces the best seasonal agreement for 25 of the 42 AERONET stations, including 15 of the 18 North African stations (Fig. S5). However, the influence of changes in the emission scheme on seasonal variability appears limited: for a given station, the standard deviation of the four correlations produced by the four different simulations is on average only 0.05, which is only a small fraction of the mean correlation coefficient of ~0.80 (Table 1). This indicates a limited influence of the emission scheme on the seasonal variability of AOD, which is likely primarily controlled by seasonal variations in soil moisture, wind, and vegetative soil cover. Consequently, the statistically significant improvement in Simulation IV's ability to reproduce the seasonal cycle of dust AOD results in only a modest improvement in the correlation coefficient (Table 1).

The comparison of model results to the measured daily variability of dust AOD at the different AERONET stations produces results that are qualitatively similar to those for the seasonal cycle. That is, Simulation IV again produces a statistically significant improvement in the model's ability to reproduce the daily AOD variability (Table 1), and produces best agreement at 18 of the 31 available stations, including 13 of the 18 North African stations. However, the emission scheme appears to also have limited influence on the daily AOD variability, which is probably largely controlled by the daily variations in wind speed and in soil moisture, which controls the dust emission threshold (see Section 2.1.1). Indeed, for a given station, the standard deviation of the four correlations produced by the four different simulations is on average only 0.03, which is only a small fraction of the mean correlation coefficient for daily variability of ~0.45 (Table 1). Consequently, the absolute improvement in the correlation coefficient produced by the statistically significant improvement in the model's ability to capture daily variability in the AOD is again modest (Table 1).

3.2.3. Dust optical depth and dust mass path off the West African coast

Evan et al. (2014) analyzed satellite data to estimate both the dust optical depth and the dust column mass path (DMP) off the West African coast over the region of 10º-20º N, 20º-30º W around Cape Verde. They found that most models that participated in the Coupled Model Intercomparison Project Phase 5 (CMIP5) underestimated the dust optical depth for this region, and that all models substantially underestimated the dust mass path. We find that the dust optical depth in Simulations I, III, and IV are close to the satellite estimates, and that all four simulations produce a DMP that is in better agreement with the satellite estimates than that of the CMIP5 models, which includes a previous version of CESM (Fig. 6). As already suggested by Evan et al. (2014), these improvements most likely occur because our newer CESM version uses the size distribution of Kok (2011b), which corrects a bias towards fine dust aerosols in most large-scale models. Consequently, using this size distribution results in a higher dust mass path per unit of dust AOD, which is in better agreement with measurements.

Although all four simulations are in better agreement with the Evan et al. (2014) estimates of DMP than the CMIP5 models, Simulations I and II still underestimate the DMP, whereas Simulations III and IV are consistent with the lower uncertainty range of the satellite estimates. The likely reason for the improved performance of Simulations III and IV is that these simulations shift emissions towards West Africa (see Figs. 2 – 4), resulting in a higher, and thus more realistic, value of DMP off the West African coast.

Note that the simulated values of DMP and the dust AOD in Fig. 6 both depend on the tuning constant C_{tune} scaling the dust emissions (see Eqs. 1 and 8). It's thus possible to obtain better agreement with these measures by choosing a different method to set C_{tune}, although doing so would degrade the model's comparison against AERONET AOD (Figs. 5, S5). Also note that the dust optical depth and dust emissions are sensitive to dust radiative effects and dust optical properties (Perlwitz et al., 2001; Albani et al., 2014).

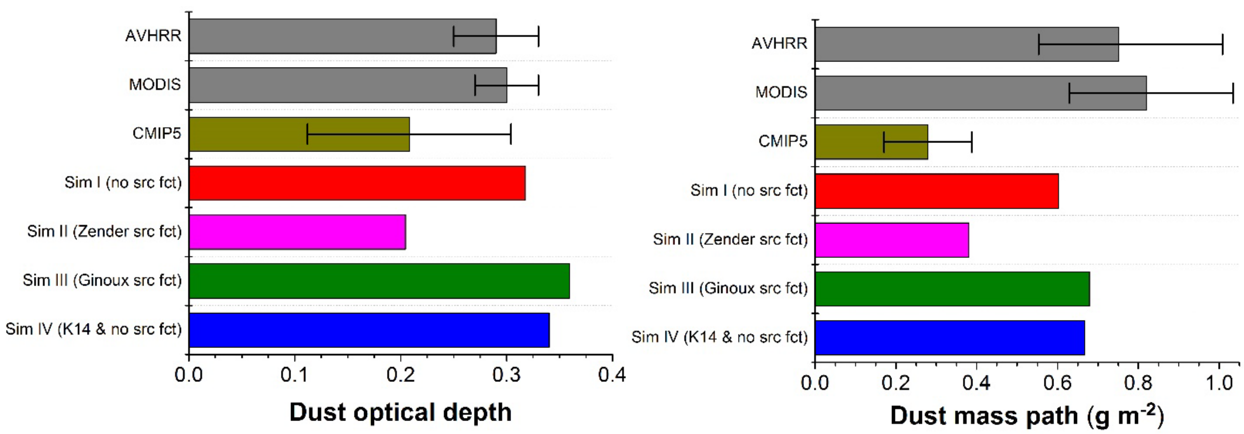

Figure 6. Dust optical depth (left) and dust mass path (right) averaged over the region 10˚-20˚ N and 20˚-30˚ W. Satellite-derived estimates for AVHRR (1982-2005) and MODIS (2001-2012), as well as the ensemble average of CMIP5 models (1982-2005), are from Evan et al. (2014). Error bars denote the uncertainty on the satellite estimates, and the standard deviation of the available CMIP5 model results (23 models for the dust optical depth, and 11 models for the dust mass path; see Evan et al. (2014)). The dust optical depth and dust mass paths calculated from the four CESM simulations were averaged over the period 2001 – 2011 to be most comparable to the MODIS results.

3.3. Comparisons against other measurements of the dust cycle

The previous section evaluated possible improvements in CESM's representation of dust emission through comparisons against measurements of aerosol optical depth close to source regions. In this section, we evaluate whether these improvements propagate into the simulation of other dust cycle properties further from source regions. Specifically, we compare the simulation results against measurements of dust surface concentration and deposition, which are generally taken further from source regions (Table 2). We find that Simulation IV, which uses the K14 scheme, produces a statistically insignificant improvement against both the surface dust concentration climatology and seasonal cycle (Figs. 7 and S6). We also find that Simulation IV produces agreement against dust deposition flux measurements that is slightly less than that of the other simulations (Fig. 8).

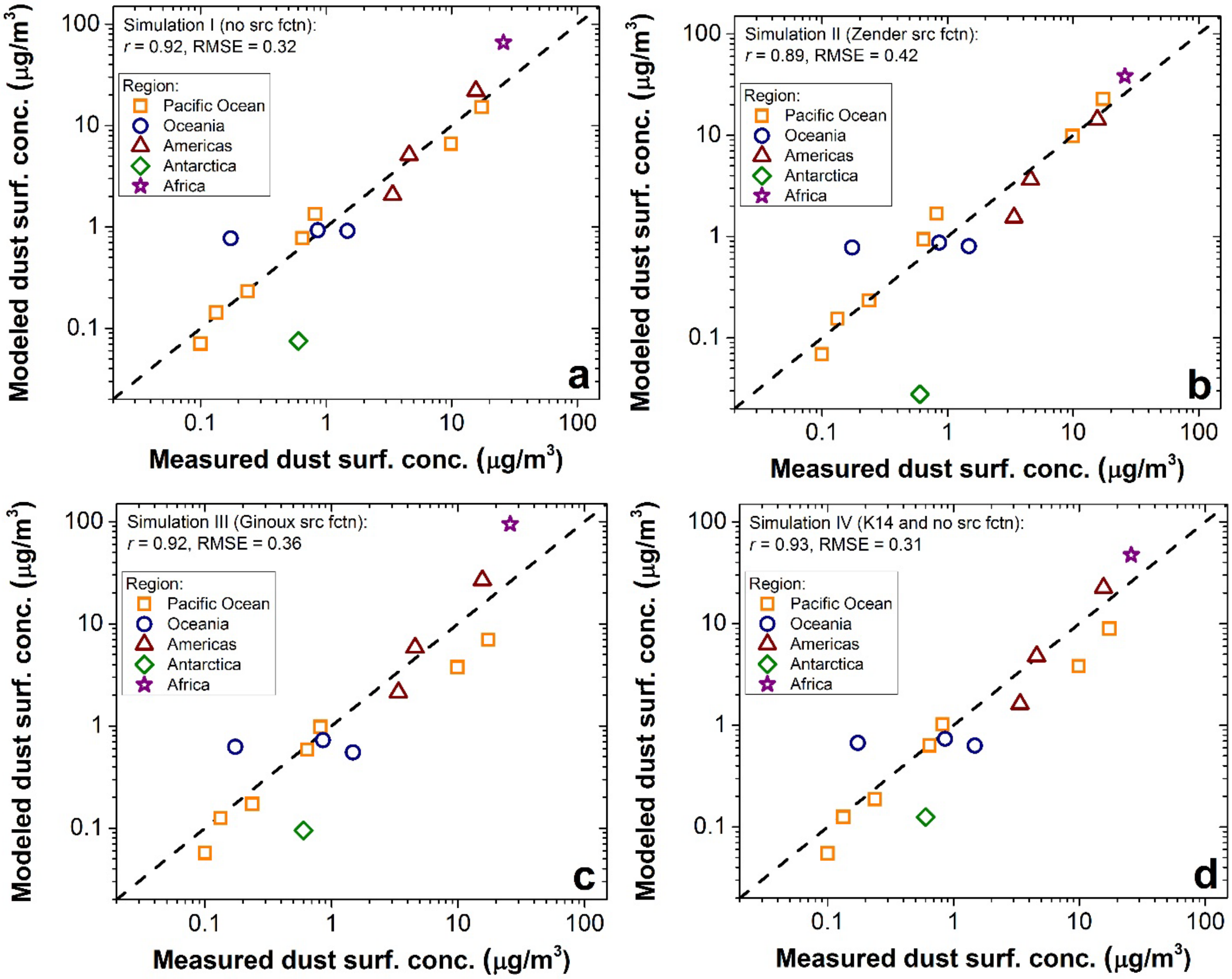

Figure 7: Comparison of the annually-averaged modeled dust surface concentration with that measured at 15 stations (see Section 2.3.1). Results are shown for (**a**) Simulation I (no source function), (**b**) Simulation II (Zender et al. (2003b) source function), (**c**) Simulation III (Ginoux et al. (2001) source function), and (**d**) Simulation IV (no source function, and dust flux is parameterized following K14 instead of Z03). For each panel, the root mean square error (RMSE) and correlation coefficient (r) in log10-space are noted.

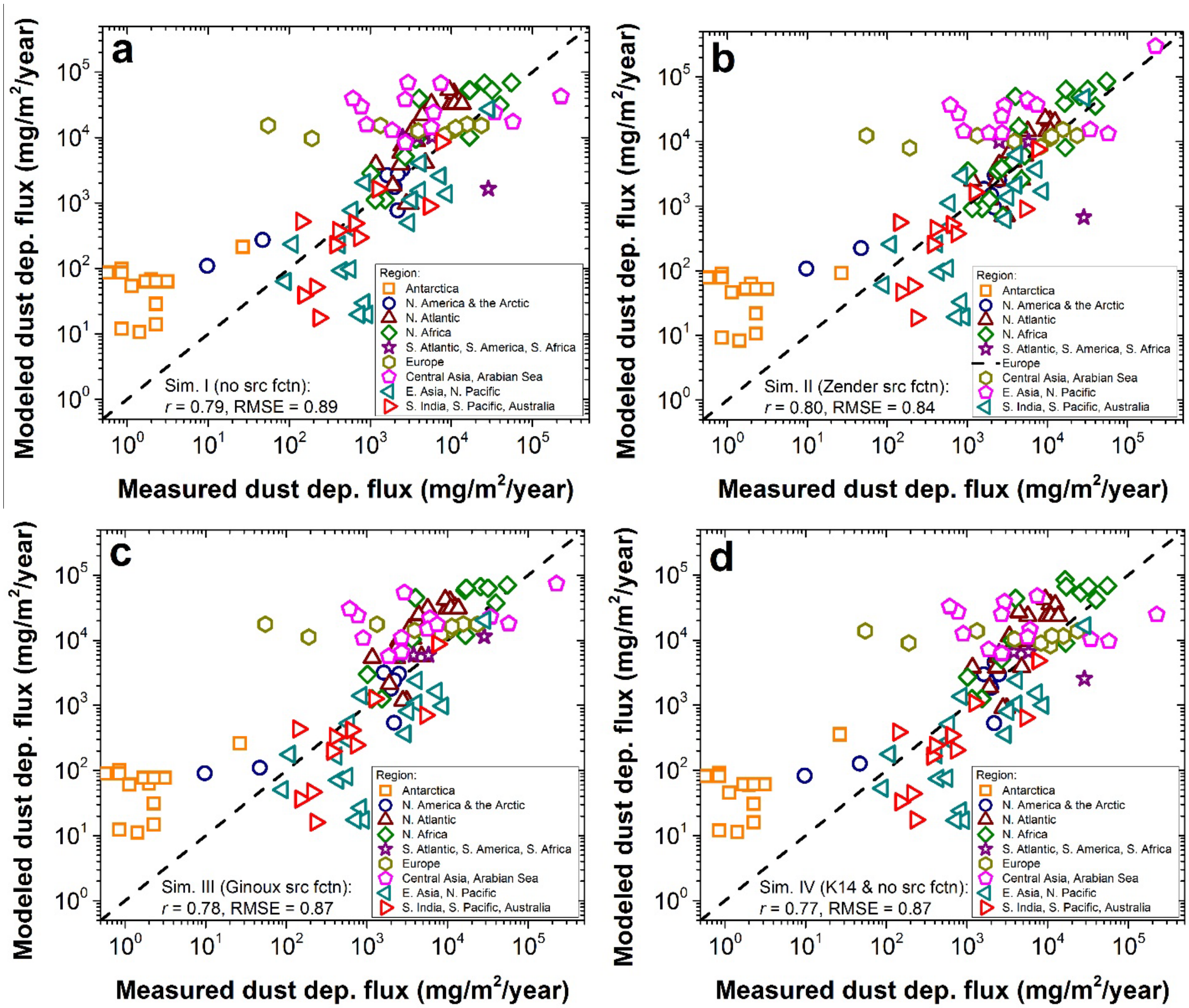

Figure 8: Comparison of the modeled dust deposition flux with that measured at 110 stations (see Section 2.3.2). Results are shown for (**a**) Simulation I (no source function), (**b**) Simulation II (Zender et al. (2003b) source function), (**c**) Simulation III (Ginoux et al. (2001) source function), and (**d**) Simulation IV (no source function, and dust flux is parameterized following K14 instead of Z03). For each panel, the root mean square error (RMSE) and correlation coefficient (*r*) in log10-space are noted.

Table 2. Statistics of the comparison of the four CESM simulations against data sets taken further from source regions, namely dust surface concentration measurements and dust deposition fluxes. Simulations and measurements are compared with respect to their climatology for both data sets and their seasonal cycle for the surface concentration. Statistically significant improvements (see Section 2.4) of Simulations II-IV relative to the 'control' Simulation I are indicated with bold font. Additionally, simulation results that are statistically significantly improved over the results of each of the other three simulations are both bold and underlined.

Simulation	**Dust flux parameter-ization**	**Dust source function**	**Surf. conc. climatology, *r***	**Surf. conc. climatology, RMSE**	**Surf. conc. seasonal cycle, *r***	**Dep. flux climatology, *r***	**Dep. flux climatology, RMSE**

I	Zender et al. (2003a)	None	0.92	0.32	0.62	0.79	0.88
II	Zender et al. (2003a)	Zender et al. (2003b)	0.88	0.42	0.61	**0.80**	**<u>0.84</u>**
III	Zender et al. (2003a)	Ginoux et al. (2001)	0.92	0.36	0.63	0.78	0.87
IV	Kok et al. (2014)	None	0.93	0.31	0.63	0.77	0.87

4. Discussion

The simulations reported in the previous section were designed to (i) evaluate the performance of the K14 dust emission scheme in CESM, and (ii) test the hypothesis in Kok et al. (2014) that the K14 scheme reduces the need to use a source function in dust cycle simulations. The next two sections discuss these two objectives, after which we discuss the implications of our results for the dust cycle's sensitivity to climate changes.

4.1. Evaluation of the K14 dust emission scheme in CESM

Relative to the 'control' (Sim. I), the simulation using K14 (Sim. IV) shows statistically significant improvements against measurements most characteristic of dust emission, namely (i) AERONET AOD climatology (Fig. 5), (ii) variations in AERONET AOD on daily and seasonal timescales (Table 1 and Fig. S5), and (iii) satellite-derived estimates of dust optical depth and dust mass path off the West African coast (Fig. 6). The representation of dust emission in Simulation IV is also statistically significantly improved over the simulations using either the Zender et al. (2003b) or the Ginoux et al. (2001) source function.

We find that the improvement in CESM's dust emission module by the K14 scheme does not propagate into a statistically significant improvement of the model's ability to reproduce surface measurements of dust concentration (Figs. 7 and S6), or of dust deposition (Fig. 8). Since most stations in these data sets are far from source regions, this indicates that the improvement in CESM's dust emission scheme does not produce comparable improvements in simulated dust cycle properties further from source regions. This could be caused by model errors in other processes, particularly in dust transport and deposition. This is especially likely to explain the lack of improvement in the simulated dust deposition fluxes, which is known to be subject to large model errors (Huneeus et al., 2011). In addition, it is possible that tuning of parameters describing processes such as transport and deposition in previous model versions (e.g., Albani et al. (2014)) degrades the model performance with the new K14 parameterization.

4.2. Does the K14 scheme reduce the need to use a dust source function?

The main reason for the improved representation of dust emissions with K14 is likely that this scheme accounts for a soil's increased ability to produce dust as its erodibility increases (Kok et al., 2014). This results in an increased sensitivity of the dust flux to a soil's standardized dust emission threshold (Fig. 1), which quantifies a soil's susceptibility to wind erosion. Since the dust emission threshold in CESM is parameterized mainly in terms of soil moisture, the dust emission coefficient in the K14 scheme (Fig. 2c) is strongly anti-correlated with soil moisture (Fig. S4). Consequently, relative to the 'control' simulation with the Z03 scheme, the simulation with K14 produces a shift of emissions and dust AOD to hyper-arid - and thus typically highly erodible - regions such as North Africa (Figs. 2c, 3d, 4d). This effect is remarkably similar to that of applying the Ginoux et al. (2001) source function (Figs. 2b, 3c, 4c), which was developed to shift emissions to regions with high dust loadings observed by the TOMS satellite (Prospero et al., 2002). This similarity between the effects of the K14 scheme and the Ginoux et al. (2001) source function suggests that the K14 scheme replaces some of the empiricism introduced by this source function with an improved description of the physics of dust emission.

The K14 scheme thus reduces, or even eliminates, the need to use a source function in CESM. Although further work is needed to investigate whether the K14 scheme produces similar improvements in other large-scale models, the additional dust emission physics accounted for in K14 could aid in moving dust modules beyond the widespread use of empirical source functions. Such a transition towards a more physically-explicit treatment of dust emission is necessary for better understanding past and forecasting future changes in the global dust cycle: although empirical descriptions of dust emission can work well for the current climate, such descriptions are unlikely to accurately capture the effect of climate-driven changes in soil erodibility and other relevant factors.

Note that parallel efforts to improve the fidelity of dust modules might also help to reduce the reliance on empirical source functions in dust cycle simulations. Indeed, since many source functions were formulated for models that did not account for the spatial variability of the aerodynamic roughness length (Ginoux et al., 2001; Tegen et al., 2002; Zender et al., 2003b), the use of drag partition schemes employing high-resolution maps of roughness length (Laurent et al., 2008; Chappell et al., 2010; Menut et al., 2013) might be particularly effective. In addition, a more accurate description of the land surface through higher resolution and more detailed soil data sets could further reduce the reliance on empirical parameterizations in dust modules.

4.3. Implications for the dust cycle's sensitivity to climate changes

An important result from Kok et al. (2014) is that current parameterizations in climate models likely underestimate the dust flux's sensitivity to the soil's threshold friction velocity, which is further supported by the results presented here (Figs. 1 - 4). This underestimation might have important implications for evaluating the global dust cycle's response to climate changes. In particular, since soil erodibility is affected by climate, which partially determines the soil moisture content, aggregation state, and crusting of the soil (Zobeck, 1991; Kok et al., 2012), our results here and in Kok et al. (2014) suggest that many climate models underestimate the dust cycle's climate sensitivity.

This result could help explain a series of observations. For instance, climate models have difficulty reproducing the increase in North African dust emissions during the Sahel drought in the 1980s (Mahowald et al., 2002; Evan et al., 2014; Ridley et al., 2014), which is likely partially due to the underestimation of the dust flux's sensitivity to drought conditions (Fig. 1). Furthermore, an increased sensitivity of dust emissions to climate changes could help explain the large differences in the global dust cycle between different climates, such as the much larger dust deposition fluxes measured for the Last Glacial Maximum (Rea, 1994; Harrison et al., 2001), which climate models also have difficulty reproducing without positing large changes in source areas (Werner et al., 2002; Mahowald et al., 2006b).

5. Summary and Conclusions

We used CESM simulations to both evaluate the performance of the K14 dust emission scheme developed in the companion paper (Kok et al., 2014), and to test the hypothesis that the K14 scheme reduces the need to use an empirical source function in dust cycle simulations.

We find that implementing the K14 scheme has an effect that is strikingly similar to that of implementing the Ginoux et al. (2001) source function. That is, it shifts emissions and dust AOD towards the most erodible regions, especially North Africa (Figs. 2- 4). Indeed, the spatial pattern of the dust emission coefficient C_d, which scales the dust flux in K14 using only the dust emission threshold and can thus be interpreted as a physically-based and dynamic source function, is remarkably similar to that of the Ginoux et al. (2001) source function (Fig. 2). We further find that the K14 scheme improves CESM's representation of dust emission, as evidenced by statistically significant improvements of the model's ability to reproduce AERONET AOD measurements in dusty regions (Table 1, Figs. 5, S5) and satellite observations of dust optical depth and dust mass path off the West African coast (Fig. 6). These improvement substantially exceed those produced by implementing either the Zender et al. (2003b) or the Ginoux et al. (2001) source functions.

These results suggest that the K14 scheme replaces some of the empiricism introduced by the use of a source function with an improved description of the physics of dust emission. As such, the K14 scheme reduces, or even eliminates, the need to use a source function in dust cycle simulations in CESM. Further work is required to investigate whether the K14 scheme can similarly improve other large-scale models.

Our results further suggest that many large-scale models have used source functions to empirically account for a part of the sensitivity of the dust flux to the soil threshold friction velocity (Figs. 1 – 4). Because climate changes affect this dust emission threshold, for instance by affecting the soil moisture content and soil aggregation (Zobeck, 1991; Fecan et al., 1999; Shao, 2008; Kok et al., 2012), many models might underestimate the dust cycle's sensitivity to climate changes. Since the K14 scheme accounts for this missing component of the dust flux' sensitivity to the soil threshold friction velocity, namely the effect that a more erodible soil will produce more dust per saltator impact (Kok et al., 2014), we expect that it can improve the accuracy of dust cycle simulations for past and future climates.

Accounting for the dust flux's increased sensitivity to the soil state will thus affect simulations of the global dust cycle's response to future climate changes. In particular, since arid regions are generally predicted to become drier in most climate models (Solomon et al., 2007), accounting for the dust flux' increased sensitivity to the soil threshold friction velocity would likely produce an increase in the future global dust emission rate, and thus in the global dust radiative forcing, relative to simulations that do not account for this. Since the dust cycle is sensitive to a variety of processes, including CO_2 fertilization (Mahowald et al., 2006b), land use change (Ginoux et al., 2012), and changes in sediment availability (Harrison et al., 2001), a substantial body of further work is required to assess the dust cycle's response to future climate changes.

Acknowledgments

We thank two anonymous referees, the editor Yves Balkanski, and Shanna Shaked for helpful comments that improved the manuscript. We also gratefully acknowledge Joseph Prosperoand Nicolas Huneeus for providing dust surface concentration data from in situ measurements from the University of Miami Ocean Aerosol Network. We further thank the AERONET principal investigators and their staff for establishing and maintaining the 42 sites used in this investigation. This work was supported by the National Science Foundation (NSF) under grant numbers 0932946, 1137716, and 1358621. The CESM simulations were conducted at the National Center for Atmospheric Research's Computation Information Systems Laboratory, an NSF-funded facility.

References

Albani, S., Mahowald, N. M., Perry, A. T., Scanza, R. A., Zender, C. S., Heavens, N. G., Maggi, V., Kok, J. F., and Otto-Bliesner, B. L.: Improved dust representation in the Community Atmosphere Model, J. Adv. Model. Earth Syst., doi: 10.1002/2013MS000279, 2014. 2014.

Andronache, C.: Estimated variability of below-cloud aerosol removal by rainfall for observed aerosol size distributions, Atmospheric Chemistry and Physics, 3, 131-143, 2003.

Arimoto, R., Duce, R. A., Ray, B. J., Ellis, W. G., Cullen, J. D., and Merrill, J. T.: Trace-elements in the atmosphere over the north-atlantic, Journal of Geophysical Research-Atmospheres, 100, 1199-1213, 1995.

Ashpole, I. and Washington, R.: A new high-resolution central and western Saharan summertime dust source map from automated satellite dust plume tracking, Journal of Geophysical Research-Atmospheres, 118, 6981-6995, 2013.

Balkanski, Y. J., Jacob, D. J., Gardner, G. M., Graustein, W. C., and Turekian, K. K.: Transport and residence times of tropospheric aerosols inferred from a global 3-dimensional simulation of pb-210, Journal of Geophysical Research-Atmospheres, 98, 20573-20586, 1993.

Barchyn, T. E., Martin, R., Kok, J., and Hugenholtz, C. H.: Fundamental mismatches between measurements and models in aeolian sediment transport prediction: The role of small-scale variability, Aeolian Research, in press, 2014.

Bevington, P. R. and Robinson, D. K.: Data reduction and error analysis, McGraw-Hill, New York, 2003.

Cakmur, R. V., Miller, R. L., Perlwitz, J., Geogdzhayev, I. V., Ginoux, P., Koch, D., Kohfeld, K. E., Tegen, I., and Zender, C. S.: Constraining the magnitude of the global dust cycle by minimizing the difference between a model and observations, Journal of Geophysical Research-Atmospheres, 111, D06207, 2006.

Cakmur, R. V., Miller, R. L., and Torres, O.: Incorporating the effect of small-scale circulations upon dust emission in an atmospheric general circulation model, Journal of Geophysical Research-Atmospheres, 109, 2004.

Chappell, A., Van Pelt, S., Zobeck, T., and Dong, Z. B.: Estimating aerodynamic resistance of rough surfaces using angular reflectance, Remote Sensing of Environment, 114, 1462-1470, 2010.

Claquin, T., Schulz, M., and Balkanski, Y. J.: Modeling the mineralogy of atmospheric dust sources, Journal of Geophysical Research-Atmospheres, 104, 22243-22256, 1999.

Colarco, P. R., Nowottnick, E. P., Randles, C. A., Yi, B. Q., Yang, P., Kim, K. M., Smith, J. A., and Bardeen, C. G.: Impact of radiatively interactive dust aerosols in the NASA GEOS-5 climate model: Sensitivity to dust particle shape and refractive index, Journal of Geophysical Research-Atmospheres, 119, 753-786, 2014.

Crouvi, O., Schepanski, K., Amit, R., Gillespie, A. R., and Enzel, Y.: Multiple dust sources in the Sahara Desert: The importance of sand dunes, Geophysical Research Letters, 39, 2012.

Dee, D. P., Uppala, S. M., Simmons, A. J., Berrisford, P., Poli, P., Kobayashi, S., Andrae, U., Balmaseda, M. A., Balsamo, G., Bauer, P., Bechtold, P., Beljaars, A. C. M., van de Berg, L., Bidlot, J., Bormann, N., Delsol, C., Dragani, R., Fuentes, M., Geer, A. J., Haimberger, L., Healy, S. B., Hersbach, H., Holm, E. V., Isaksen, L., Kallberg, P., Kohler, M., Matricardi, M., McNally, A. P., Monge-Sanz, B. M., Morcrette, J. J., Park, B. K., Peubey, C., de Rosnay, P., Tavolato, C., Thepaut, J. N., and Vitart, F.: The ERA-Interim reanalysis: configuration and performance of the data assimilation system, Quarterly Journal of the Royal Meteorological Society, 137, 553-597, 2011.

Dubovik, O., Holben, B., Eck, T. F., Smirnov, A., Kaufman, Y. J., King, M. D., Tanre, D., and Slutsker, I.: Variability of absorption and optical properties of key aerosol types observed in worldwide locations, J. Atmos. Sci., 59, 590-608, 2002.

Dubovik, O., Sinyuk, A., Lapyonok, T., Holben, B. N., Mishchenko, M., Yang, P., Eck, T. F., Volten, H., Munoz, O., Veihelmann, B., van der Zande, W. J., Leon, J. F., Sorokin, M., and Slutsker, I.: Application of spheroid models to account for aerosol particle nonsphericity in remote sensing of desert dust, Journal of Geophysical Research-Atmospheres, 111, D11208, 2006.

Eck, T. F., Holben, B. N., Reid, J. S., Dubovik, O., Smirnov, A., O'Neill, N. T., Slutsker, I., and Kinne, S.: Wavelength dependence of the optical depth of biomass burning, urban, and desert dust aerosols, Journal of Geophysical Research-Atmospheres, 104, 31333-31349, 1999.

Efron, B.: The jackknife, the bootstrap, and other resampling plans, Capital City Press, Montpelier, Vermont, 1982.

Evan, A. T., Flamant, C., Fiedler, S., and Doherty, O.: An analysis of aeolian dust in climate models, Geophysical Research Letters, doi: 10.1002/2014GL060545, 2014. 2014.

Evan, A. T. and Mukhopadhyay, S.: African Dust over the Northern Tropical Atlantic: 1955-2008, Journal of Applied Meteorology and Climatology, 49, 2213-2229, 2010.

FAO: Harmonized World Soil Database (version 1.2), FAO, Rome, Italy and IIASA, Laxenburg, Austria, 2012.

Fecan, F., Marticorena, B., and Bergametti, G.: Parametrization of the increase of the aeolian erosion threshold wind friction velocity due to soil moisture for arid and semi-arid areas, Ann Geophys-Atm Hydr, 17, 149-157, 1999.

Forster, P., Ramaswamy, V., Artaxo, P., Berntsen, T., Betts, R., Fahey, D. W., Haywood, J., Lean, J., Lowe, D. C., Myhre, G., Nganga, J., Prinn, R., Raga, G., Schulz, M., and Dorland, R. V.: Changes in Atmospheric Constituents and in Radiative Forcing. In: Climate Change 2007: The Physical Science Basis., Solomon, S., D. Qin, M. Manning, Z. Chen, M. Marquis, K.B. Averyt, M.Tignor and H.L. Miller (Ed.), Cambridge University Press, Cambridge, United Kingdom and New York, NY, USA, 2007.

Gillette, D. A.: Environmental factors affecting dust emission by wind erosion. In: Saharan dust, Morales, C. (Ed.), Wiley, New York, 1979.

Gillette, D. A. and Passi, R.: Modeling dust emission caused by wind erosion, Journal of Geophysical Research-Atmospheres, 93, 14233-14242, 1988.

Ginoux, P., Chin, M., Tegen, I., Prospero, J. M., Holben, B., Dubovik, O., and Lin, S. J.: Sources and distributions of dust aerosols simulated with the GOCART model, J. Geophys. Res., 106, 20255-20273, 2001.

Ginoux, P., Prospero, J. M., Gill, T. E., Hsu, N. C., and Zhao, M.: Global-scale attribution of anthropogenic and natural dust sources and their emission rates based on MODIS Deep Blue aerosol products, Reviews of Geophysics, 50, Rg3005, 2012.

Grini, A., Myhre, G., Zender, C. S., and Isaksen, I. S. A.: Model simulations of dust sources and transport in the global atmosphere: Effects of soil erodibility and wind speed variability, Journal of Geophysical Research-Atmospheres, 110, 2005.

Harrison, S. P., Kohfeld, K. E., Roelandt, C., and Claquin, T.: The role of dust in climate changes today, at the last glacial maximum and in the future, Earth-Sci. Rev., 54, 43-80, 2001.

Holben, B. N., Eck, T. F., Slutsker, I., Tanre, D., Buis, J. P., Setzer, A., Vermote, E., Reagan, J. A., Kaufman, Y. J., Nakajima, T., Lavenu, F., Jankowiak, I., and Smirnov, A.: AERONET - A

federated instrument network and data archive for aerosol characterization, Remote Sensing of Environment, 66, 1-16, 1998.
Huneeus, N., Schulz, M., Balkanski, Y., Griesfeller, J., Prospero, J., Kinne, S., Bauer, S., Boucher, O., Chin, M., Dentener, F., Diehl, T., Easter, R., Fillmore, D., Ghan, S., Ginoux, P., Grini, A., Horowitz, L., Koch, D., Krol, M. C., Landing, W., Liu, X., Mahowald, N., Miller, R., Morcrette, J. J., Myhre, G., Penner, J., Perlwitz, J., Stier, P., Takemura, T., and Zender, C. S.: Global dust model intercomparison in AeroCom phase I, Atmospheric Chemistry and Physics, 11, 7781-7816, 2011.
Hurrell, J. W., Holland, M. M., Gent, P. R., Ghan, S., Kay, J. E., Kushner, P. J., Lamarque, J. F., Large, W. G., Lawrence, D., Lindsay, K., Lipscomb, W. H., Long, M. C., Mahowald, N., Marsh, D. R., Neale, R. B., Rasch, P., Vavrus, S., Vertenstein, M., Bader, D., Collins, W. D., Hack, J. J., Kiehl, J., and Marshall, S.: The Community Earth System Model A Framework for Collaborative Research, Bulletin of the American Meteorological Society, 94, 1339-1360, 2013.
Iversen, J. D. and White, B. R.: Saltation threshold on earth, mars and venus, Sedimentology, 29, 111-119, 1982.
Jansen, E., Overpeck, J., Briffa, K. R., Duplessy, J.-C., Joos, F., Masson-Delmotte, V., Olago, D., Otto-Bliesner, B., Peltier, W. R., Rahmstorf, S., Ramesh, R., Raynaud, D., Rind, D., Solomina, O., Villalba, R., and Zhang, D.: Palaeoclimate. In: Climate Change 2007: The Physical Science Basis. Contribution of Working Group I to the Fourth Assessment Report of the Intergovernmental Panel on Climate Change, Solomon, S., Qin, D., Manning, M., Chen, Z., Marquis, M., Averyt, K. B., Tignor, M., and Miller, H. L. (Eds.), Cambridge University Press, Cambridge, United Kingdom and New York, NY, USA, 2007.
Kaufman, Y. J., Koren, I., Remer, L. A., Tanre, D., Ginoux, P., and Fan, S.: Dust transport and deposition observed from the Terra-Moderate Resolution Imaging Spectroradiometer (MODIS) spacecraft over the Atlantic ocean, Journal of Geophysical Research-Atmospheres, 110, 2005.
Kok, J. F.: Does the size distribution of mineral dust aerosols depend on the wind speed at emission?, Atmospheric Chemistry and Physics, 11, 10149-10156, 2011a.
Kok, J. F.: A scaling theory for the size distribution of emitted dust aerosols suggests climate models underestimate the size of the global dust cycle, Proc. Natl. Acad. Sci. U. S. A., 108, 1016-1021, 2011b.
Kok, J. F., Mahowald, N. M., Fratini, G., Gillies, J. A., Ishizuka, M., Leys, J. F., Mikami, M., Park, M.-S., Park, S.-U., Van Pelt, R. S., and Zobeck, T. M.: An improved dust emission model. Part 1: Model description and comparison against measurements, Atmospheric Chemistry and Physics, this issue, 2014.
Kok, J. F., Parteli, E. J. R., Michaels, T. I., and Karam, D. B.: The physics of wind-blown sand and dust, Reports on Progress in Physics, 75, 106901, 2012.
Koven, C. D. and Fung, I.: Identifying global dust source areas using high-resolution land surface form, Journal of Geophysical Research-Atmospheres, 113, 2008.
Laurent, B., Marticorena, B., Bergametti, G., Leon, J. F., and Mahowald, N. M.: Modeling mineral dust emissions from the Sahara desert using new surface properties and soil database, Journal of Geophysical Research-Atmospheres, 113, 2008.
Lawrence, C. R. and Neff, J. C.: The contemporary physical and chemical flux of aeolian dust: A synthesis of direct measurements of dust deposition, Chemical Geology, 267, 46-63, 2009.
Lawrence, D. M., Oleson, K. W., Flanner, M. G., Thornton, P. E., Swenson, S. C., Lawrence, P. J., Zeng, X. B., Yang, Z. L., Levis, S., Sakaguchi, K., Bonan, G. B., and Slater, A. G.:

Parameterization Improvements and Functional and Structural Advances in Version 4 of the Community Land Model, J. Adv. Model. Earth Syst., 3, 27, 2011.
Liu, X., Easter, R. C., Ghan, S. J., Zaveri, R., Rasch, P., Shi, X., Lamarque, J. F., Gettelman, A., Morrison, H., Vitt, F., Conley, A., Park, S., Neale, R., Hannay, C., Ekman, A. M. L., Hess, P., Mahowald, N., Collins, W., Iacono, M. J., Bretherton, C. S., Flanner, M. G., and Mitchell, D.: Toward a minimal representation of aerosols in climate models: description and evaluation in the Community Atmosphere Model CAM5, Geoscientific Model Development, 5, 709-739, 2012.
Ma, P.-L., Rasch, P. J., Wang, H., Zhang, K., Easter, R. C., Tilmes, S., Fast, J. D., Liu, X., Yoon, J.-H., and Lamarque, J.-F.: The role of circulation features on black carbon transport into the Arctic in the Community Atmosphere Model version 5 (CAM5), Journal of geophysical research: Atmospheres, 118, 4657-4669, 2013.
Mahowald, N. M., Albani, S., Kok, J. F., Engelstaedter, S., Scanza, R., Ward, D. S., and Flanner, M. G.: The size distribution of desert dust aerosols and its impact on the Earth system, Aeolian Research, doi: 10.1016/j.aeolia.2013.09.002, 2014. 2014.
Mahowald, N. M. and Dufresne, J. L.: Sensitivity of TOMS aerosol index to boundary layer height: Implications for detection of mineral aerosol sources, Geophysical Research Letters, 31, 2004.
Mahowald, N. M., Engelstaedter, S., Luo, C., Sealy, A., Artaxo, P., Benitez-Nelson, C., Bonnet, S., Chen, Y., Chuang, P. Y., Cohen, D. D., Dulac, F., Herut, B., Johansen, A. M., Kubilay, N., Losno, R., Maenhaut, W., Paytan, A., Prospero, J. A., Shank, L. M., and Siefert, R. L.: Atmospheric Iron Deposition: Global Distribution, Variability, and Human Perturbations, Annual Review of Marine Science, 1, 245-278, 2009.
Mahowald, N. M., Kloster, S., Engelstaedter, S., Moore, J. K., Mukhopadhyay, S., McConnell, J. R., Albani, S., Doney, S. C., Bhattacharya, A., Curran, M. A. J., Flanner, M. G., Hoffman, F. M., Lawrence, D. M., Lindsay, K., Mayewski, P. A., Neff, J., Rothenberg, D., Thomas, E., Thornton, P. E., and Zender, C. S.: Observed 20th century desert dust variability: impact on climate and biogeochemistry, Atmospheric Chemistry and Physics, 10, 10875-10893, 2010.
Mahowald, N. M., Lamarque, J. F., Tie, X. X., and Wolff, E.: Sea-salt aerosol response to climate change: Last Glacial Maximum, preindustrial, and doubled carbon dioxide climates, Journal of Geophysical Research-Atmospheres, 111, 2006a.
Mahowald, N. M., Muhs, D. R., Levis, S., Rasch, P. J., Yoshioka, M., Zender, C. S., and Luo, C.: Change in atmospheric mineral aerosols in response to climate: Last glacial period, preindustrial, modern, and doubled carbon dioxide climates, J. Geophys. Res., 111, D10202, 2006b.
Mahowald, N. M., Zender, C. S., Luo, C., Savoie, D., Torres, O., and del Corral, J.: Understanding the 30-year Barbados desert dust record, Journal of Geophysical Research-Atmospheres, 107, 4561, 2002.
Marticorena, B. and Bergametti, G.: Modeling the atmospheric dust cycle .1. Design of a soil-derived emission scheme, Journal of Geophysical Research-Atmospheres, 100, 16415-16430, 1995.
Martin, J. H., Gordon, R. M., and Fitzwater, S. E.: The case for iron, Limnology and Oceanography, 36, 1793-1802, 1991.
McKenna Neuman, C. and Nickling, W. G.: A theoretical and wind-tunnel investigation of the effect of capillary water on the entrainment of sediment by wind, Canadian Journal of Soil Science, 69, 79-96, 1989.

Menut, L., Perez, C., Haustein, K., Bessagnet, B., Prigent, C., and Alfaro, S.: Impact of surface roughness and soil texture on mineral dust emission fluxes modeling, Journal of Geophysical Research-Atmospheres, 118, 6505-6520, 2013.

Miller, R. L. and Tegen, I.: Climate response to soil dust aerosols, Journal of Climate, 11, 3247-3267, 1998.

Mokhtari, M., Gomes, L., Tulet, P., and Rezoug, T.: Importance of the surface size distribution of erodible material: an improvement on the Dust Entrainment And Deposition (DEAD) Model, Geoscientific Model Development, 5, 581-598, 2012.

Neale, R. B., Chen, C.-C., Gettelman, A., Lauritzen, P. H., Park, S. U., Williamson, D. L., Conley, A. J., Garcia, R., Kinnison, D., Lamarque, J. F., D., M., Mills, M., Smith, A. K., Tilmes, S., Vitt, F., Morrison, H., Cameron-Smith, P., Collins, W. D., Jacono, M. J., Easter, R. C., Ghan, S. J., Liu, X., Rasch, P. J., and Taylor, M. A.: Description of the NCAR Community Atmosphere Model (CAM 5.0), NCAR Technical Note, TN-486, pp. 268, 2010.

Oleson, K. W., Lawrence, D. M., Gordon, B. B., Flanner, M. G., Kluzek, E., Lawrence, P. J., Levis, S., Swenson, S. C., Thornton, P. E., Dai, A., Decker, M., Dickinson, R., Feddema, J., Heald, C. L., Hoffman, F., Lamarque, J.-F., Mahowald, N., Niu, G.-Y., Qian, T., Randerson, J., Running, S., Sakaguchi, K., Slater, A., Stockli, R., Wang, A., Yang, Z.-L., Zeng, Z., and Zeng, X.: Technical Description of version 4.0 of the Community Land Model (CLM), 2010.

Perlwitz, J., Tegen, I., and Miller, R. L.: Interactive soil dust aerosol model in the GISS GCM 1. Sensitivity of the soil dust cycle to radiative properties of soil dust aerosols, Journal of Geophysical Research-Atmospheres, 106, 18167-18192, 2001.

Prospero, J. M.: Assessing the impact of advected African dust on air quality and health in the eastern United States, Hum. Ecol. Risk Assess., 5, 471-479, 1999.

Prospero, J. M., Ginoux, P., Torres, O., Nicholson, S. E., and Gill, T. E.: Environmental characterization of global sources of atmospheric soil dust identified with the Nimbus 7 Total Ozone Mapping Spectrometer (TOMS) absorbing aerosol product, Reviews of Geophysics, 40, 1002, 2002.

Prospero, J. M. and Lamb, P. J.: African droughts and dust transport to the Caribbean: Climate change implications, Science, 302, 1024-1027, 2003.

Prospero, J. M. and Nees, R. T.: Impact of the north african drought and el-nino on mineral dust in the barbados trade winds, Nature, 320, 735-738, 1986.

Prospero, J. M., Uematsu, M., and Savoie, D. L.: Mineral aerosol transport to the Pacific Ocean. In: Chemical Oceanography, Riley, J. P. (Ed.), Academic Press, New York, 1989.

Ravi, S., D'Odorico, P., Over, T. M., and Zobeck, T. M.: On the effect of air humidity on soil susceptibility to wind erosion: The case of air-dry soils, Geophysical Research Letters, 31, 2004.

Ravi, S., Zobeck, T. M., Over, T. M., Okin, G. S., and D'Odorico, P.: On the effect of moisture bonding forces in air-dry soils on threshold friction velocity of wind erosion, Sedimentology, 53, 597-609, 2006.

Rea, D. K.: The paleoclimatic record provided by eolian deposition in the deep-sea - The geologic history of wind, Reviews of Geophysics, 32, 159-195, 1994.

Ridley, D. A., Heald, C. L., and Prospero, J. M.: What controls the recent changes in African mineral dust aerosol across the Atlantic?, Atmospheric Chemistry and Physics, 14, 5735-5747, 2014.

Schepanski, K., Tegen, I., Todd, M. C., Heinold, B., Bonisch, G., Laurent, B., and Macke, A.: Meteorological processes forcing Saharan dust emission inferred from MSG-SEVIRI

observations of subdaily dust source activation and numerical models, Journal of Geophysical Research-Atmospheres, 114, 2009.
Shao, Y. P.: Physics and Modelling of Wind Erosion, Springer, Heidelberg, 2008.
Solomon, S., Qin, D., Manning, M., Alley, R. B., Berntsen, T., Bindoff, Z., Chen, Z., Chidthaisong, A., Gregory, J. M., Hegerl, G. C., Heimann, M., Hewitson, B., Hoskins, B. J., Joos, F., Jouzel, J., Kattsov, V., Lohmann, U., Matsuno, T., Molina, M., Nicholls, N., Overpeck, J., Raga, G., Ramaswamy, V., Ren, J., Rusticucci, M., Somerville, R., Stocker, T. F., Whetton, P., Wood, R. A., and Wratt, D.: Technical Summary. In: Climate Change 2007: The Physical Science Basis. Contribution of Working Group I to the Fourth Assessment Report of the Intergovernmental Panel on Climate Change Solomon, S., Qin, D., Manning, M., Chen, Z., Marquis, M., Averyt, K. B., Tignor, M., and Miller, H. L. (Eds.), Cambridge University Press, Cambridge, United Kingdom and New York, NY, USA, 2007.
Tegen, I., Harrison, S. P., Kohfeld, K., Prentice, I. C., Coe, M., and Heimann, M.: Impact of vegetation and preferential source areas on global dust aerosol: Results from a model study, Journal of Geophysical Research-Atmospheres, 107, 2002.
Tegen, I., Werner, M., Harrison, S. P., and Kohfeld, K. E.: Relative importance of climate and land use in determining present and future global soil dust emission, Geophysical Research Letters, 31, 2004.
Videen, G. and Chylek, P.: Scattering by a composite sphere with an absorbing inclusion and effective medium approximations, Optics Communications, 158, 1-6, 1998.
Washington, R., Bouet, C., Cautenet, G., Mackenzie, E., Ashpole, I., Engelstaedter, S., Lizcano, G., Henderson, G. M., Schepanski, K., and Tegen, I.: Dust as a tipping element: The Bodele Depression, Chad, Proc. Natl. Acad. Sci. U. S. A., 106, 20564-20571, 2009.
Werner, M., Tegen, I., Harrison, S. P., Kohfeld, K. E., Prentice, I. C., Balkanski, Y., Rodhe, H., and Roelandt, C.: Seasonal and interannual variability of the mineral dust cycle under present and glacial climate conditions, Journal of Geophysical Research-Atmospheres, 107, 4744, 2002.
Wilks, D. S.: Statistical Methods in the Amtospheric Sciences, Academic Press, Oxford, UK, 2011.
Zender, C. S., Bian, H. S., and Newman, D.: Mineral Dust Entrainment and Deposition (DEAD) model: Description and 1990s dust climatology, Journal of Geophysical Research-Atmospheres, 108, 4416, 2003a.
Zender, C. S., Newman, D., and Torres, O.: Spatial heterogeneity in aeolian erodibility: Uniform, topographic, geomorphic, and hydrologic hypotheses, Journal of Geophysical Research-Atmospheres, 108, 4543, 2003b.
Zobeck, T. M.: Soil properties affecting wind erosion, Journal of Soil and Water Conservation, 46, 112-118, 1991.